EFFECTS OF FREESTREAM TURBULENCE ON TURBINE BLADE HEAT TRANSFER IN TRANSONIC FLOW

by

Loren Patton Johnson

Thesis submitted to the Faculty of the

Virginia Polytechnic Institute and State University

in partial fulfillment of the requirements for the degree of

Master of Science

in

Mechanical Engineering

APPROVED:

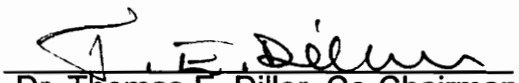

Dr. Thomas E. Diller, Co-Chairman

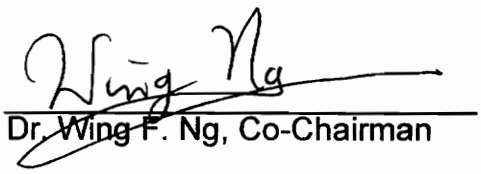

Dr. Wing F. Ng, Co-Chairman

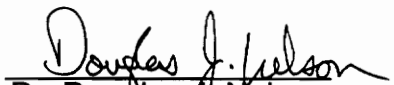

Dr. Douglas J. Nelson

May, 1995

Blacksburg, Virginia

EFFECTS OF FREESTREAM TURBULENCE ON TURBINE BLADE HEAT TRANSFER IN TRANSONIC FLOW

by

Loren P. Johnson

Dr. Thomas E. Diller and Dr. Wing F. Ng, Co-Chairmen

Mechanical Engineering

(ABSTRACT)

The effects of grid generated freestream turbulence on surface heat transfer to turbine blades were measured experimentally. Time-resolved and unsteady heat flux measurements were made with **H**eat **F**lux **M**icrosensors at two positions on the suction side of turbine blades. The experiments were conducted on a stationary cascade of aluminum turbine blades for heated runs at transonic conditions. Non-dimensional flow parameters were matched to actual engine conditions including the design exit Mach number of 1.26 and the gas-to-wall temperature ratio of 1.4.

Methods for determining the adiabatic wall temperature and heat transfer coefficient are presented and the results are compared to computer predictions for these blades. Heat transfer measurements were taken with a new, directly deposited HFM gage near the trailing edge shock on nitrogen cooled blades. The average heat transfer coefficient for Mach 1.26 was 765 W/(m^2 °C) and matched well with a predicted value of 738 W/(m^2 °C). Freestream turbulence effects were studied at a second gage location 1.0 cm from the stagnation point on uncooled blades. Results at this location show an increase in freestream turbulence from 1% to 8% led to a 15% increase of the average heat transfer

coefficient and also matched well with predictions. The fast response time of the HFM illustrated graphically the increase in energy spectra due to freestream turbulence at the 0 - 10 kHz range. The heat flux turbulence intensity (Tu_q) was defined as another physical quantity important to turbine blade heat transfer.

DEDICATION

I would like to dedicate this body of work to my two grandfathers, H. Loren Johnson and Leo R. Call, Sr., who passed away during my collegiate years at Virginia Tech. I will always cherish their love, kindness, and support.

ACKNOWLEDGMENTS

First, and foremost, I would like to thank my two advisors, Dr. Diller and Dr. Ng. I talked to Dr. Diller, first, about working on this project, and I'm deeply indebted to his patience and wisdom. I had many questions about this project and he answered them all. Dr. Ng was insightful and helpful, especially at our weekly meetings. I would also like to thank my third committee member, Dr. Nelson, for his time and outside guidance.

I could not have done the work without the assistance from my fellow team members Alex Mezynski and Angela Wesner (and her photo assistance). I would like to thank Terry Reid for his help with Kulites and tunnel expertise. I especially want to thank David Holmberg for his invaluable time in the tunnel helping to run the heat flux experiments. I would like to thank Jamie Hale and Missy Fasold, new members to the project, for helping with tunnel repairs and all their assistance. I would also like to thank D.J. Osborne and Tim Yang for their assistance. Also, thanks to the guys in the shop, Johnny, Jerry, Timmy, Red, and Bill. I would like to give special thanks to Dr. Tibor Kiss for all his help on how the tunnel works. Finally, thanks to the guys at Vatell, John Hager and Jim Terrel, for their technical assistance with the Heat Flux Microsensor.

Obviously I can not leave out my love to my parents. Thanks, dad, you're my inspiration, and a tough act to follow. Thanks, mom, for all your love and support. Seattle is far but only a phone call away.

I would finally like to thank the Air Force for funding this project.

TABLE OF CONTENTS

LIST OF FIGURES

Programs

LIST OF TABLES

NOMENCLATURE

A_{tot}	-	Total screen surface area [m^2]
Cp	-	Specific Heat [J/(kg K)]
D	-	Diameter [m]
d_W	-	Hot wire diameter [m]
E	-	Voltage signal [V]
Eq	-	Heat flux sensor output [V]
E_T	-	Temperature sensor output [V]
h	-	Heat transfer coefficient [W/(m^2 K)]
k	-	Thermal conductivity [W/(m K)]
L	-	Blade Chord [m], Length [m]
L_W	-	Hot wire length
Ma	-	Mach number
M	-	Mesh size [m]
P_{ATM}	-	Atmospheric pressure [Pa]
P_{TOT}	-	Total upstream pressure [Pa]
P_S	-	Static pressure [Pa]
P_{SUR}	-	Surface pressure [Pa]
q"	-	Heat flux [W/cm^2]
q"'	-	Fluctuating component heat flux [W/cm^2]
R	-	Universal gas constant
R_W	-	Hot wire operating resistance
r	-	Recovery factor
S	-	Gage sensitivity [μV/(W/cm^2)]
t	-	Time [s]
T_∞	-	Freestream temperature
T_{AW}	-	Adiabatic wall temperature [ºC]
T_I	-	Initial reference for temperature sensor [ºC]
T_M	-	Film temperature [K]
T_{TOT}	-	Inlet total temperature [ºC]
T_R	-	Recovery temperature [ºC]
T_{REF}	-	Reference temperature [ºC]
T_S	-	Static temperature [ºC,K]
T_{SUR}	-	Surface temperature (from RTS) [ºC]
T_W	-	Hot wire temperature [K]
Tx	-	Temperature exponent
u'	-	Fluctuating component of flow velocity [m/s]
U	-	Instantaneous velocity [m/s]
U_∞	-	Freestream velocity [m/s]
V	-	Hot wire voltage
x	-	Distance from turbulence grid to center blade
Tu	-	Freestream velocity turbulence intensity
Tu_q	-	Heat flux turbulence intensity
Nu	-	Nusselt number - h D / k
Pr	-	Prandtl number - ν/α

Re	-	Reynolds number - $U_\infty l / \nu$
Fr	-	Frossling number - $Nu/\mathrm{Re}^{1/2}$

Greek Symbols

α	-	Thermal diffusivity [m^2/s]
γ	-	Specific heat ratio
μ	-	Dynamic viscosity [$(Ns)/m^2$]
ν	-	Kinematic viscosity [m^2/s]
ρ	-	Density of air [kg/m^3]

Acronyms and Abbreviations

AC	-	Fluctuating component
BASIC	-	Beginner's All-Purpose Instruction Code
°C	-	Celsius
DC	-	Mean Component
Hz	-	Hertz
IBM PC	-	International Business Machines Personal Computer
K	-	Kelvin
ms	-	Milliseconds
Pa	-	Pascal
RMS	-	Root mean square
VPI&SU		Virginia Polytechnic Institute and State University
HFS	-	Heat Flux Sensor
RTS	-	Resistance Temperature Sensor
HFM	-	Heat Flux Microsensor (both HFS and RTS)
CFD	-	Computational Fluid Dynamics
μs	-	Microseconds

Chapter 1.0

INTRODUCTION

1.1 Background

An important emphasis in the gas turbine engine industry is to increase the thrust to weight ratio of a turbine engine. An increase in thrust implies an increase of the thermal load in the engine while a reduction in weight requires lighter, stronger materials. These improvements require an understanding of the thermal stresses and flow fields on and around the components in the engine.

The study of heat transfer is a key tool in the ability to determine critical thermal loads. With this tool, better cooling schemes can be implemented to minimize the thermal stresses on key components. An increased knowledge in the dynamics of this heating process can lead to advanced designs to optimize the system.

An area of interest inside the turbine engine is the turbine blades. It is important to know where and how to cool the blades, which are subjected to high thermal loads.

It is known that freestream turbulence augments the heat transfer to the turbine blades. Several studies have been conducted on the increase of heat transfer from a circular cylinder due to freestream turbulence. Little study has been done on measuring the time-resolved heat flux due to varying turbulence intensity on an actual, modeled turbine blade in a heated transonic wind tunnel.

The use of thin-film gages to measure heat flux has become more common in recent years. In the past, these gages were placed on a substrate that was then recessed into a bored hole on the cylinder or blade. Now, newer

techniques allow for the direct deposit of a gage on the surface of a turbine blade. The ability to measure heat flux and surface temperature directly on a portion of the blade with a surface gage has not previously been reported.

1.2 Objective

Here at Virginia Tech, a unique wind tunnel was created in order to simulate in a stationary turbine blade cascade non-dimensional flow conditions that exist in an engine. These conditions include Reynolds number, Mach number and temperature ratios. The focus of this thesis is the detailed measurements of time-resolved heat flux due to varying turbulence intensity using new and unique instrumentation. Heat transfer measurements were taken at the leading and trailing edge of the suction side of high performance blades in the cascade. Different turbulence grids were studied in order to increase the freestream turbulence and augment the heat transfer to the blades. The experimental data can then be compared with computer predictions and help eventually to piece together the "complete" picture.

The surface blade temperature and heat flux were measured by new thin-film gages. Two versions of the Heat Flux Microsensor (HFM) were used to take time-resolved and unsteady heat transfer measurements. The Heat Flux Microsensors are more fully explained in the literature review of chapter 2.0. Also in chapter 2.0 is a background review on freestream turbulence. In Chapter 3.0, details about the experimental set-up, including the tunnel facility and cascade design, are discussed. The experimental procedure, including discussion of the turbulence grids, is explained in chapter 4.0. The results of the

experiments are given in chapter 5.0 followed by discussion of the results. Some final comments and conclusions are made in chapter 6.0.

Chapter 2.0

BACKGROUND

There are two subjects covered in this review, the study of freestream turbulence and the development of the Heat Flux Microsensor. First, a background review is given on the effects of freestream turbulence on turbine blade heat transfer. Second, background on the Heat Flux Microsensor is given but with special emphasis on the new, directly deposited gage.

2.1 Freestream Turbulence

Many researchers have investigated different aspects of turbine blade heat transfer due to freestream turbulence effects. Several experiments were conducted on the effects of heat transfer from freestream turbulence on cylinders and flat plates.

To model freestream turbulence, the flow velocity can be expressed as a mean velocity component and a fluctuating component that changes in magnitude with respect to time.

$$U_\infty = \overline{U}_\infty + U'_\infty \qquad [1]$$

Characterizations of turbulent flow depend on the frequencies and amplitudes of the fluctuating components of velocity. The integral length scale, λ, can be measured from the autocorrelation coefficient

$$\rho(\tau) = \frac{\lim_{t_O \to T} \dfrac{\dfrac{1}{t_O}\displaystyle\int_0^{t_O} u'(t)u'(t+\tau)dt}{\dfrac{1}{t_O}\displaystyle\int_0^{t_O}[u'(t)]^2 dt}}{} \qquad [2]$$

where τ is the time delay and T is the length of the time record. The integral time scale, T_1, can then be defined as

$$T_1 = \int_0^\infty \rho(\tau) d\tau \qquad [3]$$

so that finally the integral length scale equals the time scale multiplied by the mean velocity.

$$\lambda = T_1 \bullet U \qquad [4]$$

The turbulence intensity is then defined as

$$Tu = \frac{\frac{1}{3}\left(\overline{U'^2} + \overline{V'^2} + \overline{W'^2}\right)^{1/2}}{U} \qquad [5]$$

The further assumption of isotropy reduces the turbulence intensity equation to

$$Tu = \frac{\sqrt{\overline{u'^2}}}{U_\infty} \qquad [6]$$

where Tu is the turbulence intensity ratio, U_∞ is the mean flow velocity and u' is the fluctuating component of velocity.

Kestin [1966] summarized previous flat plate and circular cylinder experiments, studying the increase in turbulence intensity versus Nusselt number. Some of his conclusions were that freestream turbulence has an effect on a laminar boundary layer, but little effect on a turbulent boundary layer. He did show that increases in freestream turbulence did increase heat transfer but he questioned whether a standardized method could be formulated for the correlation of freestream turbulence to heat transfer. Studies were done on the increase of heat transfer through the laminar boundary layer on a cylinder and demonstrated that the stagnation point heat transfer was a function of freestream

turbulence. Kestin [1971] proposed the following relationship to describe the effects of freestream turbulence

$$Fr = \frac{Nu}{\mathrm{Re}^{1/2}} = 0.945 + 3.48\left(\frac{Tu\,\mathrm{Re}^{1/2}}{100}\right) - 4.0\left(\frac{Tu\,\mathrm{Re}^{1/2}}{100}\right)^2 \qquad [7]$$

Lowery and Vachon [1973] showed upwards of a 20% increase in heat transfer at the stagnation point on a cylinder due to increased freestream turbulence. They proposed a new equation for the Frossling number defined as

$$Fr = \frac{Nu}{\mathrm{Re}^{1/2}} = 1.010 + 2.624\left[\frac{Tu\,\mathrm{Re}^{1/2}}{100} - 3.070\frac{Tu\,\mathrm{Re}^{1/2}}{100}\right] \qquad [8]$$

As turbulence intensity increased, the heat transfer increased at the forward stagnation point and in the boundary layer over the front of the cylinder [Gundappa and Diller, 1991]. O'Brien and Van Fossen [1985] found that high turbulence intensity levels at the stagnation region of a circular cylinder in crossflow increased the heat transfer and confirmed an additional Reynolds effect. Van Fossen and Simoneau [1987] found that the boundary layer had laminar characteristics in the presence of freestream turbulence. The heat transfer was high at a stagnation point on the cylinder where the turbulent fluctuations were high and the velocity low.

Glezer, et. al., [1994] studied more closely ways to emulate and reproduce actual engine freestream turbulence. Difficulties arose due to problems in evaluating the effectiveness of cooling in an engine and hot cascade environment. Through their research, they improved the formula given by Lowery and Vachon as

$$\mathrm{Fr} = 1.01\left(\frac{\mathrm{Re_D}}{100000}\right)^{0.05} + 0.058\left(Tu\,\mathrm{Re}_D^{1/2}\right)^{0.65} \qquad [9]$$

for an extended $Tu\sqrt{\mathrm{Re}}$ range.

One way of varying and increasing the freestream turbulence is by the use of turbulence grids. A detailed theoretical discussion on the effects of different grid mesh sizes versus isotropy and boundary analysis is given by Corrsin [1963]. Moss and Oldfield [1994] found that an increase of freestream turbulence led to an increase in heat transfer due to the penetration of freestream turbulence eddies deep into the boundary layer. Their research studied the effect of eddy structures on a flat plate .

Sohn, Obrien and Reshotko [1989] studied the effects of low turbulence 0.3% - 6.0% on a heated flat plate. They examined how six freestream turbulence intensity cases affected laminar, transitional, and low Reynolds number turbulent boundary layers on a flat plate.

Uberoi and Wallis [1969] reported on the study of turbulence decay and the structure of grid generated turbulence by measuring spectra of u and v components of turbulence. They found that some turbulent eddies caused an anisotropic effect.

Grid turbulence is characterized by the turbulence length scale level and spectra [Tan-Atichat, et al. 1981]. Young and Han [1988] studied the effects of high freestream turbulence on turbulent boundary layer heat transfer. Their studies focused on how Tu, U_∞, and temperature effected the heat transfer from a flat plate. They studied the effects of the turbulence integral scales, microscales, turbulence intensity and the relation to surface heat transfer.

All these studies are important in the prediction of the thermal flow fields around the turbine blades. Many computer programs and CFD codes have been written to simulate the effects of freestream turbulence. Most notably, the

STAN5 computer code [Crawford, 1976] can be modified to simulate certain flow regimes.

2.2 The Heat Flux Microsensor

Over the past several years there have been great advances in heat transfer measurement [Diller,1993]. Doorly and Oldfield [1986, 1987] proposed techniques to create new thin-film gages on metal turbine blades that measured surface heat flux. These gages were dependent on the idea of placing a thermal resistance layer on a substrate to measure transient surface temperatures. If the properties of the thermal resistance layer and the substrate were known along with a proper analytical model, then the surface heat flux could be determined.

Hager, et. al., [1991a] discussed the design of a new heat flux gage made from microfabrication techniques. The gages had fast time response and could measure high heat flux levels. Many versions of the **H**eat **F**lux **M**icrosensor have been created. These gages consist of a passive heat flux gage (**H**eat **F**lux **S**ensor), which measures the temperature difference across a thin thermal resistance layer (see Fig. 1) and a second active temperature gage (**R**esistance **T**emperature **S**ensor). The HFS consists of many thermocouple pairs in series which boost the heat flux signal to a measurable level and allow an output signal directly proportional to the heat flux (Fig. 2). The HFM has a fast response time of 10 μs (100 kHz) and allows for a continuous readout.

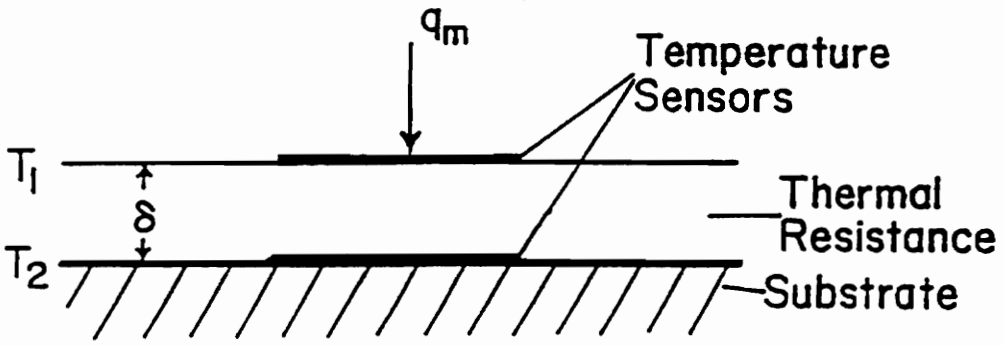

Figure 1. Cross Section of Resistance Layer for HFM

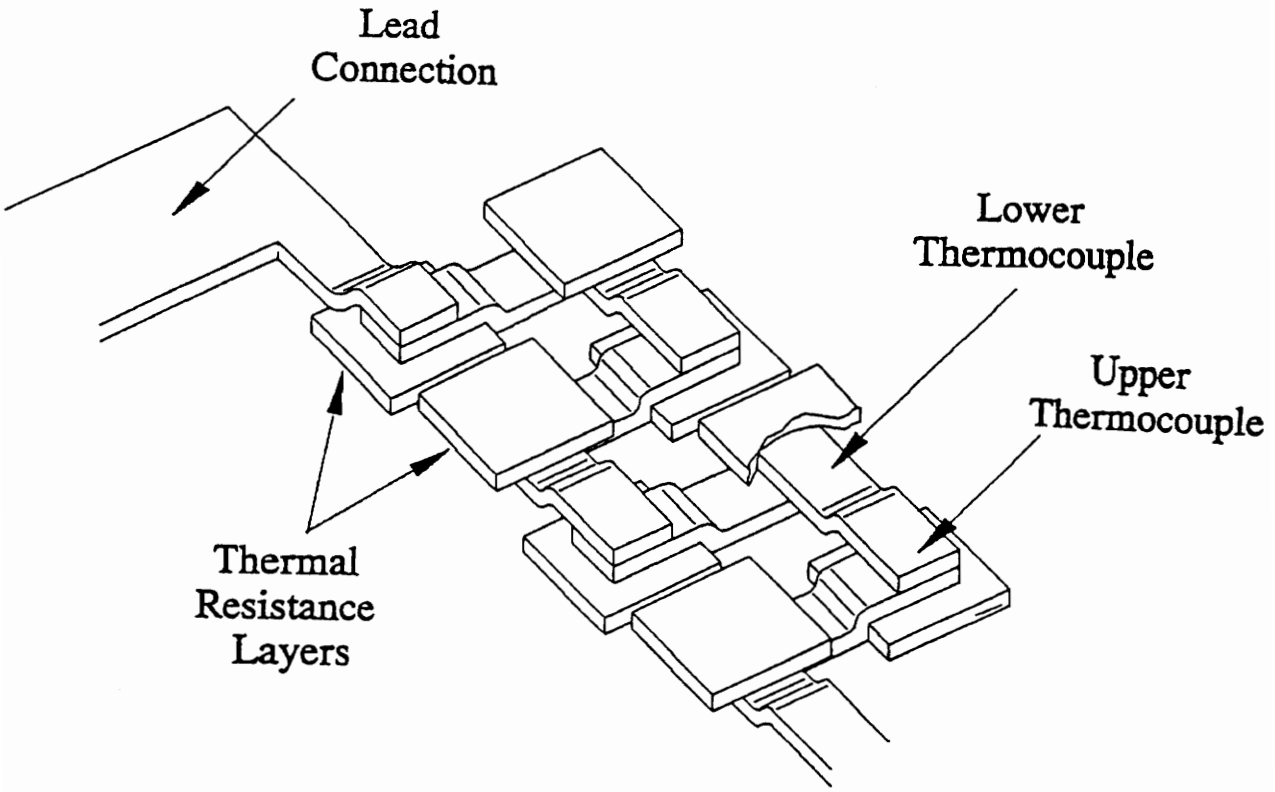

Figure 2. Detailed Section of HFM Thermopile

The HFM has been previously reported in several papers. Swisher, et. al. [1992] measured the time-resolved unsteady heat flux in a junction vortex flow. Holmberg, et. al. [1994] measured the heat transfer from a shock wave through a turbine blade passage. Simmons, Hager, and Diller [1991] measured time-resolved surface heat flux with the HFM due to freestream turbulence at a stagnation point on a circular cylinder. Many more ideas on the uses of the HFM are mentioned by Hager, et. al. [1991b].

Chapter 3.0

EXPERIMENTAL SET-UP

In this chapter the wind tunnel facility, the test section, and the cascade of turbine blades are discussed in detail. A description of the nitrogen cooling set-up is also explained.

3.1 Wind Tunnel Facility

The Cascade Wind Tunnel has been modified to create a unique set-up at Virginia Tech. It is a blow-down wind tunnel with an added heating loop (see Fig. 3). In the following paragraphs, an explanation is given on the air flow through particular sections of the tunnel.

First, a four stage compressor pumps air through a dryer into two large, outside holding tanks. The air is then piped to the tunnel room, where it passes through a throttling valve and a safety valve before entering the main tunnel section. An IBM PC running a compiled tunnel control program regulates the throttle by controlling a compressed air-bottle, set at 138 kPa (20 psi). A more detailed explanation on the tunnel control set-up, including the computer programs, is given by Bersch [1990]. The safety valve was set at a gage pressure of 207 kPa (30 psig) to prevent structural damage to the test section. Next, the air flow enters the wind tunnel. An inlet total pressure can be maintained at 160 kPa (22 psig) with a mass flow rate of 2.1 kg/s for about 20-30 seconds. As the pressure in the tanks decreases, the computer program opens

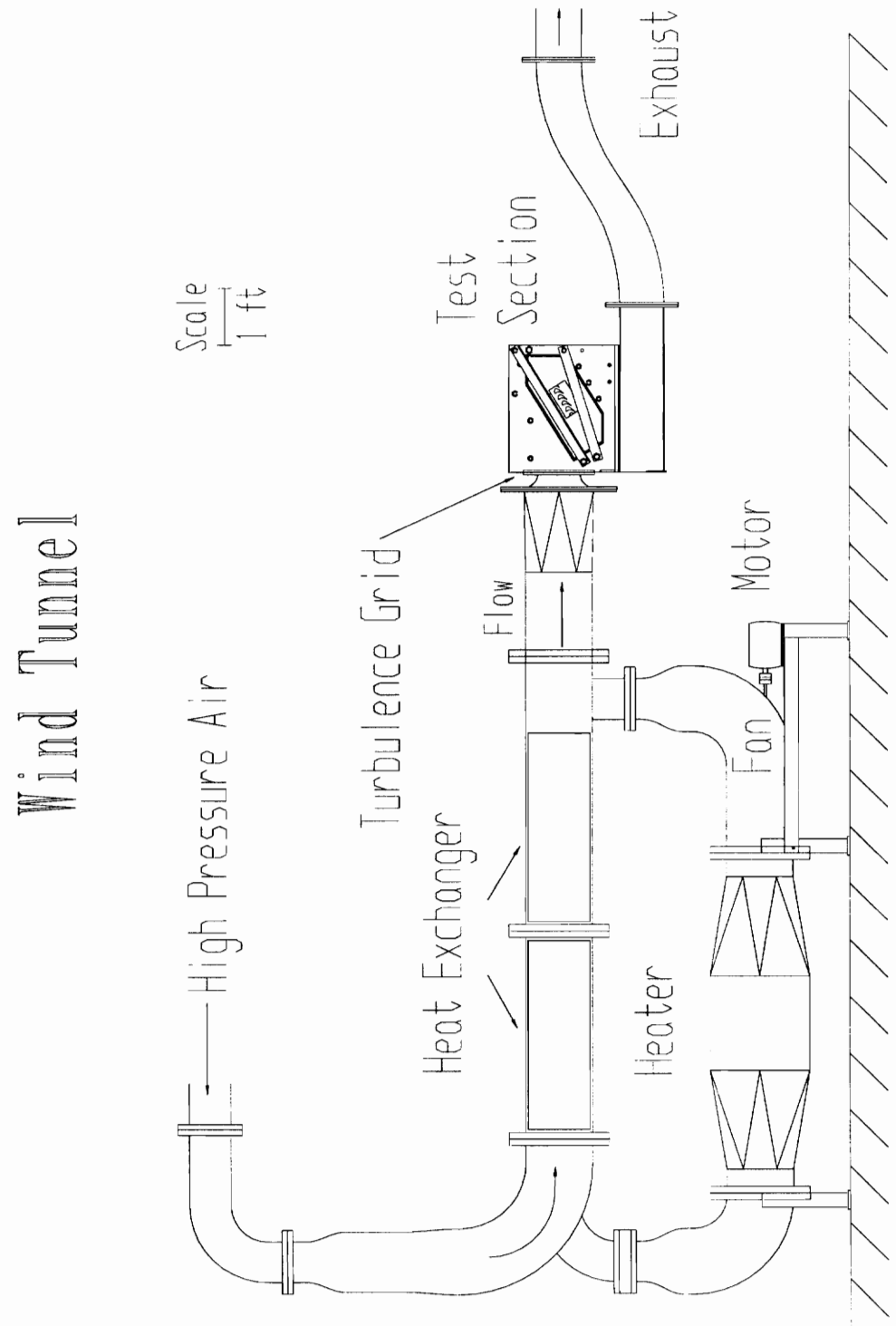

Figure 3. Wind Tunnel.

the throttle and a constant inlet pressure can be maintained. The supply tanks take about 5-10 minutes to recharge for a tank pressure of 827 kPa (120 psig).

Unique to this tunnel is the circulating heating loop. The air enters the main tunnel set-up where it passes through two bundles of 1 meter long 1.59 cm diameter copper heat exchanger tubes. The air is then heated by these tubes. Approximately 350 tubes, held in place by stainless steel screens and weighing 136 kg per bundle were used to store thermal energy. This created an effective surface area of 70 m^2. For the trailing edge tests, the heat exchanger tubes consisted of 250 kg, 2 cm diameter galvanized steel tubes with an effective surface area of 28m^2.

By closing two valves, a heating loop is created (see Fig. 4 and Fig. 5). To heat the copper tubes, a 36 kW electric heater was turned on along with a Dayton three-phase axial flow fan to help circulate the air at 2 m/s. The desired heating temperature was measured by two type K thermocouples. One thermocouple was cemented at the end of one copper tube (44.5 cm [17.5 in] from downstream flange) and another "air" thermocouple (41.3 cm [16.25 in] from downstream flange) was placed 0.3 m (1 ft) downstream of the tube bundle directly in the center of the large pipe and was designated as the total temperature thermocouple. A third thermocouple measured the electric heater temperature.

Upon reaching the desired tube temperature, generally either 90°C (190°F) or 169°C (330°F), the heaters were turned off and the fan was allowed to normalize the temperature to 93°C (200°F) or 177°C (350°F). Typically, the heater reached 370°C,510°C (700°F,950°F), before it was turned off. The fan was then turned off and the flapper valves opened to allow the tunnel to run. On

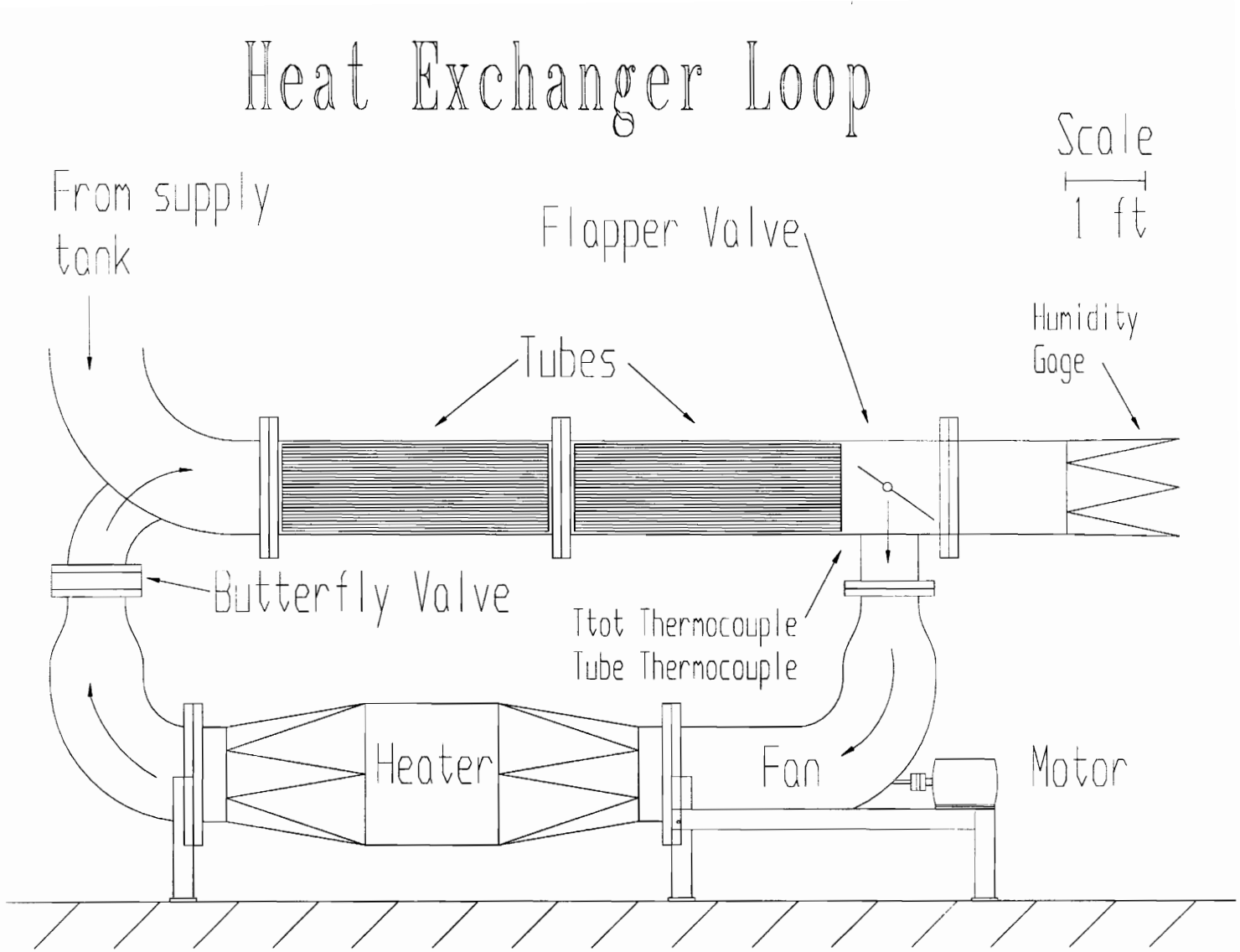

Figure 4. Heat Exchanger Loop

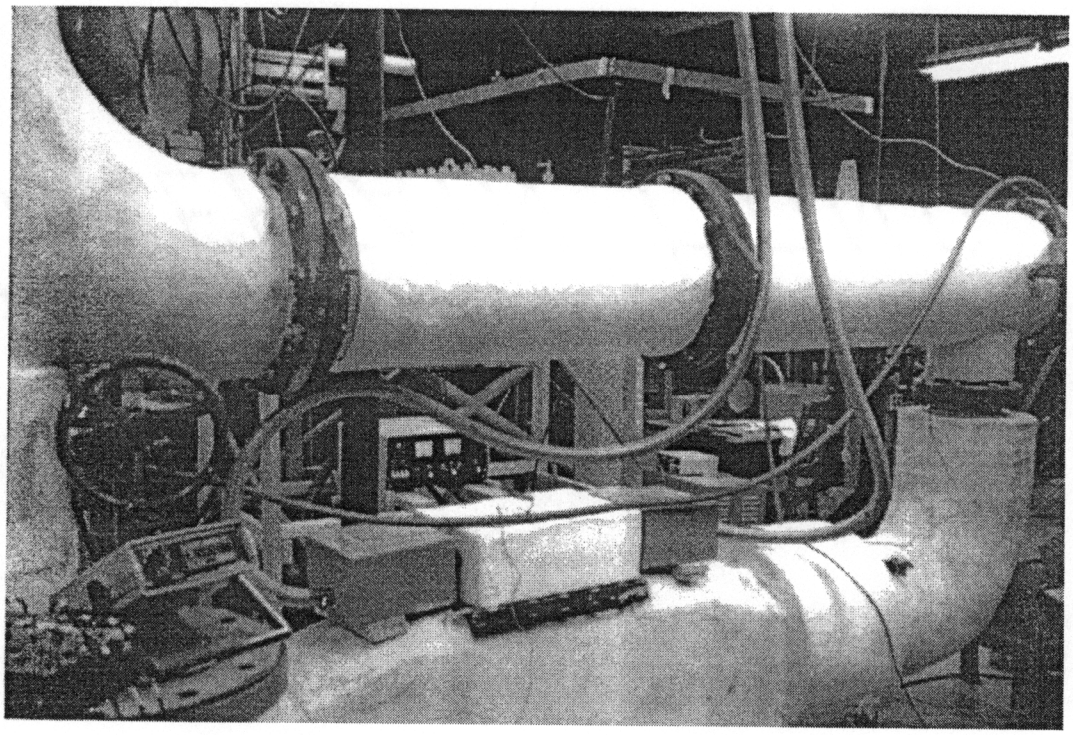

Figure 5. Heat Exchanger Loop Photo

a given day the first heating took approximately 20 minutes to 1 hour, and subsequent runs took 7-15 minutes for recharging. For a 30 second run when the tube temperature started at 93°C (200°F), it cooled to 57°C (135°F). This allowed for gas-to-wall temperature ratios closely matching actual engine ratios of 1.4

The air then passes through a nozzle and into the test section. Next, the air passes over the blades and out through the exhaust portion of the tunnel where it is eventually vented to the atmosphere. For a heated run, the heating loop procedure was repeated again to bring the temperature of the copper tubes back to the desired temperature level.

The humidity of the air flow into the test section was recorded during all runs. A humidity gage, located in the transition piece (29.2 cm [11.5 in] from downstream flange), showed the air to initially contain 20 - 30% humidity but after approximately one run, the humidity lowered to 3.0 - 6.0%, which was considered acceptable.

To reach supersonic exit Mach numbers, the flow enters the test section at Mach 0.36. Many exit Mach numbers were examined during the course of the experiments, but this thesis focused on a design average exit Mach number of 1.26.

The Reynolds number based on exit conditions and true chord is 1.0×10^6 with a gas-to-wall temperature ratio of 1.4. For heated runs, a nitrogen cooling scheme was employed to lower the blade temperature and enhance the heat transfer to the blade. The Reynolds number based on inlet conditions and true chord is 3.4×10^5 with an inlet Mach number of 0.36. To maintain a gas-to-wall ratio of 1.4, a series of cooling tests were performed. The best nitrogen cooling

scheme implemented in this thesis was to start the heated tunnel and cooling simultaneously during a run. Over a 93°C (200°F) run, the temperature dropped 36°C, and the Reynolds number increased to 1.2×10^6.

3.2 Cooling Set-up

For runs heated to 177°C(350°F), the blades were cooled using boil off from liquid nitrogen. A 160 liter high pressure nitrogen tank was connected to a copper tube which spliced the flow of nitrogen into 3 separate channels. Each channel was cemented to the Plexiglas endwall of the cascade where the nitrogen then entered a horseshoe internal channel in the blade (Fig. 6). The nitrogen circulated through each blade and back into an exhaust copper tube which vented the nitrogen to the atmosphere.

The nitrogen was initially pressurized at 1586 kPa (230 psi). After each run, the tank was repressurized to approximately 1448 kPa (210 psi). The nitrogen flow choked at less than 414 kPa (60 psi) but allowed a 15-20 second cooled run. The nitrogen was turned on and off manually. In between runs, a cooling fan was placed directly into a plug hole above the cascade of blades and helped cool the surface of the blades as well as the surrounding test section.

3.3 Test Section and Cascade

The test section (Fig. 7 and Fig. 8) consisted of eleven aluminum blades mounted between two 1.27 cm (0.5 in) thick Plexiglas plates. The Plexiglas is translucent and can allow optical information to be recorded such as shadowgraphs and flow visualization. The blades are 5.08 cm (2.00 in) in span with a 3.81 cm (1.50 in) aerodynamic chord and are spaced 3.81 cm (1.50 in)

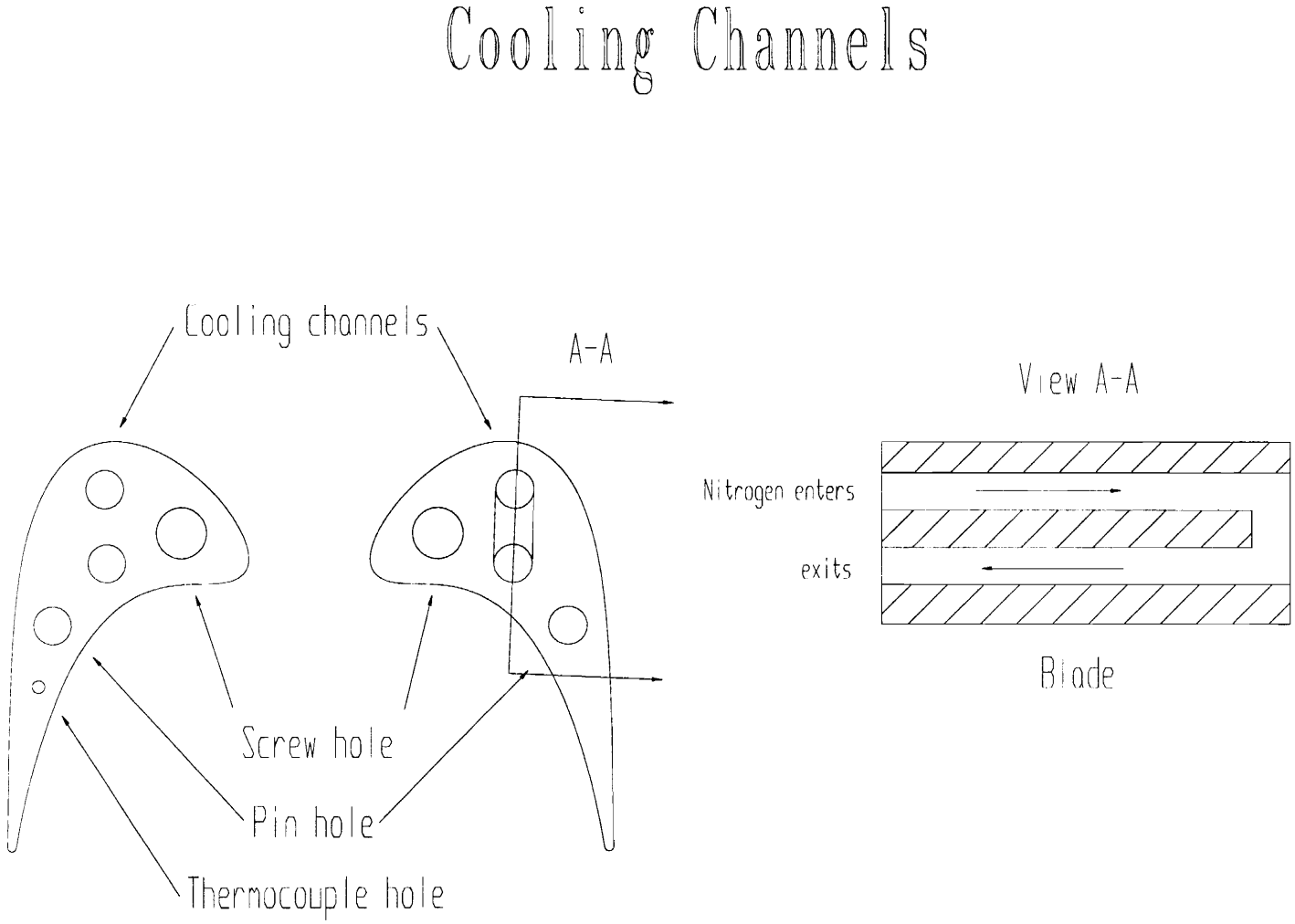

Figure 6. Cooling Set-up in Turbine Blade

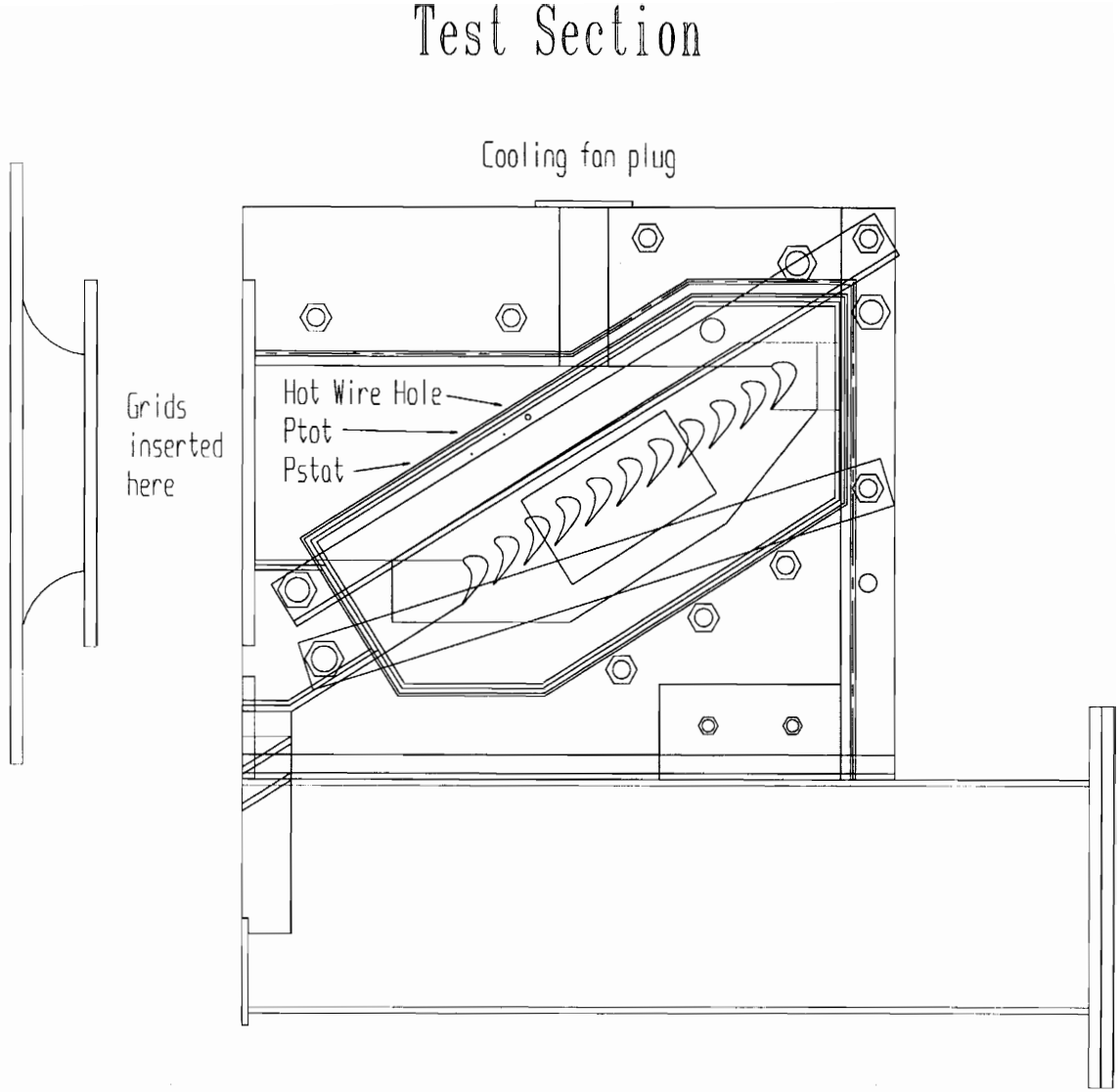

Figure 7. Test Section.

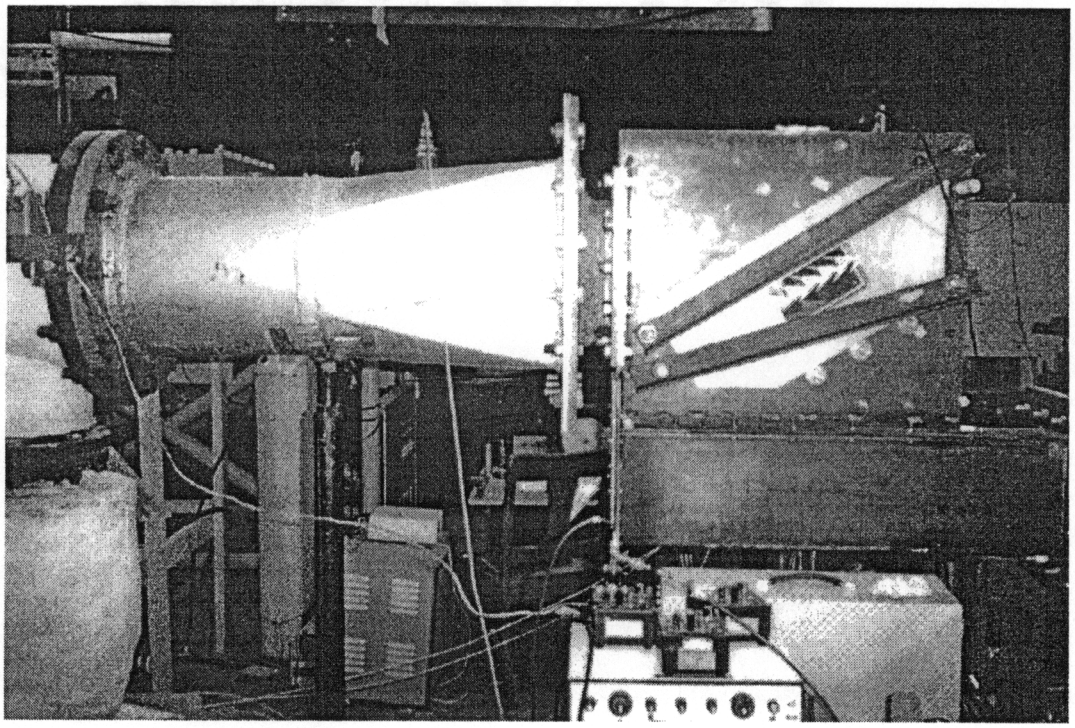

Figure 8. Test Section and Transition Piece Photo

apart. The blades are connected to each Plexiglas wall by a pin and screw combination (Fig. 9). The three middle blades are the primary blades of interest. These blades each have two cooling holes for the nitrogen cooling scheme aforementioned. These three blades also have a thermocouple hole near the side of the trailing edge for interior temperature measurements. The instrumented blade was the sixth blade from the bottom of the cascade and was the middle of the three cooled blades to maximize the uniformity of its flow and temperature conditions.

3.4 HFM-6 Insert Gage and Kulite

For this project, two different HFM gages were used to measure heat flux and surface temperature from the turbine blade. The HFM-6, shown in figure 10, was used in conjunction with a XCQ-062 Kulite miniature pressure transducer to measure heat transfer, surface temperature, and surface pressure along the same span on the leading edge of the blade. This gage had to be inserted into a bored hole in the turbine blade.

The HFM-6 gage is located 1.27 cm (0.5 in) from midspan of the blade to the center of the gage and 1.00 cm (0.375 in) from the stagnation point. The gage housing has a diameter of 0.64 cm (0.25 in) with the actual gage measuring 0.476 cm (0.1875 in) in diameter. The HFM gage bored hole is 0.89 cm (0.35 in) in depth and the lead wires continue through a 0.476 cm (0.188 in) diameter hole for another 0.38 cm (0.15 in) until connecting to one internal

Figure 9. Profile Views of Cascade of Blades.

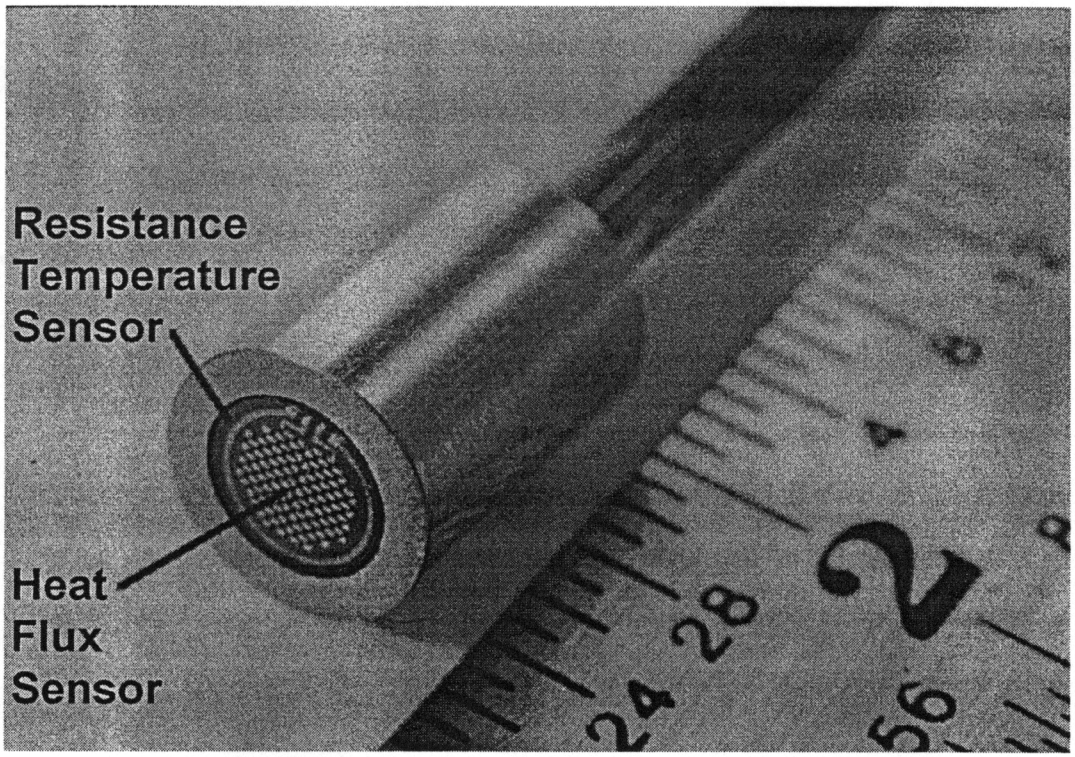

Figure 10. HFM-6 Gage

cooling chamber in the blade (Fig. 11).

The Kulite pressure transducer has a 0.159 cm (0.063 in) diameter and is located 0.794 cm (0.313 in) from blade midspan opposite of the HFM gage. A hole of 0.953 cm (0.375 in) was bored and the lead wires traveled another 0.318 cm (0.125 in) through a 0.119 cm (0.047 in) hole to an internal cooling hole chamber in the blade.

Both gages were inserted into their holes with thermal paste. The HFM gage was secured through the blade screw hole with a 0.476 cm (0.188 in) set screw. The lead wires of the HFM and Kulite came through the internal cooling hole channel. The HFM's 0.008 cm (0.003 in) platinum wires were soldered to 0.008 cm (0.003 in) copper wires that were then soldered to a male Lemo plug. A 91.4 cm (36.0 in) cable with two female Lemo connectors made the connection between the HFM Lemo and an amplifier.

A third hole was drilled at midspan to insert a type-K thermocouple and acted as a surface temperature reference with the RTS. The bead of 0.008 cm (0.003 in) thermocouple wire was soldered to a 0.318 cm (0.125 in) length, 0.159 cm (0.063 in) outer diameter copper sheath. The sheath was press fit into a 0.159 cm (0.063 in) hole that connected to the cooling hole. The Chromium-Alumel lead wires were then connected to an Omega Amplifier.

3.5 HFM-2a Line Gages

A new technique by Vatell Corporation was used to deposit an HFM directly on the turbine blade (HFM-2a), shown in figure 12. The aluminum turbine blade was anodized to prevent the gage from shorting to the aluminum blade. The gage was placed onto the blade through a sputtering process

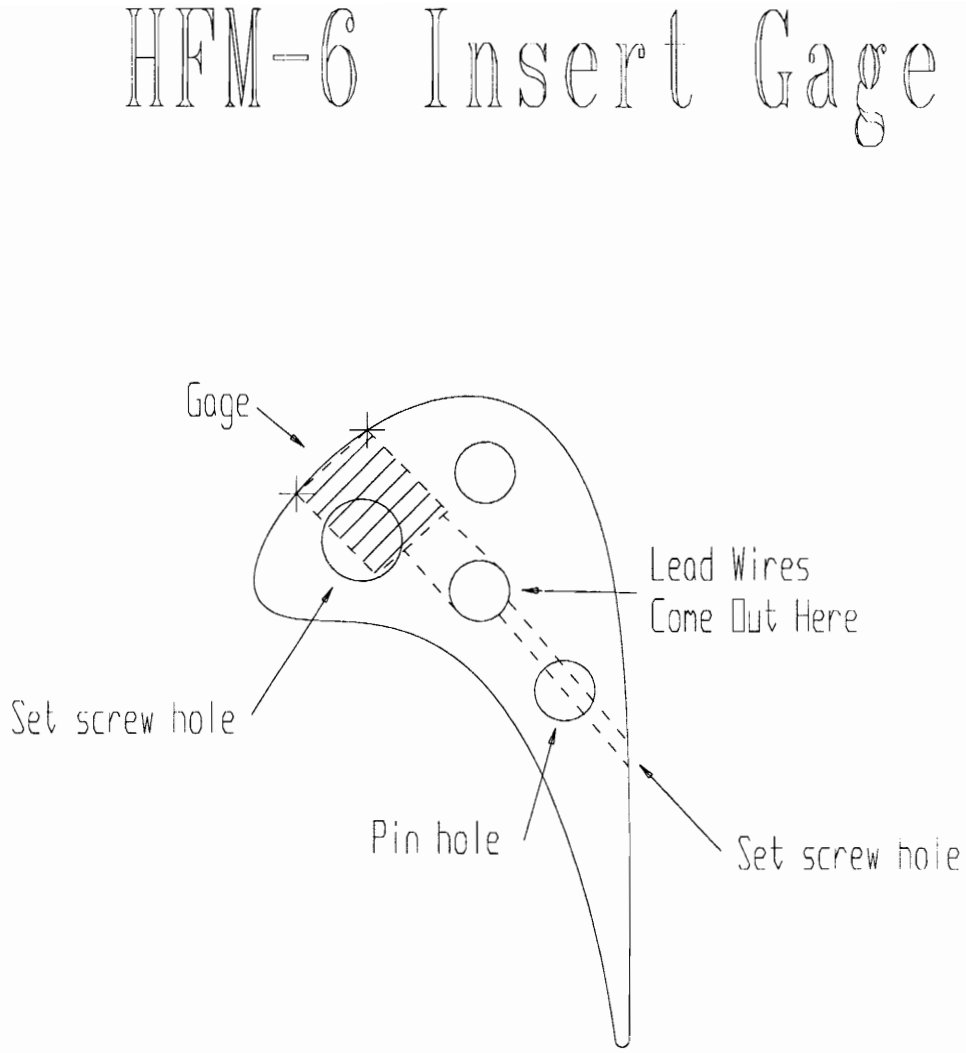

Figure 11. HFM-6 Position in Turbine Blade.

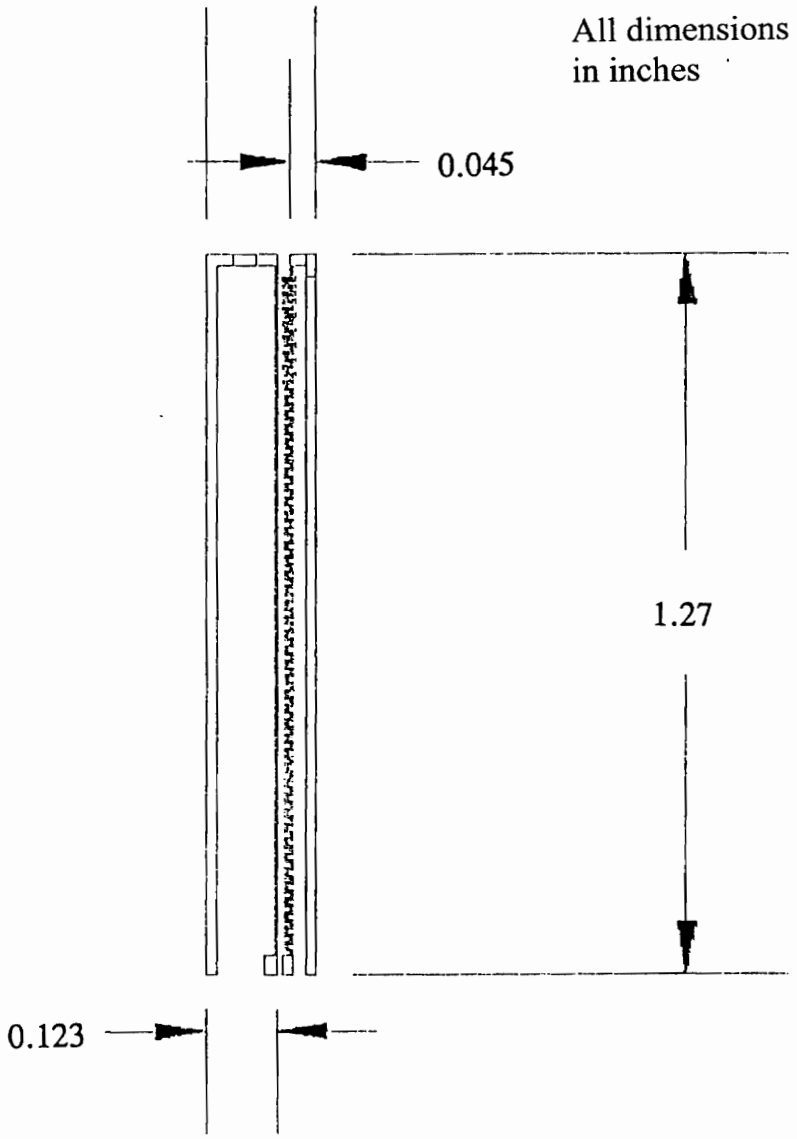

Figure 12. HFM-2a Line Gage Pattern

[Hager, et. al., 1991] and due to this technique, this line gage could be placed on curved portions of the blade where other gages would not fit due to size limitations or could disrupt the physical flow.

This line gage was fabricated in two locations. The first location was at the trailing edge of the turbine blade, 1.5 cm (0.6 in) from the trailing edge (see top of Fig. 13). The second location, placed on a different turbine blade, was at the leading edge (see bottom of Fig. 13), approximately 1.0 cm (0.375 in) from the stagnation point.

Four wires 0.008 cm (0.003 in) came off each blade, two from the HFS and two from the RTS. For both line gages, the lead wires were attached by epoxy and silver paint and pulled off the side of the blade.

Figure 13. Line Gage Locations on Blade

Chapter 4.0

Experimental Procedure

This chapter provides an overview on the instrumentation and data acquisition systems used to run the cascade tunnel and the experimental apparatus. The procedure to obtain freestream turbulence levels and heat flux information from the blades is also discussed.

4.1 Instrumentation and Data Acquisition

The following paragraphs describe the instrumentation and data acquisition necessary to run the cascade wind tunnel. Data was digitally recorded by computer or visually monitored and recorded by hand. Properties monitored during tunnel runs were total upstream pressure, static exit pressure, humidity, and tube temperatures.

Gage pressure in the test section was recorded by a 780B Pressure Sensor Industries Machine. An upstream Pitot pressure tap and an upstream static tap were placed on the aluminum door and above the blades to monitor inlet pressure conditions. Twenty-one static pressure taps were placed directly 1.27 cm (0.5 in) below the trailing edge of the blades on the Plexiglas window (Fig. 9) to monitor exit pressure conditions. These pressure taps were then plugged into a ESP-32 channel pressure transducer. Channels 1 - 21 were designated for the exit static taps while channels 31,32 were designated for the upstream Pitot and static tap, respectively. An IBM PC running a BASIC program recorded the information from the transducer's signal. With this

information, an estimate of the average exit Mach number could be calculated from the Pitot pressure and averaged trailing edge static pressures assuming an isentropic ideal gas relationship. Atmospheric pressure was read daily from a barometer.

Another IBM PC ran the data acquisition program Labtech Notebook. This program could record data at low sampling rates (1 - 100 Hz). The upstream pressure, amplified by a 2310 Signal Conditioner, and total upstream temperature, amplified by an Omega Thermocouple D.C. millivolt amplifier set at a 100 gain, were recorded by Labtech. The mounted tube thermocouple and heater thermocouple were monitored visually by a 10 channel, type K Omega 650 thermocouple readout. A humidity gage monitored the flow relative humidity. Initially the humidity was recorded on Labtech, but later was visually monitored with a voltmeter. An NGI Servogor 124 strip chart recorded the upstream gage pressure over the run. A complete instrumentation schematic is shown in figure 14.

Properties measured for the experiment were heat flux, surface temperature, static surface pressure or total upstream pressure, and total upstream temperature. Data acquisition could be separated into high frequency sampled data and low frequency sampled data. The HFS and RTS data signals along with the total temperature and surface or total pressure were recorded on an 8 channel 6810 Lecroy Waveform connected to an IBM PC. The Lecroy allowed sampling rates as high as 1 MHz. Table 4.1 explains the different set-ups and sampling rates for each heat flux gage configuration.

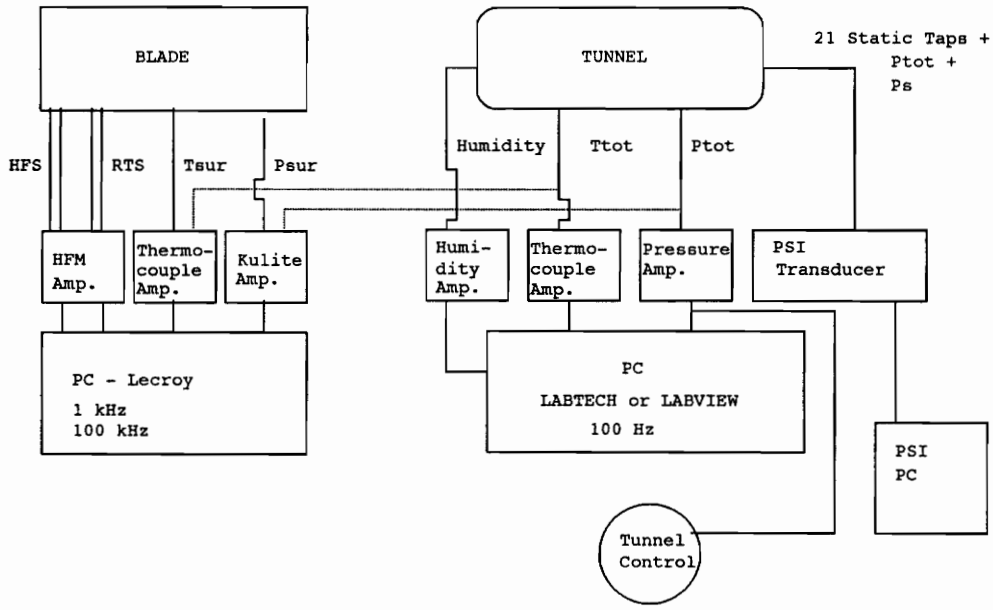

Figure 14. Instrumentation Set-up

Table 4.1 Lecroy set-up

HFM-2a - Trailing Edge Tests

50 Hz sampling rate, 41 sec. duration

Ch.1 - HFS	(q", heat flux)
Ch.2 - RTS	(surface temperature)
Ch.3 - PTOT	(total upstream surface pressure)
Ch.4 - TTOT	(total upstream temperature)

HFM-6 - Leading Edge Tests

1 kHz sampling rate, 64 sec. duration		100 kHz sampling rate, 0.64 sec. duration
Ch.1 - HFS	(q")	Ch.5 - Heat flux (q")
Ch.2 - ST	(surface temperature)	Ch.6 - Surface temperature
Ch.3 - KUL	(surface pressure)	Ch.7 - Kulite static surface pressure
Ch.4 - TT	(total upstream temperature	Ch.8 - Total upstream temperature

HFM-2a - Leading Edge Tests

1 kHz sampling rate, 64 sec. duration		100 kHz sampling rate, 0.64 sec. duration
Ch.1 - HFS	(q")	Ch.5 - Heat flux (q")
Ch.2 - RTS	(surface temperature)	Ch.6 - RTS surface temperature
Ch.3 - PTOT	(total upstream pressure)	Ch.7 - Total upstream pressure
Ch.4 - TT	(total upstream temperature	Ch.8 - Total upstream temperature

For the leading edge tests, a long duration sample was recorded to capture the tunnel run. At a stable, constant pressure region of the run, the 100 kHz sample was taken. All files recorded from the Lecroy had to be converted from a binary file to an ASCII file that could be manipulated by a PC.

The Heat Flux Microsensors operated with an AMP #6 amplifier box manufactured by Vatell Corp. The amplifier supplies a 0.1 mA current to provide the RTS measurement. The formulas to convert voltage to a heat flux or temperature value were given by the manufacturer.

Several methods were used to calibrate the different heat flux gages. The HFM-6 was calibrated using a radiation calibration. The HFM-6 was placed in a holder and then exposed to a radiative heat lamp for 5-10 seconds. A variac controlled the lamp intensity and the heat flux output. Different heat flux values

were recorded and compared to a Gardon gage. Finally, a sensitivity formula was calculated (eq. 10a). The manufacturer is confident with the results of this method.

The HFM-2a line gage sensitivity was determined using a different calibration method. The HFM-2a is a line gage and could not be accurately calibrated by the radiation method because the lamp produces a small circular spot of heat flux that would not contain the entire gage. Instead, the manufacturer, Thermateq" calibrated the line gage with a hot air jet (>100°C). The intent of the hot air jet was to produce uniform heat flux over a broader area and encompass the line gage. This method yielded a higher sensitivity and resulted in lower heat flux output than the HFM-6.

The line gage sensitivity was also verified using a conduction calibration program. For a long duration run sampled at 1 kHz, the data was reduced to a portion of the run where the temperature and heat flux rise at the beginning of tunnel start-up. Generally, the calibration program requires 1 second of data (1000 points) and requires both surface temperature (RTS) signal and heat flux (HFS) signal to calculate a sensitivity. More discussion on this method can be found in Appendix F. This method produced a sensitivity 3 times lower than the sensitivity found by the manufacturer (12 vs. 39 $\mu v/W/cm^2$). From discussion with the manufacturer, it was discovered that their method for calibration yielded large error and the conduction calibration values were chosen to determine the sensitivity. All calibrations yielded an HFS sensitivity with an uncertainty of $\pm 10\%$.

HFM-6

$$S(T) = \frac{E_q}{q''} = 8.54\,\mu V/W/cm^2 + 0.02 T_{SUR}(°C) \qquad (10a)$$

HFM-2a Trailing Edge	$S = 106.28\,\mu V/W/cm^2$	(10b)
HFM-2a Leading Edge	$S(T) = 11.86\,\mu V/W/cm^2 + 0.02T_{SUR}(^\circ C)$	(10c)

where E_q equals the unamplified voltage from the sensor and q" the heat flux. The RTS equation to convert voltage to a temperature was

HFM-6	$T_{SUR}(^oC)=(35710^oC/V)E_T+T_I(^oC)$	(11a)
HFM-2a Trailing Edge	$T_{SUR}(^oC)=(54800^oC/V)E_T+T_I(^oC)$	(11b)
HFM-2a Leading Edge	$T_{SUR}(^oC)=(37630^oC/V)E_T+T_I(^oC)$	(11c)

where E_T equals the unamplified voltage from the RTS, and T_I is the 0 voltage temperature level (ambient temperature offset).

Three different methods were used to get the lead wires from the instrumented blades to the amplifiers. The HFM-6 and Kulite wires came out through a cooling hole out of the Plexiglas. The HFM-2a trailing edge gage wires came out of a thermocouple hole in the Plexiglas. For the HFM-2a leading edge gage, a hole was drilled in the Plexiglas to take out the lead wires.

The four lead wires from the Heat Flux Microsensor were soldered to a male Lemo plug cable connector. This connection point was then wrapped in insulation to protect the junctions from thermal drift. A 91.4 cm (36 in) cable connected the connector to the amplifier. Both the HFS and the RTS could be calibrated to a zero level by turning small potentiometer knobs on the amplifier and connecting a voltmeter into the respective output channel. This was done at the beginning of each day at ambient conditions. Since no heat transfer was occurring, the heat flux was set to a zero value. The temperature was recorded with a thermometer and then the RTS was zeroed implying that room temperature became the zero volt level temperature offset.

4.2 Procedure

There were four areas of interest studied in the wind tunnel. The first tests studied the heat transfer on the suction side of the trailing edge on an instrumented blade with the HFM-2a line gage. Air was heated to 177°C (350°F) and the blades were cooled with the nitrogen set-up. The next tests studied the effectiveness of the three turbulence grids on the freestream turbulence level. A calibrated bare hot wire was used to establish the mean and fluctuating components of velocity during tunnel runs. The third set of tests focused on the heat transfer of 93°C (200°F) heated air to the blade measured by the HFM-6 gage and pressure data taken with the Kulite using the various turbulence grids on the leading edge. The last set of tests repeated all the tests conducted with the HFM-6 gage but replaced the HFM-6 gage with the HFM-2a line gage located at the leading edge.

4.2.1 Freestream Turbulence Measurements

Three different turbulence grids (Fig. 15) were used in this experiment. Two of these grids were used by Gundappa and Diller [1987] and were made from stamped 16-gage steel with square holes. Grid 1 had a mesh size of M=12.7 mm (0.5 in) with bars 3.17 mm in width allowing an open area of 56 %. Grid 2 had a mesh size of M=17.5 mm (0.687 in) with bars 4.76 in width allowing an open area of 52%. Grid 3 had a mesh size of M=1.56 mm (0.062 in) with a 70% open area and was used in an attempt to decrease the freestream

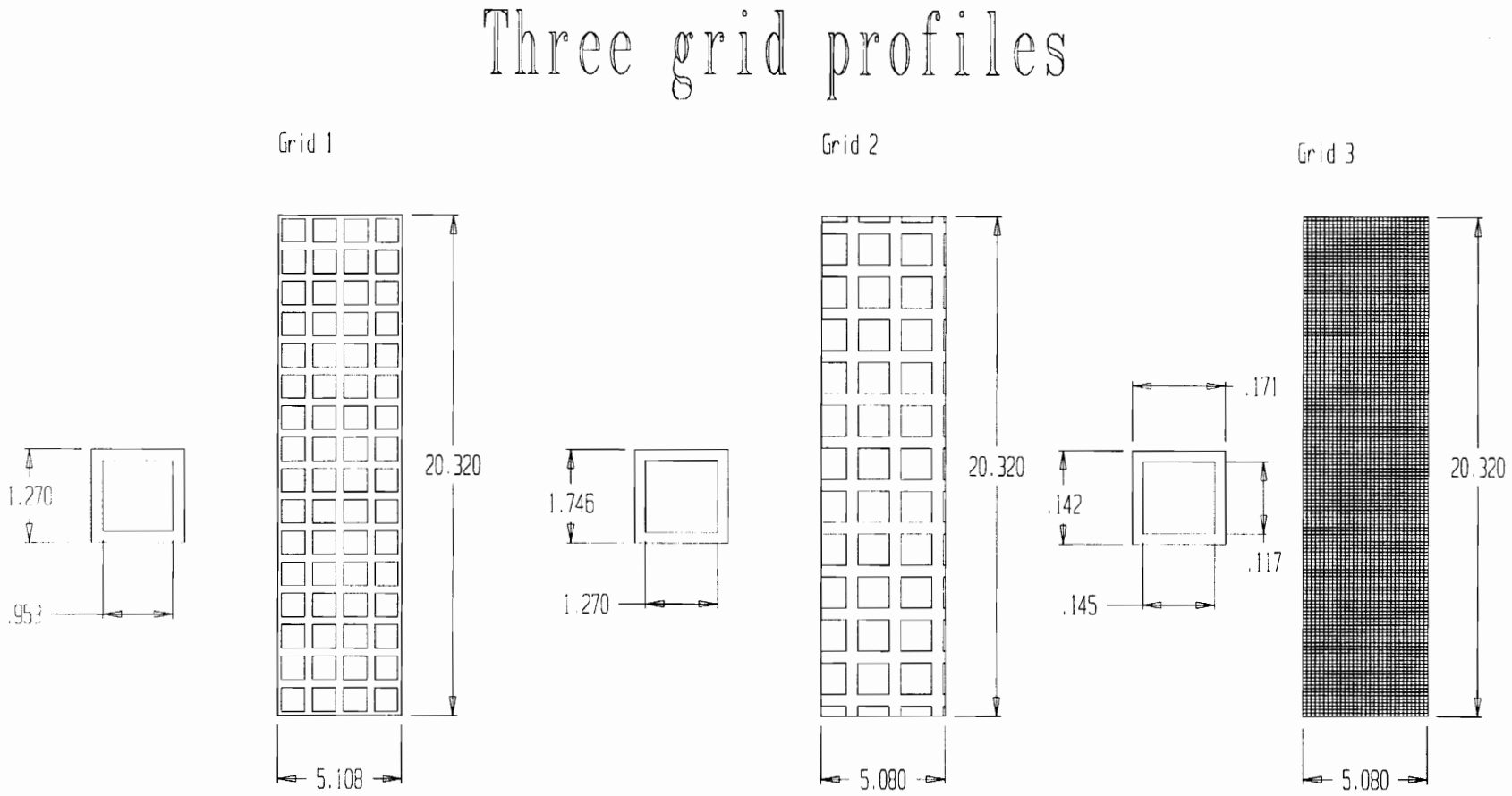

Figure 15. Freestream Turbulence Grids: Grids 1,2,3.

turbulence. It consisted of standard aluminum screen. All three grids were made 38.1 cm (15 in) wide and 25.4 cm (10 in) high to match the flange connection. Holes were made to fit the 1.9 cm diameter (3/4 in-D) screws that would hold the grids in place. The distance from the screen to the stagnation point on the middle blade was 38.1 cm (15 in). This allowed a total area of 5.0 cm (2 in) wide by 20.3 cm (8 in) high for flow to go through.

The turbulence intensity measurements were conducted with a TSI T2 straight dual hot wire. The hot wire probe was connected into a hot wire stem with a protective shield. The shield was cemented to the test section aluminum door and placed 29.7 cm (11.7 in) from the turbulence screen and 21.6 cm (8.5 in) from the top of the test section. With the shield cemented, the hot wire stem could be retracted into the test section flow. The hot wires were placed perpendicular to the flow with hot wire 1 in front of hot wire 2. For these tests, the hot wires were exposed during the complete run and were placed 2.54 cm (1 in) from the sidewall (i.e. in the center of the flow). Two BNC cables connected the hot wire stem to a TSI IFA 100 Anemometer. Although both hot wires were activated during a tunnel run, only the results of hot wire 1 are reported in this thesis. For a complete discussion on the hot wire calibration, see Appendix C.

4.2.2 Trailing Edge Tests (no turbulence screens)

The trailing edge tests had a two-fold purpose. One purpose was to see how delaying the nitrogen cooling rates affected the gas-to-wall ratio of the heated air to the blades. This was the first attempt to record data from an HFM line gage directly deposited on an aluminum blade. The trailing edge gage was deposited on a flat region of a blade for two reasons. The main reason was

ease of manufacture and the other reason was to try to determine the trailing edge shock effect on the heat transfer coefficient and compare with computer analysis. From computer prediction, turbulence grids would have only a minimal effect on the heat transfer coefficient.

A total of 10 runs were made with the HFM-2a line gage. Runs 1 and 10 did not use the cooling set-up. These runs were done to determine an adiabatic wall temperature and a recovery factor, r. Approximately 40 seconds of data was recorded for a sampling rate of 50 Hz. Runs 2 through 9 included the nitrogen cooling set-up to cool the blades during the heated run. For this test, four Mach numbers (1.12, 1.16, 1.22, 1.26) were examined in order to push the trailing edge shock closer to the trailing edge. The cooling was also delayed at three rates; cooling and tunnel started simultaneously, cooling begun 5 seconds before tunnel started, and cooling begun 10 seconds before tunnel started. These cooling tests were performed to determine the optimum scheme to achieve a 1.4 gas-to-wall temperature ratio. See Table 4.2 for the complete plan.

Table 4.2 - Trailing Edge Test Matrix

Run #	Mach # (desired)	Comments
1	1.16	No cooling
2	1.16	5 s delay
3	1.16	5 s delay
4	1.16	10 s delay
5	1.16	10 s delay
6	1.16	No delay
7	1.26	No delay
8	1.22	No delay
9	1.12	No delay
10	1.16	No cooling

4.2.3 Leading Edge Tests

For the leading edge line gage tests, turbulence grids were used to affect the heat transfer coefficient. The leading edge location was chosen as the next region to deposit a line gage due to the small curvature of the blade. This small curvature also allowed the use of the HFM-6 insert gage. The main reason for choosing this location came from computer prediction which indicated a 15% increase in the heat transfer coefficient due to increased freestream turbulence.

HFM-6 Insert Gage and Kulite

The HFM-6 insert gage tests consisted of measuring heat flux during heated runs at 93°C (200°F) for two scenarios, the no grid case and the grid 1 turbulence case. Specifically, four items were measured, heat flux from the blade, surface temperature on the blade, total upstream temperature, and Kulite surface pressure on the blade. Runs were made with a design exit Mach number of 1.26. All values were recorded on the Lecroy which sampled at two different rates. A 1 kHz sample for 64 seconds allowed for time averaged data and also allowed the use of a sensitivity analysis program to be performed on the blade (Appendix F). For data manipulation purposes a FORTRAN program removed 9 out of 10 milliseconds of data in order to reduce the sampling rate of 1 kHz to 100 Hz. The time line for the run was kept the same. A 100 kHz sample for 0.64 seconds during a steady pressure region of the run allowed for a spectral analysis and a heat flux turbulence intensity measurement. Shadowgraphs were taken to see if this gage disrupted the boundary layer during a run.

HFM-2a Line Gage

The line gage instrumented blade replaced the blade with the insert HFM-6 gage. All the tests for the HFM-6 gage were repeated with the HFM-2a line gage. The tunnel was heated to 93°C (200°F) and runs were made for the grid 1 and no grid case. The Lecroy set up was identical to the HFM-6 tests except that total pressure was measured instead of surface pressure since the HFM-2a instrumented blade did not have a Kulite.

4.2.4 HFM data reduction

The determination of the adiabatic wall temperature is essential for determining a heat transfer coefficient. T_{AW} can be found for a long heated run (>20 s) and with non-cooled blades. As the total temperature decreases (T_{TOT}) during a run, the surface temperature (T_{SUR}) increases and at a certain point in time, the heat flux may go to zero (q"=0). At that point, the difference between T_{AW} and T_{SUR} should also be zero. An assumption is then made that the difference between T_{TOT} and T_{SUR} is constant and this offset from T_{TOT} recreates the T_{AW} curve.

$$T_{AW} = T_{TOT} - \Delta T_{q"=0} \quad \text{where } \Delta T_{q"=0} = T_{TOT} - T_{SUR} \text{ at q"=0} \qquad [12]$$

A benefit of the HFM is the independent heat flux measurement made without a knowledge of the temperature field. With a T_{AW} found, the recovery temperature can be calculated as

$$T_R = T_{TOT} + \frac{U_\infty^2}{2Cp}(r-1) = T_{AW} \text{ and r can be found.} \qquad [13]$$

Once the adiabatic wall temperature is known, the heat transfer coefficient can be determined from

$$h = \frac{q''}{T_{AW} - T_{SUR}} \qquad [14]$$

since the heat flux, q", and the surface temperature, T_{SUR}, are known from the HFM gage. Comparisons can then be made between experimental heat transfer coefficients versus computer predictions. Next, the Nusselt number can be calculated from

$$Nu = \frac{hL}{k} \qquad [15]$$

where L is the blade chord length (3.81 cm) and k is the thermal conductivity at the reference temperature

$$T_{REF} = T_{\infty} + 0.5(T_{SUR} - T_{\infty}) + 0.22(T_{AW} - T_{\infty}). \qquad [16]$$

Another tool useful for evaluating the effectiveness of freestream turbulence on the heat flux value is the heat flux turbulence intensity, Tu_q. The definition of Tu_q is based on the RMS of the heat flux divided by the mean heat flux value.

$$Tu_q = \frac{\sqrt{\overline{q''^2}}}{q''} \qquad [17]$$

Chapter 5.0

RESULTS and DISCUSSION

The following sections report the results for the hot wire turbulence intensity measurements, trailing edge heat flux measurements, and the leading edge heat flux measurements based on different freestream turbulence intensities. A detailed discussion of the results is given in each section. The intent of this chapter is to give explanations on the effects of freestream turbulence on surface heat transfer.

5.1 Turbulence Intensity Measurements

The hot wire had to be calibrated in the cascade wind tunnel. For specific calibration details, see Appendix C. Runs were made for the four turbulence grid cases and Table 5.1 shows the results from the hot wire tests. The purpose of these tests was to characterize the flow entering the cascade of blades.

Table 5.1 - Turbulence Intensity Results

	NO GRID	**GRID 1**	**GRID 2**	**GRID 3**
Total Open Area - cm^2 (in^2)	103.2 (16.0)	58.1 (9.0)	53.5 (8.3)	71.9 (11.2)
% Open Area	100	56.3	51.7	69.7
Unfiltered Tu - %	2.9	8.0	6.6	2.4
Filtered Tu - %	**0.9**	**7.5**	**6.9**	**0.8**
Grid Size - mm	None	12.7	17.5	1.6
Length Scale -mm	**6.0**	**12.5**	**17.0**	**6.0**
Time Scale - ms (Frequency - kHz)	0.05 (20.0)	0.12 (8.33)	0.15 (6.67)	0.05 (20.0)

The heat flux measurement experiments were made during heated tunnel runs but the turbulence intensity measurements were made without heating the tunnel. An assumption made for these turbulence intensity experiments was that the values were valid for the heated runs.

The integral length scale for Grid 1 and Grid 2 was found to match their respective grid sizes (12.5 mm vs. 12.7 mm for Grid 1 and 17.0 mm vs. 17.5 mm for Grid 2). These length scales are much larger than the boundary layer thickness on the leading edge of the blade (<0.25 mm [<0.01 in]). Therefore, there are very large turbulent fluctuations that penetrate through the boundary layer of the turbine blade.

For the heat flux experiments, only two cases need to be examined; the no grid case and the grid 1 case. Grid 3 did not appreciably lower the turbulence intensity when compared to the no grid case (0.8% vs. 0.9% Tu). Grid 2 gave larger length scales (17 mm) but the overall intensity was less than the grid 1 case (6.9% Tu vs. 7.5% Tu). The computer model calculations were based on turbulence intensity values of 2% and 8% which are close to the experimental values of 0.9% and 7.5% from the no grid and grid 1 cases.

Fast-Fourier transforms were performed on all the signals. The power spectra graph of the 100 kHz sample (Fig. 16) indicated the presence of increased energy levels between 0 and 10 kHz for the grid 1 and 2 cases when compared to the no grid and grid 3 case. Sixty hertz noise was prevalent in the hot wire experiments but was below the frequency region of interest. The LABVIEW program (DGHSPCTM.VI) digitally removed the 60 Hz noise with a bandstop filter and removed 5 subsequent multiples of 60 Hz from the data. This 60 Hz removal also lowered the turbulence intensities for all the grid cases.

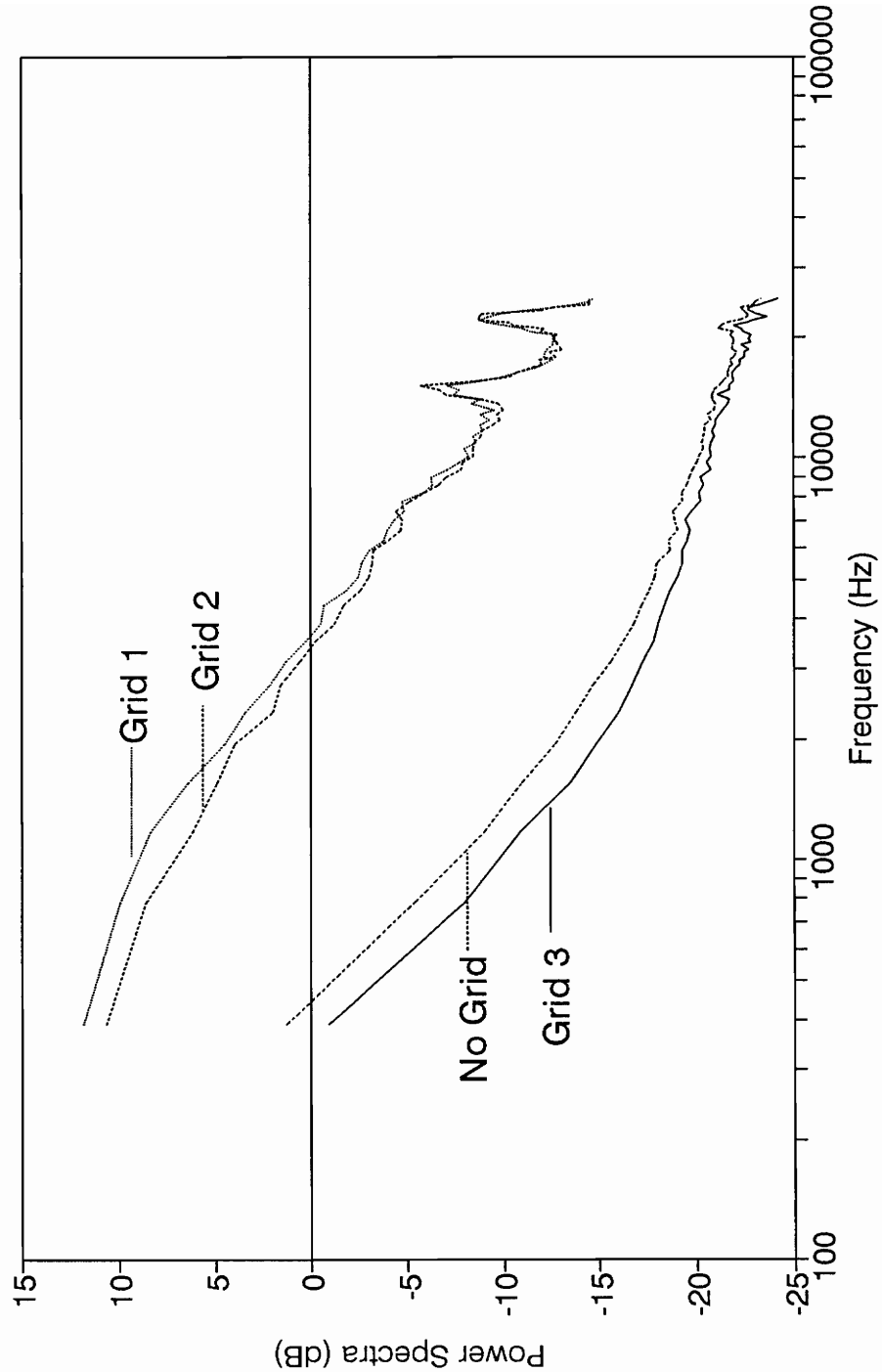

Figure 16. Hot Wire Power Spectra of 100 kHz Sample for All Grid Cases.

Table 5.1 shows the unfiltered (i.e. with 60 Hz noise) and filtered turbulence intensity value for each grid scenario.

5.2 Pressure Measurements

The static pressure distribution over the turbine blade was measured to determine the isentropic Mach number distribution. These experimental values were then compared with computer predictions (Fig. 17) [Wesner, 1994] and used as a basis for determining the freestream velocity at the two gage locations on the blade. The experimental results closely matched the curve provided by General Electric. Due to unsteadiness from the trailing edge shock, the experimental value near that location did not match with prediction, but did give correct trends.

5.3 Trailing Edge Results

The trailing edge tests were conducted to check the performance of the Heat Flux Microsensor and compare experimental heat transfer results with computer predictions. The sensor had been fabricated on a flat region of a blade and these tests were the first ever conducted with a directly deposited HFM. The location of the gage was near the trailing edge shock where shadowgraphs show the boundary layer is transitional and becoming turbulent. The trailing edge experiments were made before the use of turbulence intensity grids. If turbulence grids had been used, effects on the heat transfer may be small since freestream turbulence has smaller effects on a turbulent boundary layer when compared to a laminar boundary layer.

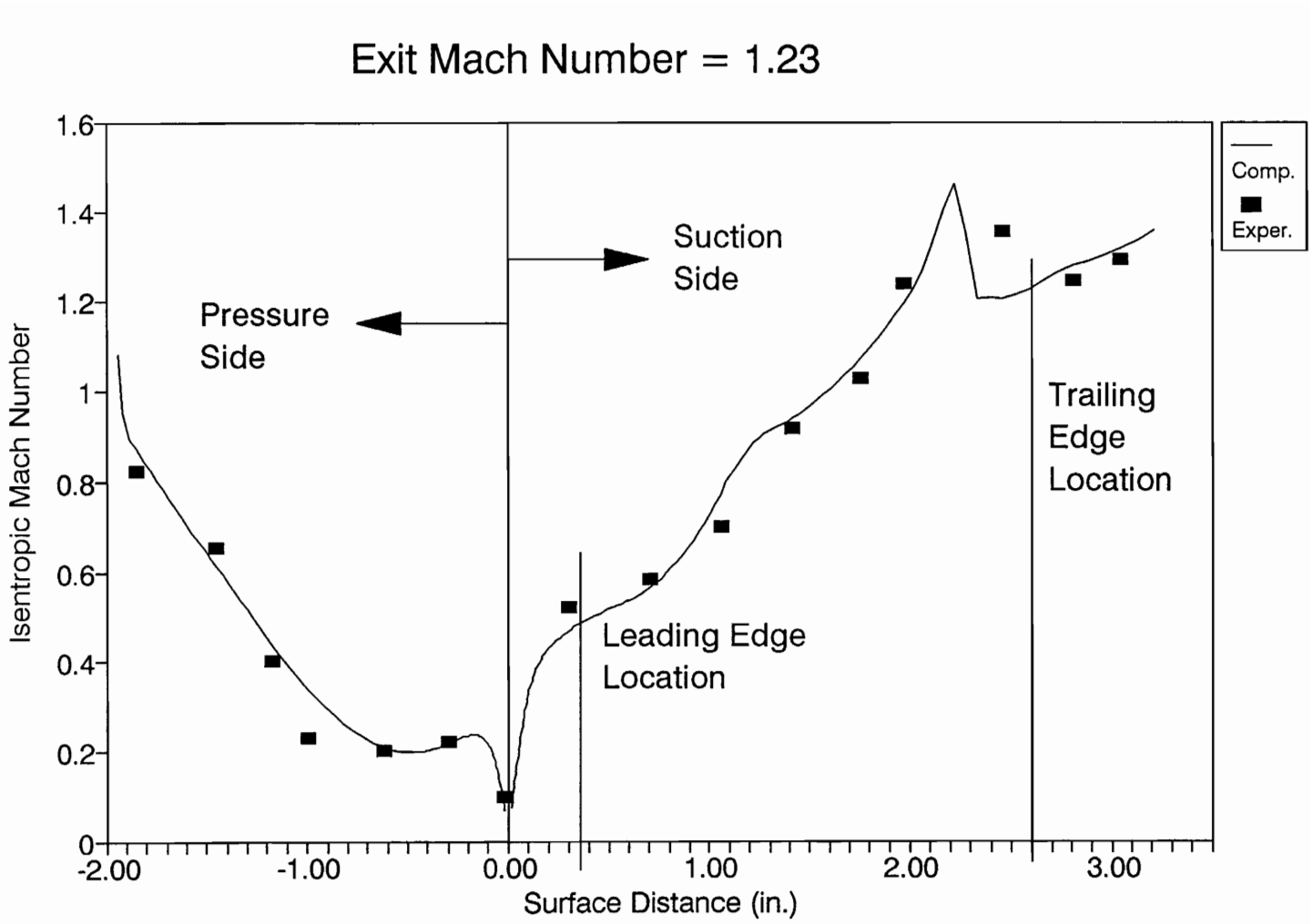

Figure 17. Isentropic Mach Number Distribution on Blade.

For run 1, the blades were not cooled during the heated run in order to determine the value of

$$(1-r)\frac{U_\infty^2}{2Cp} = T_{AW} - T_{TOT} \qquad (18)$$

from the wall temperature where q"=0. As shown in figure 18, the adiabatic wall temperature was found to be 15°C lower than the total temperature. From the non-heated, no cooled runs (Run 1 and 10), a recovery factor of r=0.88 adequately described the adiabatic wall temperature. Figure 19 shows the corresponding heat transfer coefficient, h, for run 1. The 0.88 recovery factor was used to back out heat transfer coefficients for the cooled runs (runs 2-9). A summary of the average heat transfer coefficients with a 95.0% confidence interval, based on a student-t distribution of 600-1200 points during a flat region of the particular run, is shown in Table 5.2 and figure 20.

Table 5.2 - Average Heat Transfer Coefficients and Nusselt Numbers for Trailing Edge Line Gage

Run Number	Heat Transfer Coefficient [W/(m^2 C)]	Nusselt Number	Mach Number
1	840±11	923±11	1.16
2	784±3	1024±4	1.16
3	795±5	907±5	1.16
4	843±14	965±15	1.16
5	805±4	928±4	1.16
6	807±6	917±6	1.16
7	765±10	870±10	1.26
8	636±18	732±19	1.22
9	835±5	951±5	1.12
10	984±11	1076±11	1.16

Graphs of the run data and average heat transfer coefficient for the 10 different run cases are in Appendix A.

The gage was located on the trailing edge in a flat portion

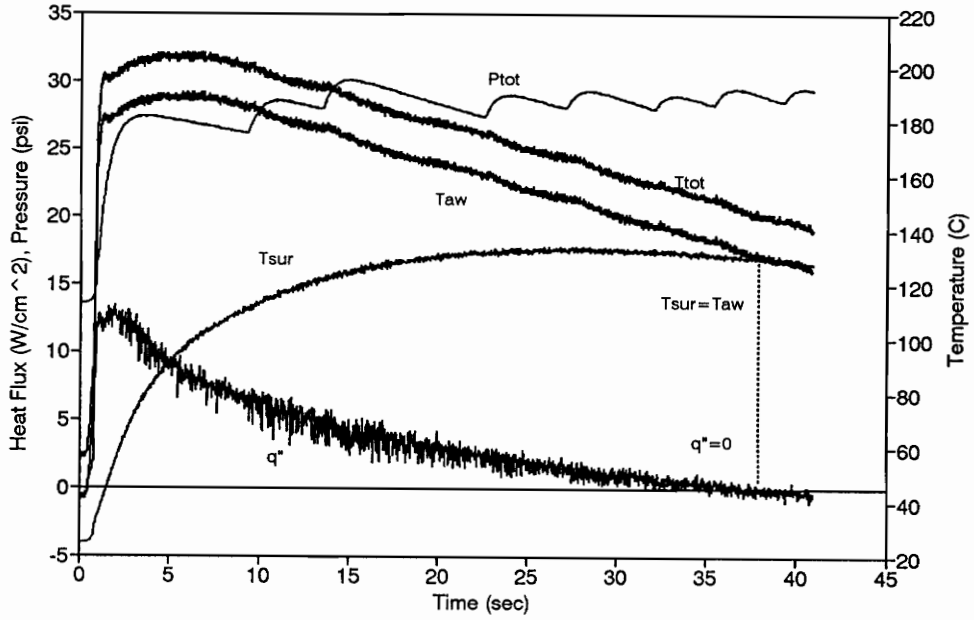

Figure 18. Example of Trailing Edge Gage Run.

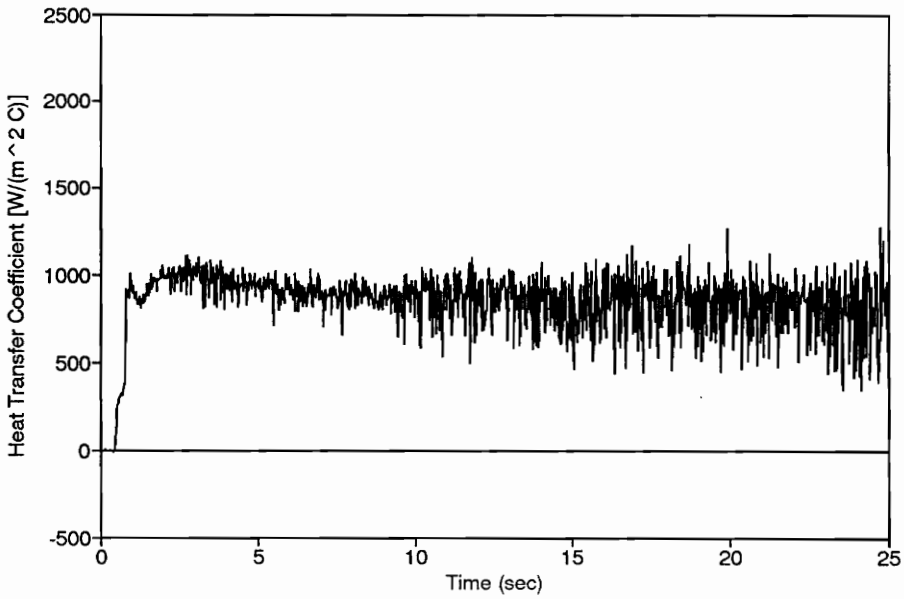

Figure 19. Heat Transfer Coefficient Calculated from Trailing Edge Run.

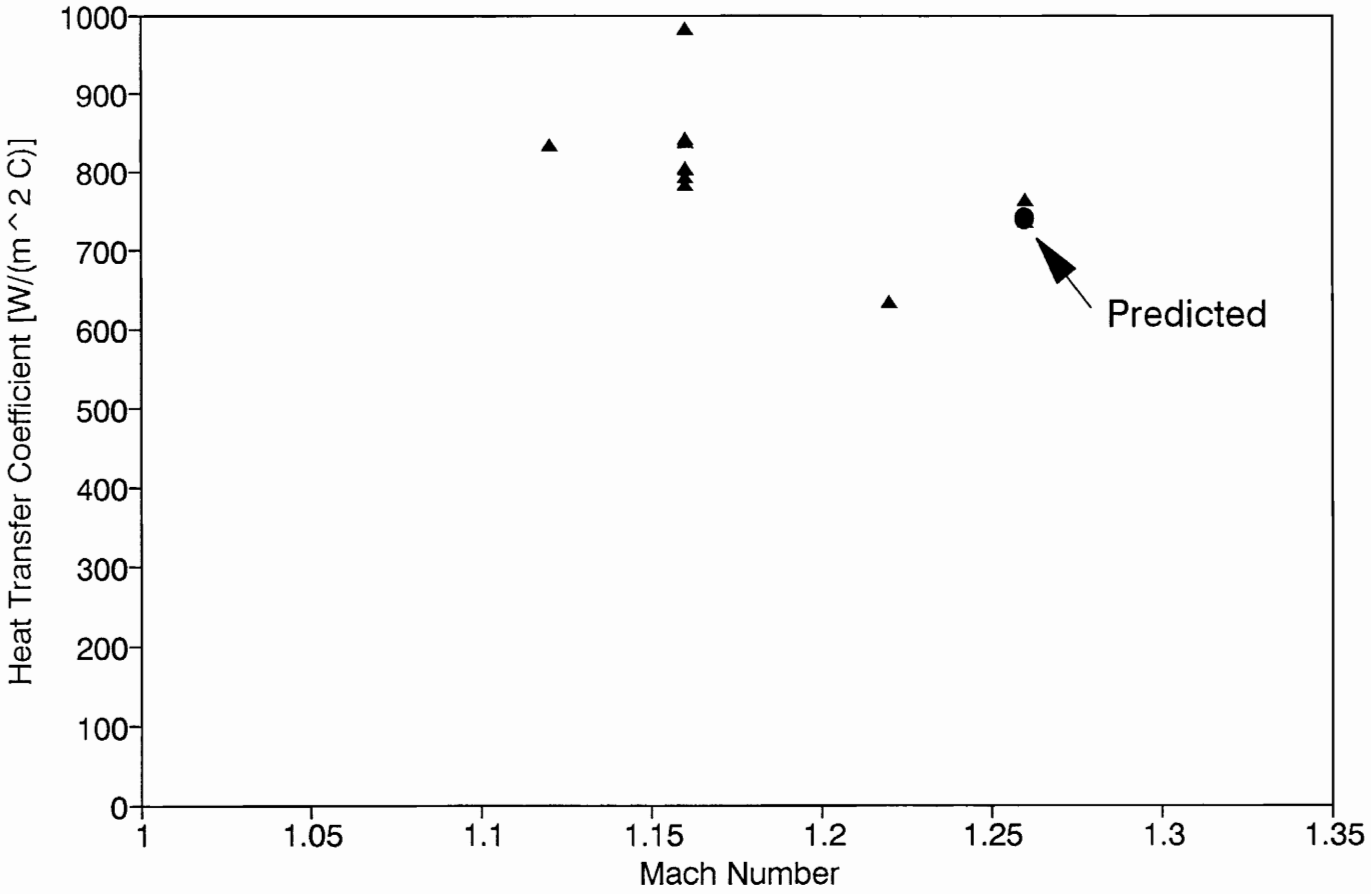

Figure 20. Average Heat Transfer Coefficient at Various Mach Numbers for Trailing Edge Gage Runs.

of the blade and the velocity at that point was based on the computer predicted value (Fig. 17). A recovery factor for the case of turbulent flow over a flat plate is typically $Pr^{1/3}$ =0.89 and matches closely with the recovery factor found experimentally of r=0.88. Notice that a constant recovery factor used to recreate the adiabatic wall temperature over the run produced a flat, steady heat transfer coefficient over the run time (Fig. 19).

From flow visualizations, for a Mach number of 1.22, a separation bubble that formed immediately behind the trailing edge shock appeared on top of the gage and lowered the heat transfer coefficient (see Figs. 21 and 22). One can see increased spikes in the heat flux (q") and the heat transfer coefficient when compared to run 1 and figures 18 and 19.

The average heat transfer coefficients at the various Mach numbers were found to be slightly higher than predictions from computer models. For an exit Mach number of 1.26 (Fig. 20), the experimental value of 765 [W/(m^2 °C)] matched well with the predicted value of 738 [W/(m^2 °C)].

5.4 HFM-6 and Kulite Leading Edge Results

Several runs were made with the HFM-6 gage; 9 runs without a grid and 13 runs with grid 1. Figure 23 shows an example run from run 5 (no grid). Figure 24 displays the heat transfer coefficient graph for the run. Figures 25 and 26 show the run data and the heat transfer coefficient for run 15 (grid 1). For all runs at the leading edge, the blades were not cooled and typically the heat flux went to zero, thus allowing for a direct way to measure T_{AW}. Recovery factors varied from 0.2-0.80. The turbulence intensity based on heat flux, Tu_q, was

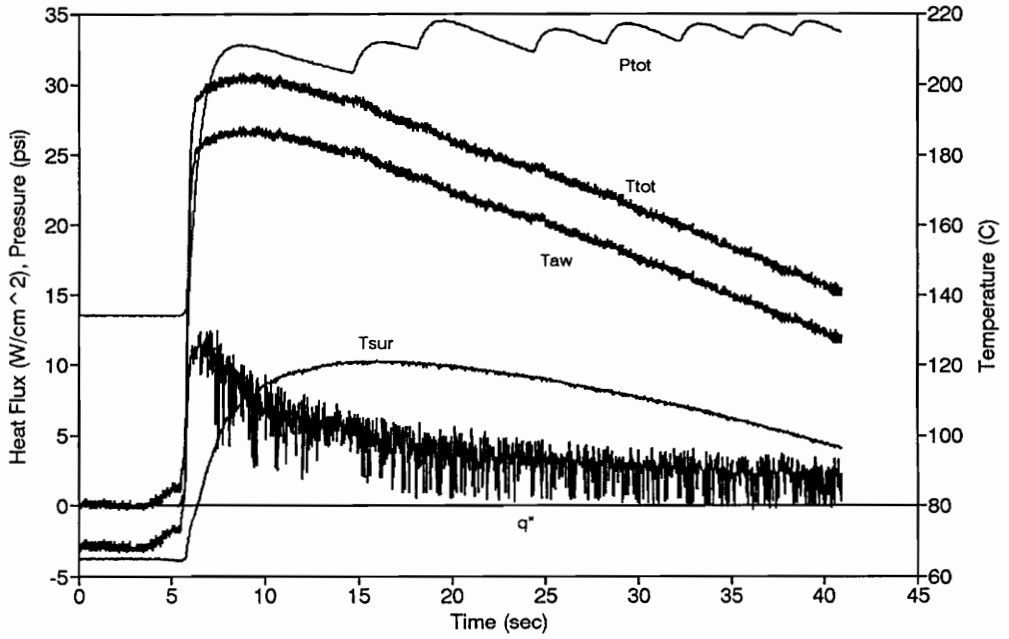

Figure 21. Example of Trailing Edge Gage Run - Trailing Edge Separation Bubble on Gage.

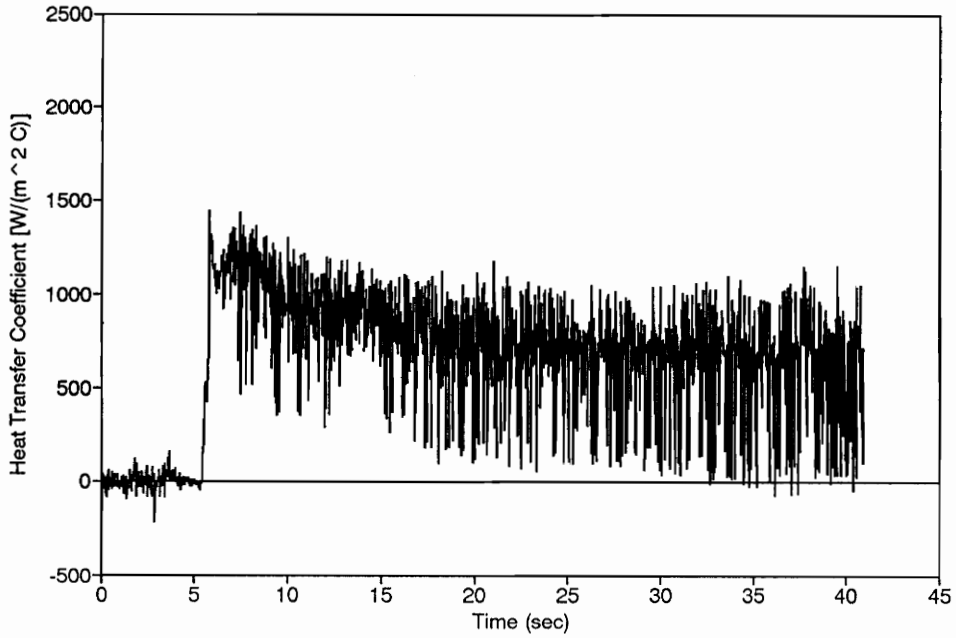

Figure 22. HTC Calculated from Trailing Edge Gage with Separation Bubble.

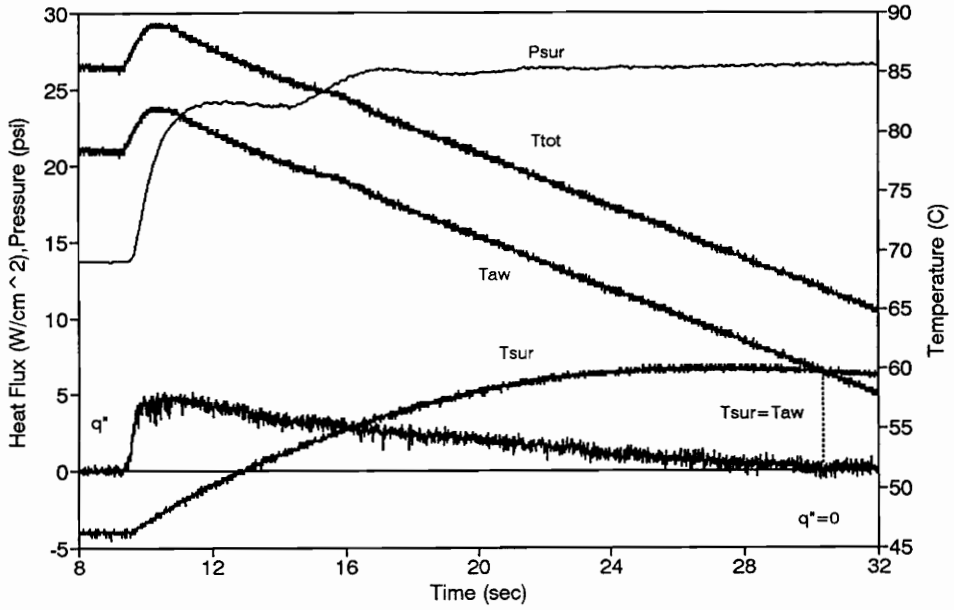

Figure 23. Example of HFM-6 Run at Leading Edge - No Grid Case.

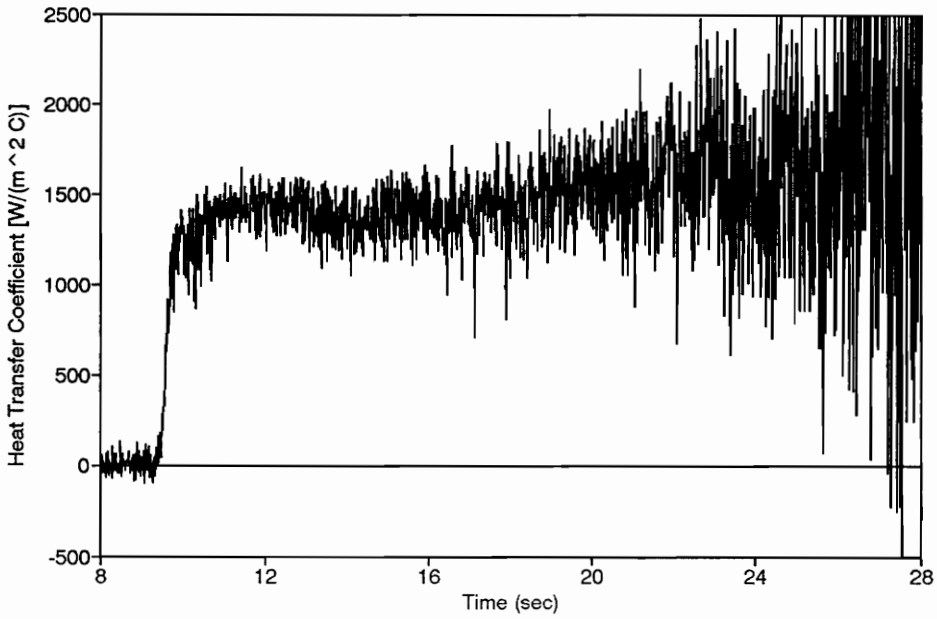

Figure 24. HTC Calculated from HFM-6 Leading Edge Gage - No Grid Case.

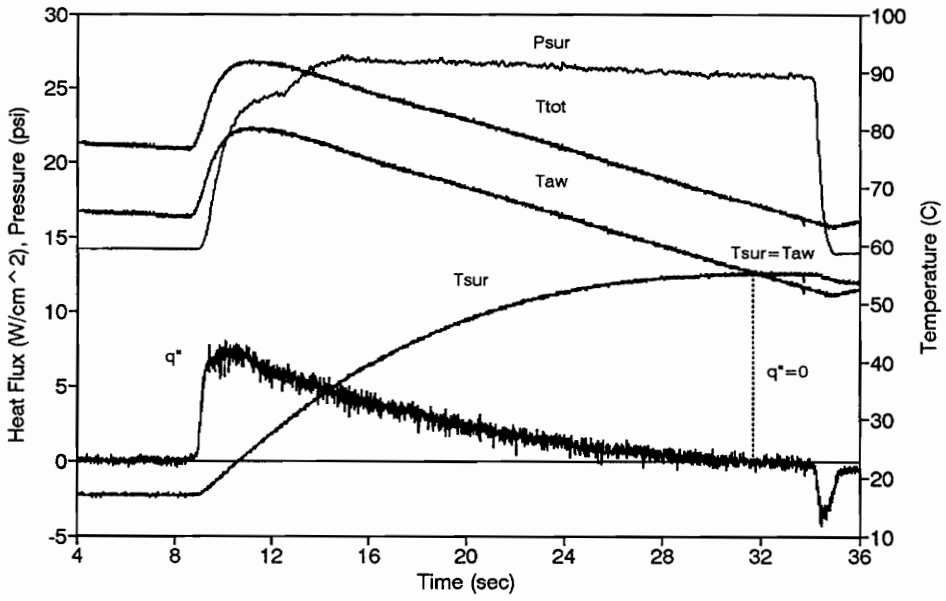

Figure 25. Example of HFM-6 Run at Leading Edge - Grid 1 Case.

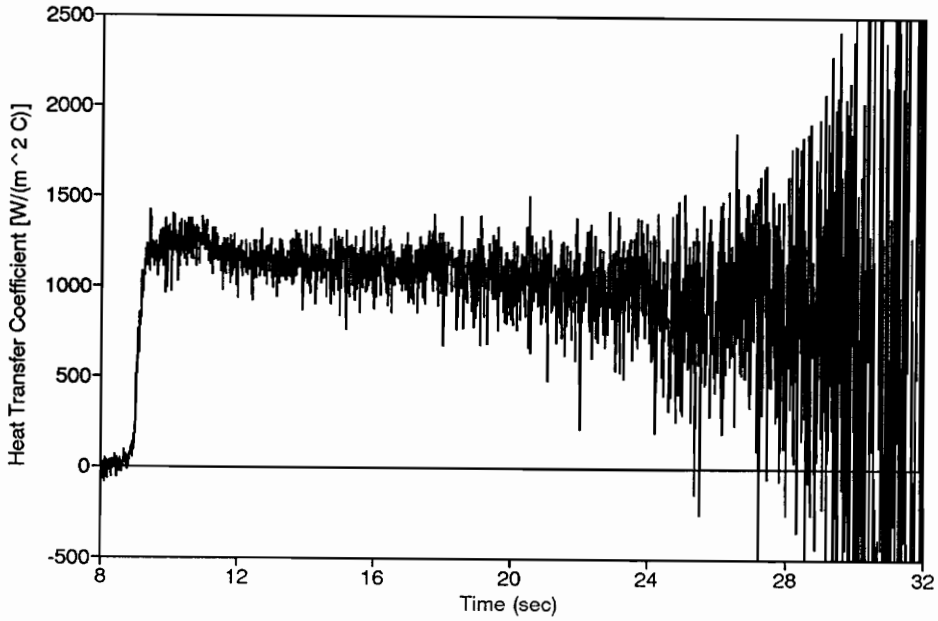

Figure 26. HTC Calculated from HFM-6 Leading Edge Gage Run - Grid 1 Case.

found for each run. A summary of the average heat transfer coefficients for the 22 runs and 2 grid cases is shown in Table 5.3a and Table 5.3b and in figure 27.

Table 5.3a - Average Heat Transfer Coefficients and Nusselt Numbers for HFM-6 Leading Edge Gage (No Grid)

Run Number	Heat Transfer Coefficient [W/(m^2 C)]	Nusselt Number	Recovery Factor	Tu_q(%)	Noise in Signal
1	1195±5.0	1600±7	0.89	N/A	N/A
2	1096±4	1467±6	0.89	N/A	N/A
3	1178±7	1566±9	0.37	11.7	Yes
4	1420±9	1874±11	0.19	13.7	Yes
5	1425±11	1872±14	0.62	20.4	Yes
6	1496±13	2010±17	0.41	35.4	Yes
7	1633±22	2176±29	0.89	35.4	Yes
8	1699±9	2282±13	0.27	0.0	No
9	1299±9	1747±12	0.36	7.7	No

Table 5.3b - Average Heat Transfer Coefficients and Nusselt Numbers for HFM-6 Leading Edge Gage (Grid 1)

Run Number	Heat Transfer Coefficient [W/(m^2 C)]	Nusselt Number	Recovery Factor	Tu_q(%)	Noise in Signal
10	1160±5	1550±7	0.89	N/A	N/A
11	1019±6	1358±7	0.89	N/A	N/A
12	1132±5	1514±7	0.89	N/A	N/A
13	1214±5	1630±7	0.89	N/A	N/A
14	1224±6	1649±8	0.89	N/A	N/A
15	1114±7	1488±10	0.89	21.2	Yes
16	1446±12	1925±16	0.73	43.0	Yes
17	985±11	1306±14	0.62	46.1	Yes
18	1388±12	1832±16	0.1	25.4	Yes
19	1301±9	1717±12	0.1	30.1	Yes
20	1440±13	1938±17	0.22	10.8	No
21	1708±12	2282±16	0.32	13.8	No
22	1759±13	2352±17	0.32	20.2	No

The gage was recessed 0.04 cm into the cylinder during later parts of testing and was no longer flush with the surface of the blade. Although the HFS continued to work properly, the RTS only worked during runs 1,2,10,11,12,13,14

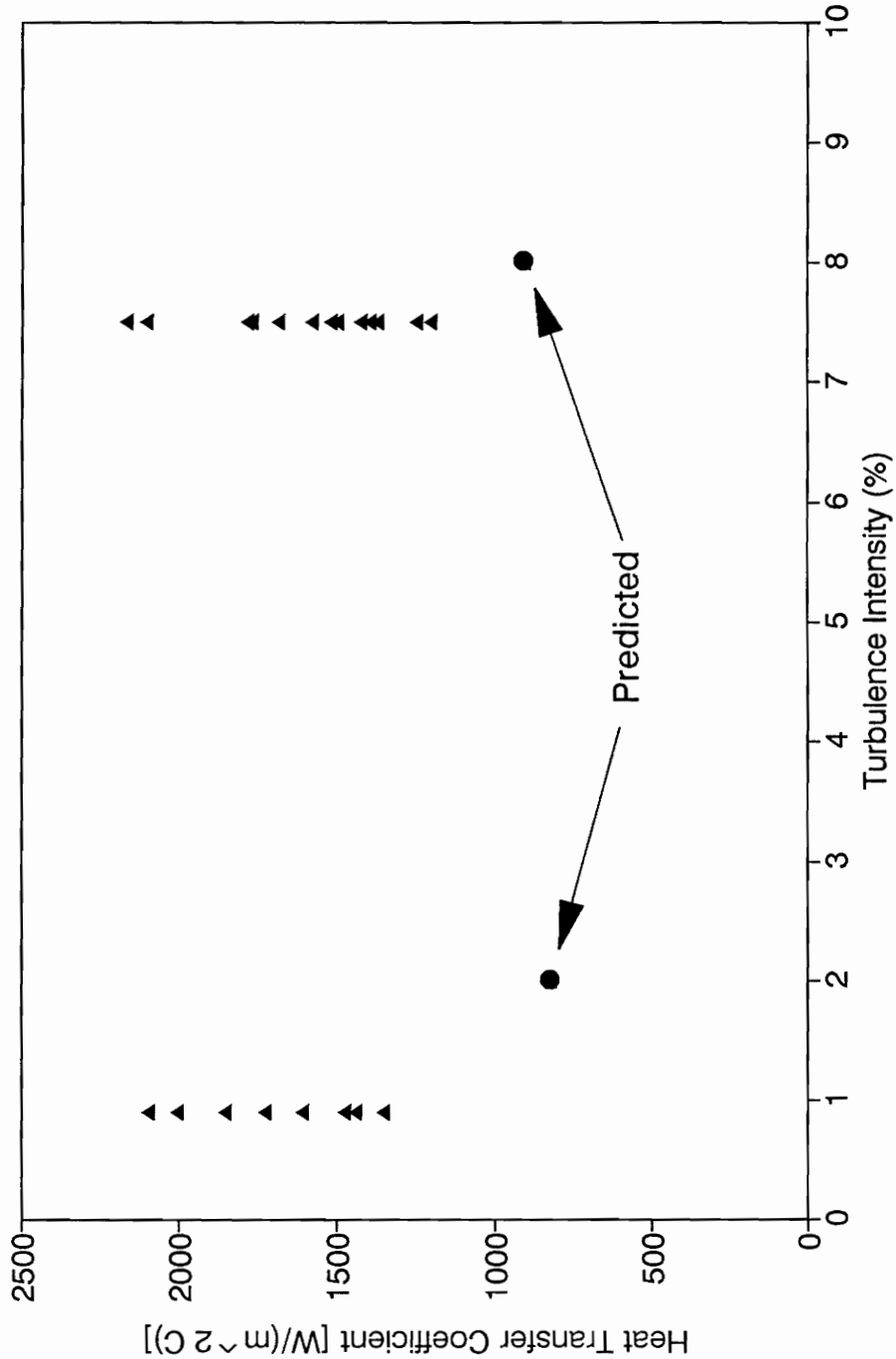

Figure 27. Average Heat Transfer Coefficient Calculated at 1.0% and 7.5% Tu for HFM-6 Leading Edge Gage Runs.

(the type-K thermocouple was not in use at the time). The calibration formula for the RTS given by the manufacturer did not produce workable data and this gage recession may have increased the resistance of the lead wires of the RTS in the gage. In order to salvage the data, temperature curves from other runs were studied. A new formula to produce surface temperature $T_{SUR}(°C)=(30130°C/V)E_T+Ti(°C)$ was used in conjunction with a recovery factor of 0.89 to produce more manageable data.

For all other runs, the surface temperature was based on the type-K thermocouple located between the HFM and the Kulite. An assumption was made that the thermocouple measured surface temperature, although the actual bead was soldered to the copper sheath and press fit into blade and was not directly exposed to surface flow. The thermocouple has an estimated uncertainty of ±0.5°C error. The response time of the thermocouple was less than the response time from an RTS.

The average heat transfer coefficient values for the two grid cases and all runs did not vary significantly. Grid 1 had an average heat transfer coefficient value of 1300 [W/(m^2 °C)] with a standard deviation of 240 [W/(m^2 °C)] while the no grid case had an average value of 1380 [W/(m^2 °C)] and a standard deviation of 208 [W/(m^2 °C)] (Fig. 27). Although the no grid case seemed to have a higher value than the grid 1 case, the deviation of the average values was large and within both grid case average values. The average heat transfer coefficients were also higher (2x) than computer predicted values of 823 [W/(m^2 °C)] for the no grid case and 908 [W/(m^2 °C)] for the grid 1 case.

The HFM gages have great frequency response (>100 kHz) and can show more resolution in the actual heat flux signals. The power spectra graphs (Figs. 28 and 29) of the HFM-6 heat flux signal sampled at 100 kHz did show an increase in frequency energy in the 0 - 10 kHz region due to an increase in freestream turbulence. At this time, it is believed that the large spikes in the spectra at 7.5 kHz, 14 kHz and 21 kHz, in figure 28 are due to electrical noise. The runs that had this noise are noted in Table 5.3. Five runs did not contain this noise; 3 runs with grid 1 and 2 runs without the grid. The power spectra for grid 1 is shown in figure 29. These five runs also showed an 8.0% increase in the average heat transfer coefficient due to freestream turbulence.

Figures 30 and 31 show the amplified heat flux voltage signal comparing the no grid and grid 1 case. Notice the 30% increase in fluctuations in the 7.5% Tu signal compared to the 1.0% Tu signal. The power spectra of the Kulite static pressure signal (Figs. 32 and 33) also shows an increase in energy due to increased freestream turbulence, although the effects are not as dramatic as the heat flux signals. The noise that was present in the heat flux signal did not appear in the static Kulite pressure signal.

The recovery factor was more difficult to estimate and typically was 10 - 85% percent lower than a recovery factor of 0.89 for a turbulent flat plate. Some of this error can be attributed to the high acceleration effects at the leading edge of the blade. One possible reason for the discrepancy in the average heat transfer coefficient values might be the disruption of the boundary layer due to the gage. Shadowgraphs did not show any obvious boundary layer disruption, although it was difficult to view the small boundary layer with the optical set-up at the time.

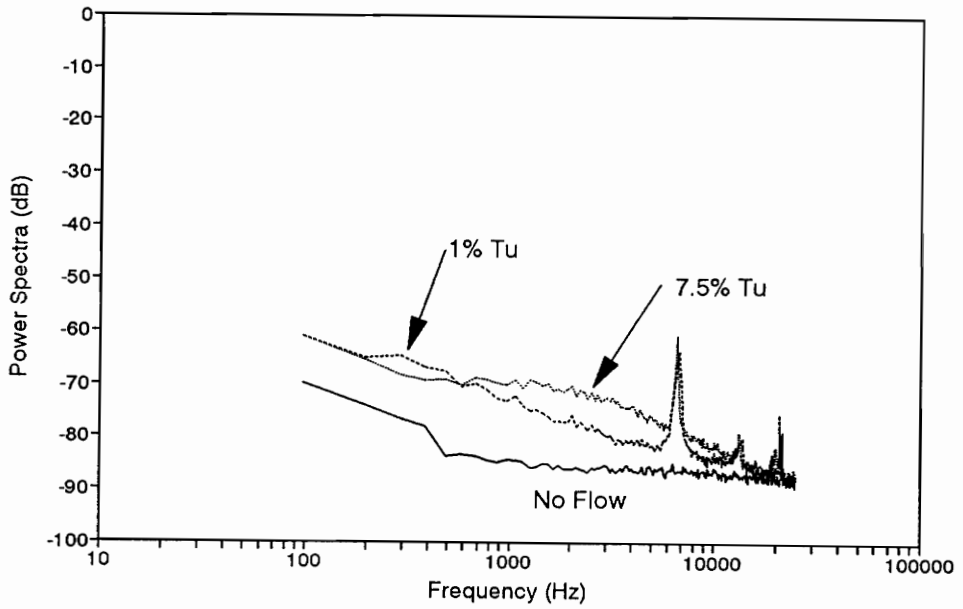

Figure 28. Power Spectra of 0.9% Tu vs. 7.5% Tu of Heat Flux Signal Sampled at 100 kHz (HFM-6).

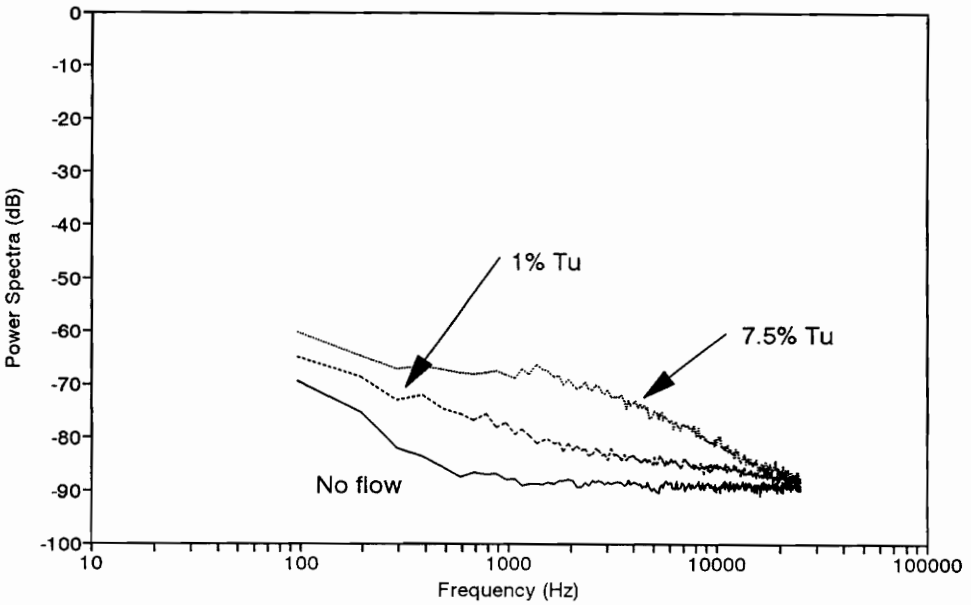

Figure 29. Power Spectra of Heat Flux Signal Sampled at 100 kHz (HFM-6).

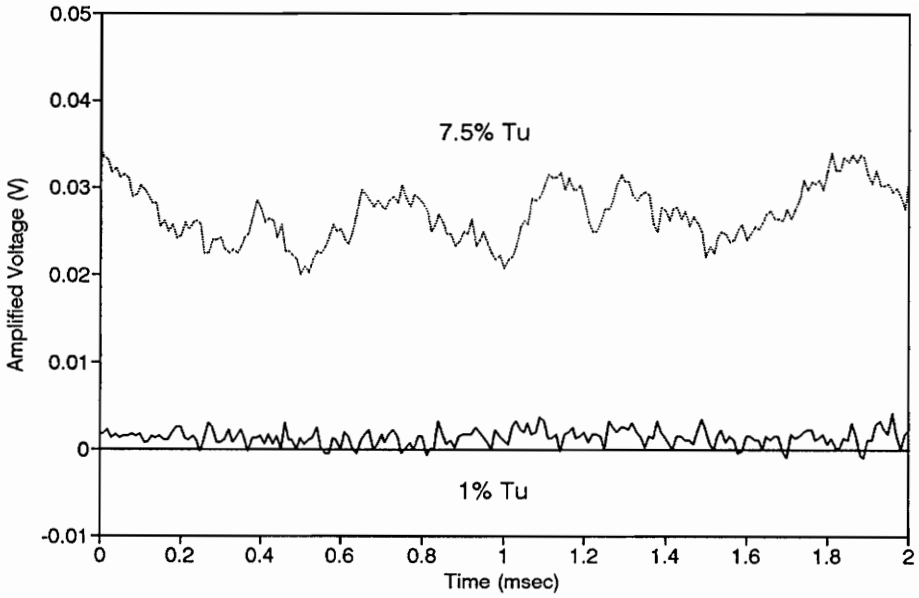

Figure 30. Raw Heat Flux Voltage Signal Sampled at 100 kHz (HFM-6).

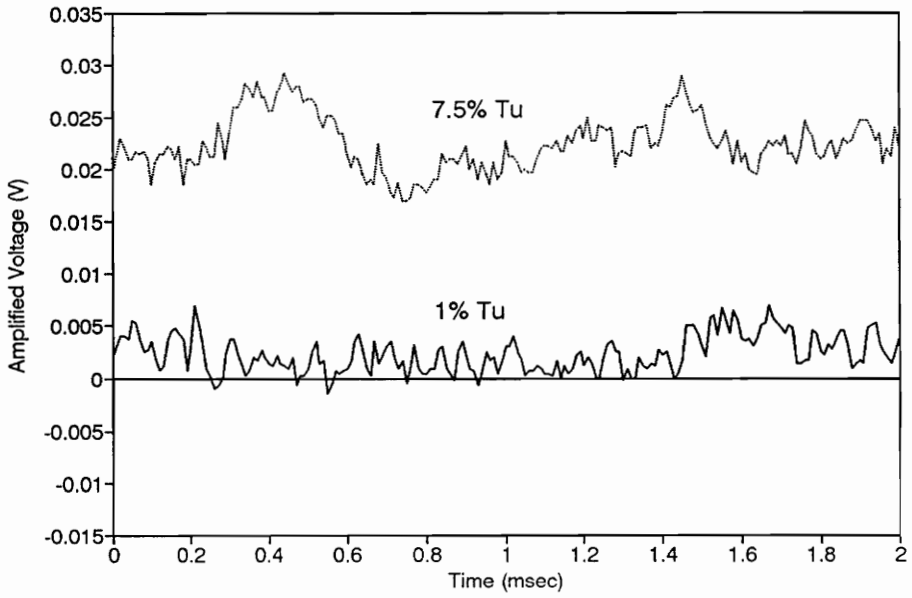

Figure 31. More Raw Heat Flux Voltage Signal Sampled at 100 kHz (HFM-6).

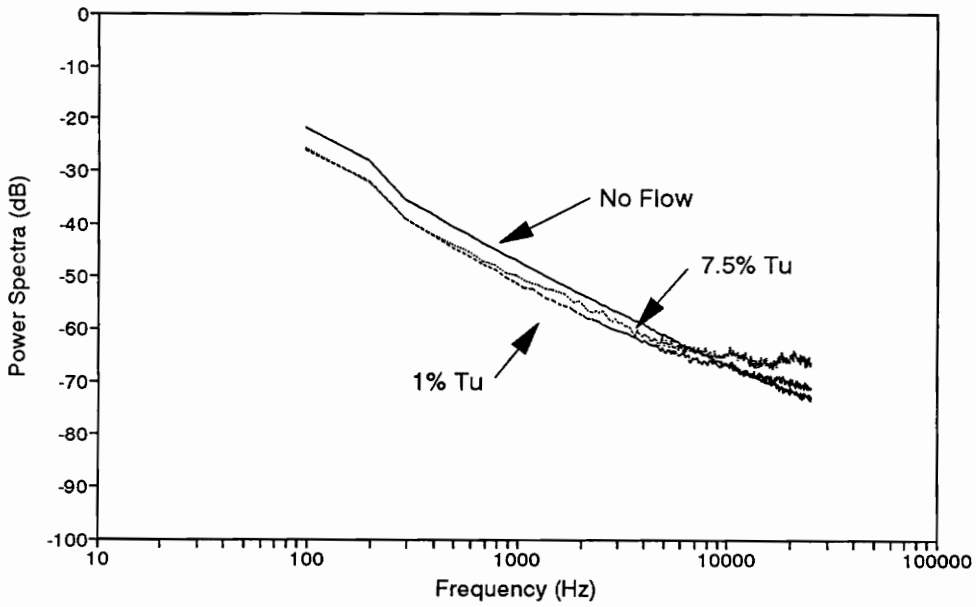

Figure 32. Power Spectra of 0.9% Tu vs. 7.5% Tu of Static Pressure Signal Sampled at 100 kHz (HFM-6).

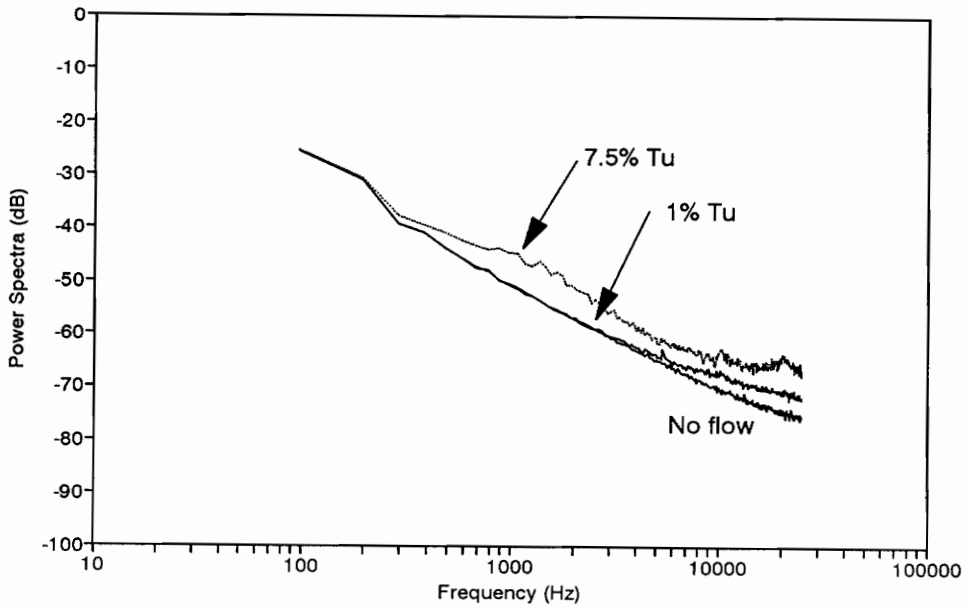

Figure 33. Power Spectra of Pressure Signal Sampled at 100 kHz (HFM-6).

5.5 Leading Edge Line Gage Results

A total of 6 runs were made with the line gage, 3 runs with the grid 1 case and 3 runs without a grid. Figures 34 and 35 show an example of the run data and the heat transfer coefficient for run 1 with grid 1. Figures 36 and 37 show the run data and heat transfer coefficient for run 5 with no grid. A summary of the average heat transfer coefficients for the 6 runs and 2 grid cases is shown in Table 5.4 and can be seen in figure 38.

Table 5.4 - Average Heat Transfer Coefficients and Nusselt Numbers for Leading Edge Line Gage

Run Number	Heat Transfer Coefficient [W/(m^2 C)]	Nusselt Number	Recovery Factor	Tu_q(%)	Noise in Signal
1 - grid 1	937±8	1242±11	0.80	206.0	Yes
2 - grid 1	981±12	1315±16	0.27	128.0	Yes
3 - grid 1	947±13	1267±17	0.47	26.6	Yes
4 - no grid	807±6	1086±8	0.51	13.9	Yes
5 - no grid	775±6	1032±8	0.75	17.4	Yes
6 - no grid	770±7	1025±9	0.79	19.3	Yes

It is evident that the line gage shows more uniformity in heat transfer coefficients due to freestream turbulence. An increase in turbulence intensity from 0.9 percent to 7.5 percent augmented the heat transfer coefficient 15 percent as seen in figure 38. The heat transfer coefficient values closely matched the values from computer predictions, which were 823 [W/(m^2 °C)] for 2% Tu and 908 [W/(m^2 °C)] for 8% Tu.

Again, power spectra of the line gage heat flux signal (Fig. 39) showed an increase in energy from 0 - 10 kHz. Noise was present in all the HFM line gage runs. A sample of the power spectra of the RTS signal (Fig. 40) showed no significant effects due to freestream turbulence. Raw heat flux voltage signals

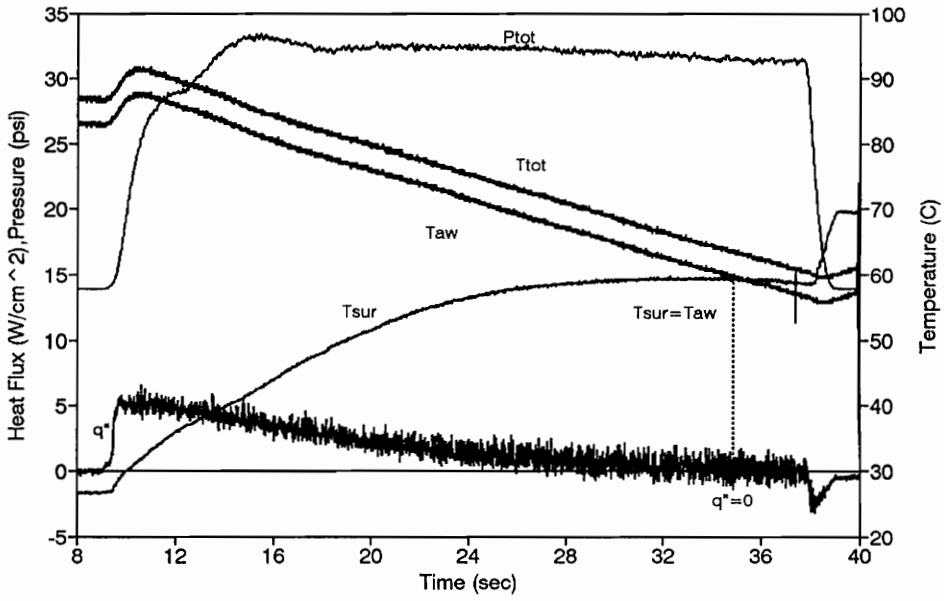

Figure 34. Example of Leading Edge Line Gage Run - Grid 1.

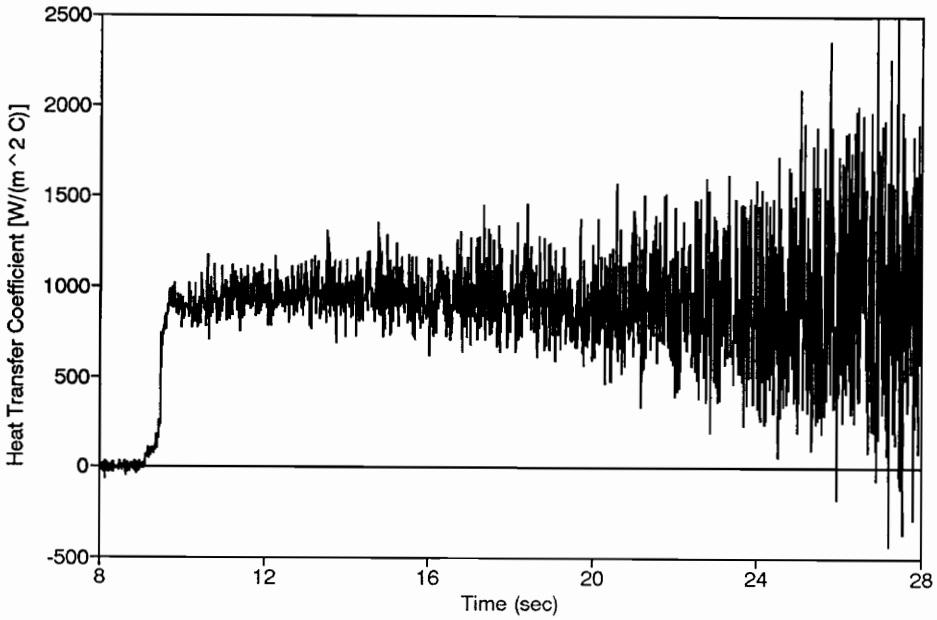

Figure 35. HTC Calculated from Leading Edge Line Gage - Grid 1.

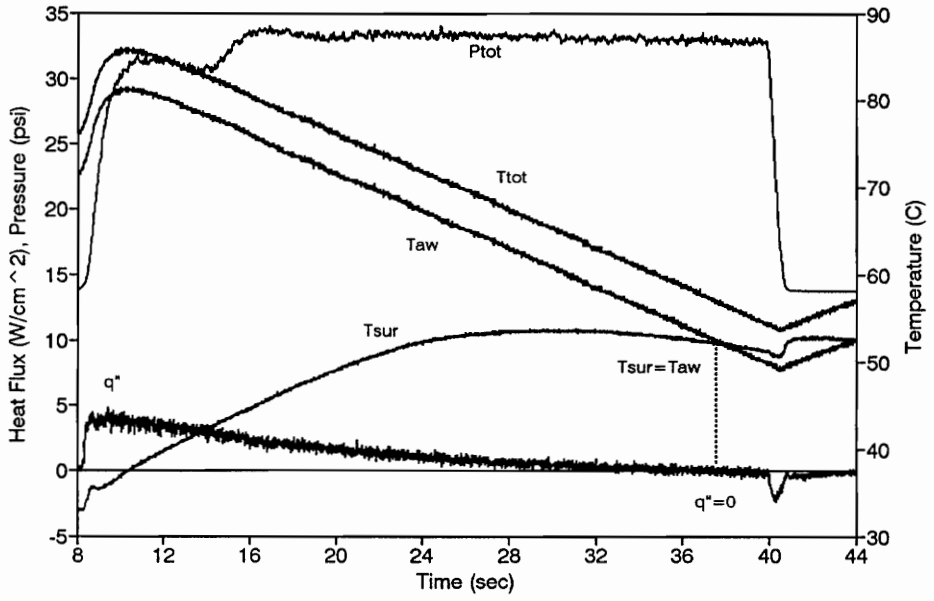

Figure 36. Example of Leading Edge Line Gage Run - No Grid.

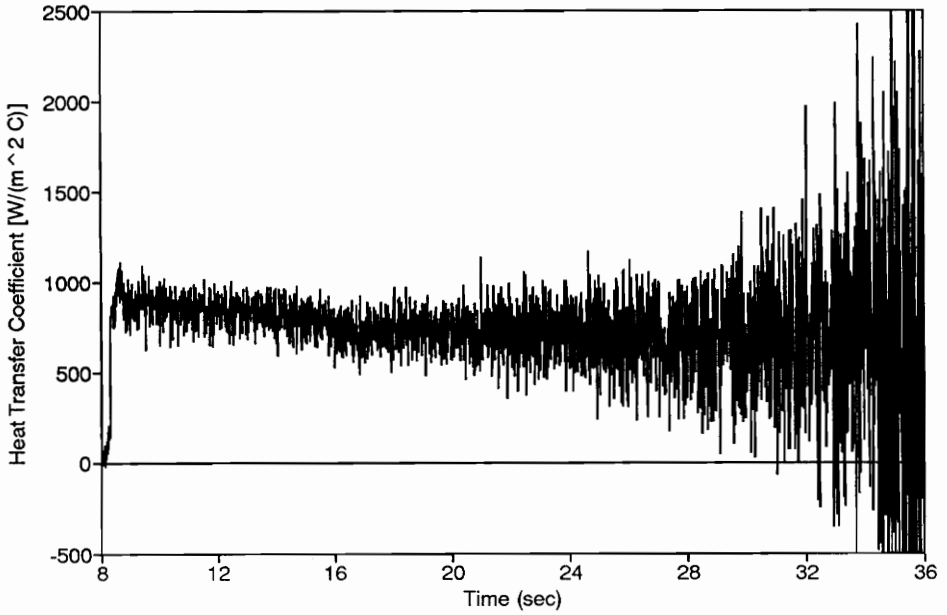

Figure 37. HTC Calculated from Leading Edge Line Gage Run - No Grid.

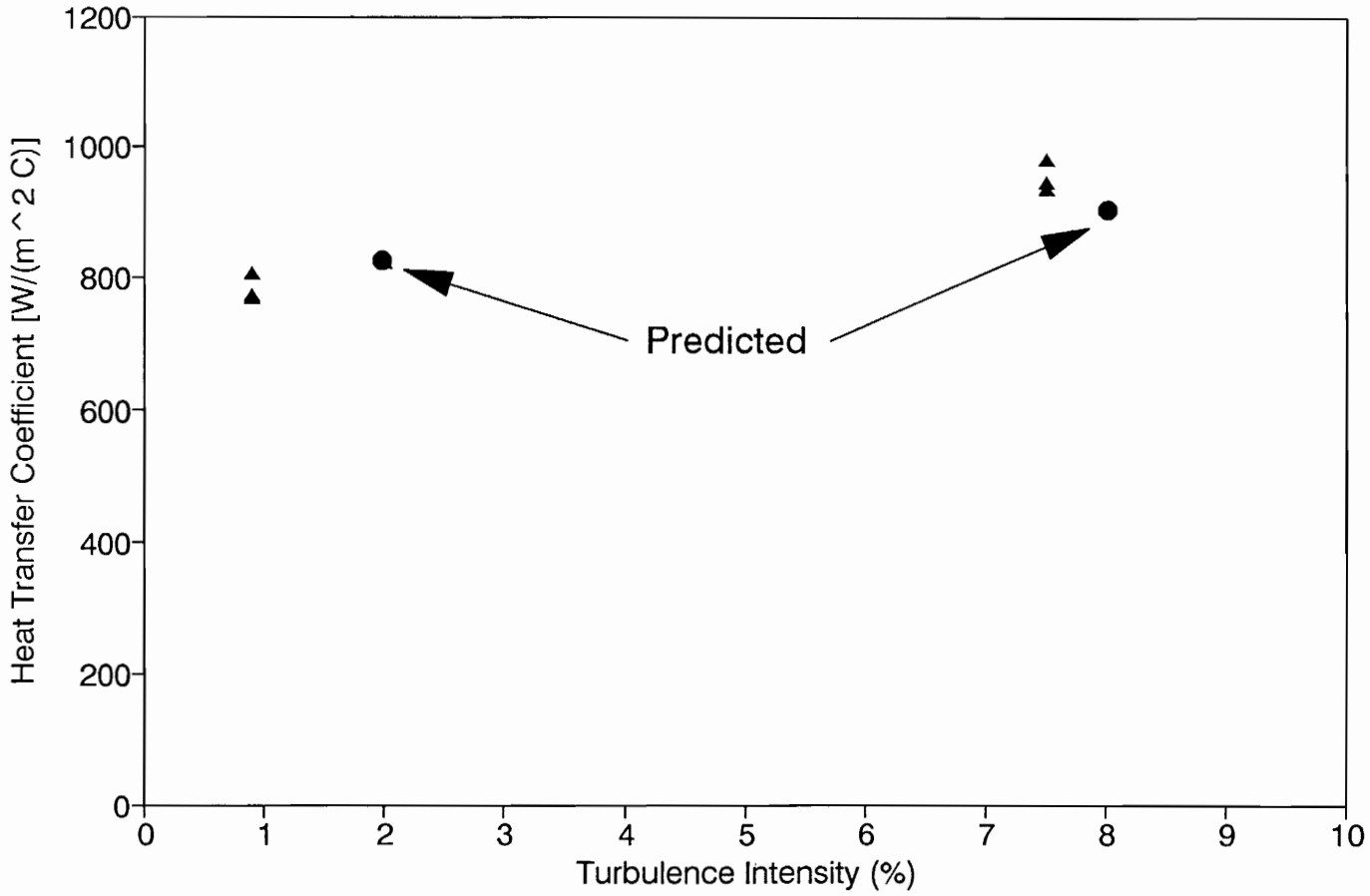

Figure. 38 Average Heat Transfer Coefficient at 1.0% and 7.5% Tu for Leading Edge Line Gage Runs.

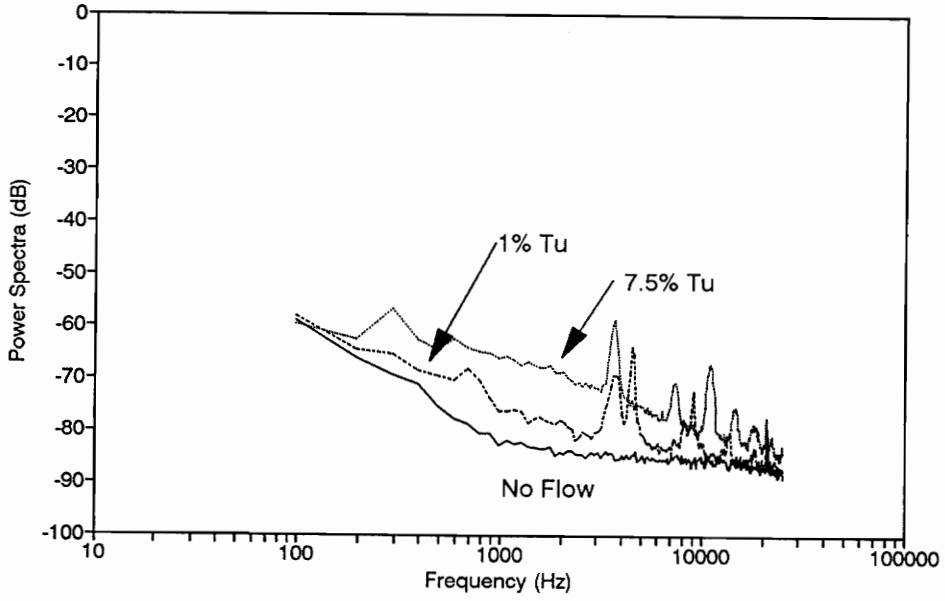

Figure 39. Power Spectra of 0.9% Tu vs. 7.5% Tu of Heat Flux Signal Sampled at 100 kHz (Leading Edge Line Gage).

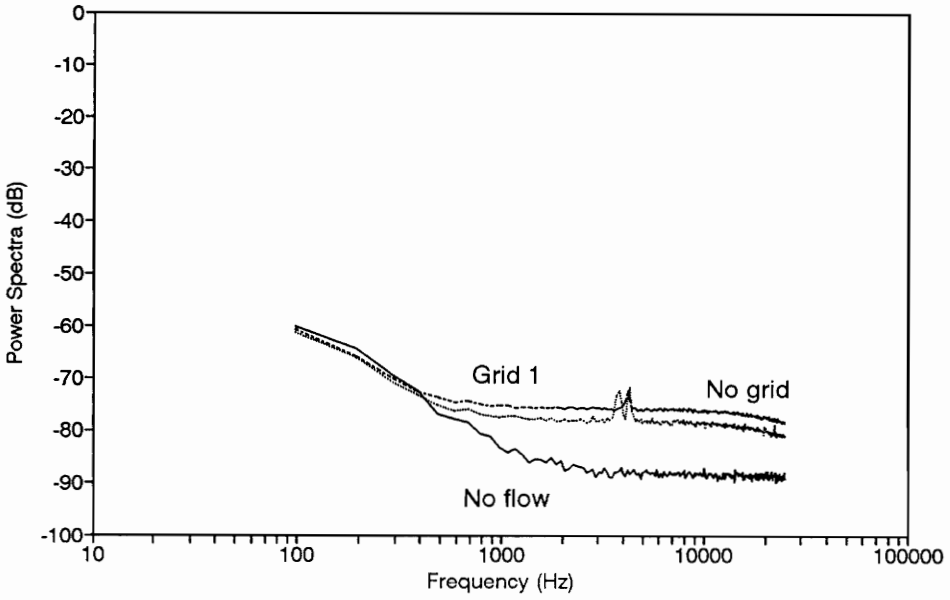

Figure 40. Power Spectra of RTS Signal Sampled at 100 kHz (LE Line Gage).

from the line gage (Fig. 41) do show larger fluctuations for the 7.5% Tu case versus the 0.9% Tu case.

Although the RTS signal worked properly during the course of a heated tunnel run with the HFM line gage, it did exhibit fluctuations before and after the tunnel run. These fluctuations can be seen at the end of both tunnel runs in figure 34 and figure 36.

5.6 Computer Prediction

General Electric supplied results from their computer codes for the heat transfer coefficient distribution over the blade. These codes were modified from the KEP code [Zerkle, 1987] which was a modification of the STAN5 code. G.E.'s results along with the experimental results from this thesis are shown in figure 42. Results from this thesis include the average heat transfer coefficient at Mach 1.26 at the trailing edge and the heat transfer coefficient values at the leading edge for the line gage; 3 runs averaged for the no grid case and 3 runs averaged for the grid 1 case.

Figure 43 shows the computer prediction of the boundary layer. G.E. predicts transition in the boundary layer occurring near the leading edge where the HFM-6 and HFM-2a gages were located. Again, from shadowgraphs, the status of the boundary layer from experiment was inconclusive.

5.7 Heat Flux Turbulence Intensity

Turbulence intensity measurements based on the heat flux have not been previously done. This new technique could only be achieved due to the fast response time of the Heat Flux Microsensor. The following results may help to

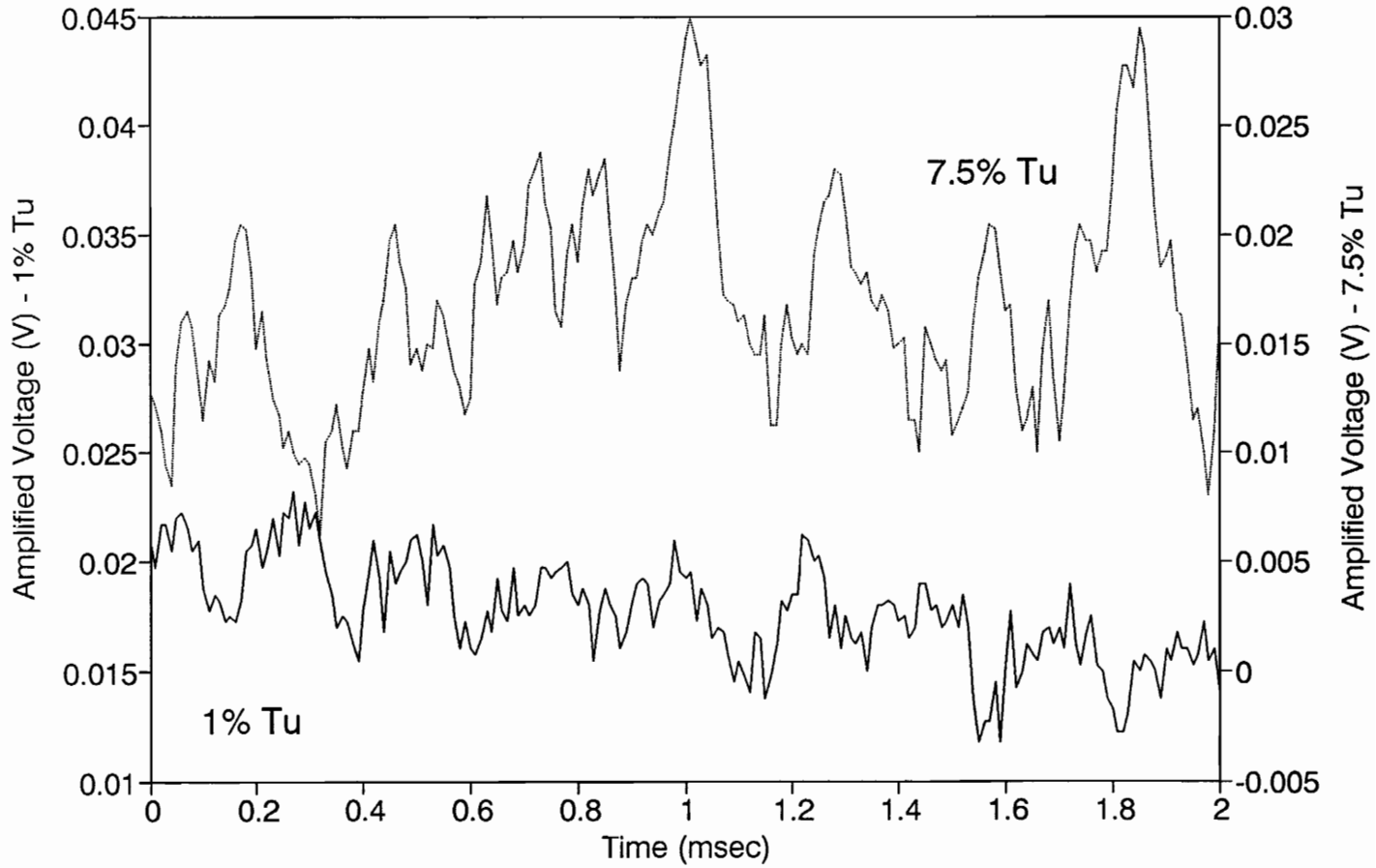

Figure 41. Raw Heat Flux Voltage Signal Sampled at 100 kHz (Leading Edge Line Gage).

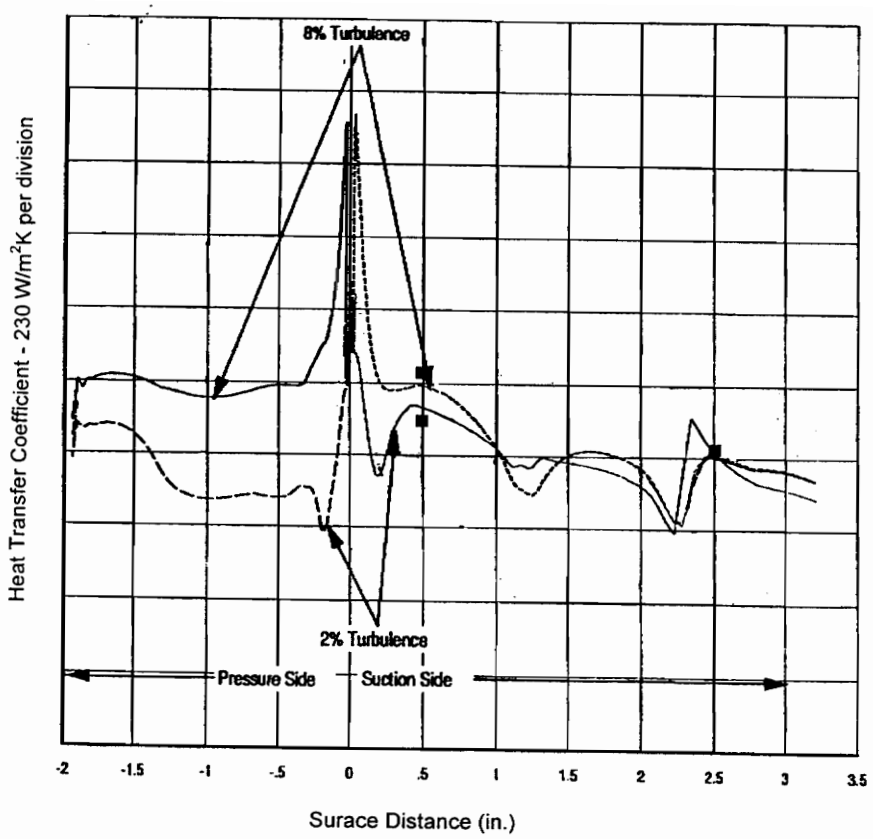

Figure 42. Experiment vs. Prediction for the Heat Transfer Coefficient.

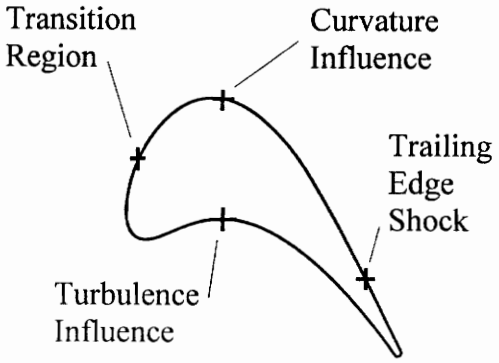

Figure 43. Boundary Layer Status from Prediction.

understand another effect that freestream turbulence has on surface heat transfer. The heat flux turbulence intensity (Tu_q) was performed on all the leading edge cases sampled at 100 kHz. A Tu_q value was averaged over every 0.25 seconds with the resulting points graphed. Figure 44 shows how Tu_q versus the mean heat flux (q") varied for all the leading edge run conditions. Tu_q at 0 is undefined by definition since the mean heat flux is zero. It does appear that the grid case had slightly higher Tu_q values than the no grid case for similar mean heat flux values. Table 5.5 displays the Mean and RMS values for heat flux, Tu_q, for the grid 1 and no grid case.

Table 5.5 Mean, RMS and Tuq comparison

Mean HFS (W/cm^2)	RMS (W/cm^2)	Tu_q (%)	Grid
-0.76	0.20	25.5	Yes
-0.48	0.24	43.0	Yes
-0.42	0.18	35.4	No
-0.27	0.62	200.3	Yes
0.18	0	0	Yes
0.48	0.20	46.1	Yes
0.54	0.12	24.5	No
0.57	0.17	35.4	No
0.71	0.20	30.1	Yes
0.78	0.16	21.5	No
0.81	0.31	40.4	Yes
0.97	0.07	7.7	No
1.14	0.22	20.2	Yes
1.15	0.22	20.4	No
1.30	0.26	21.2	Yes
1.58	0.24	15.6	No
1.71	0.22	13.7	No
1.86	0.21	11.7	No
2.01	0.27	13.8	Yes
2.57	0.27	10.8	Yes
6.63	0	0	No

In figure 45, the RMS of the heat flux versus the mean heat flux is compared. The RMS values are grouped between 0.1 and 0.3 W/cm^2. Due to difficulties with the cascade tunnel pressure control system, it was difficult to maintain repeatability in recording a 100 kHz sample of heat flux during a steady pressure region of the run. Therefore, each 100 kHz heat flux sample was recorded at different times after the tunnel initially started.

Noise from the gage seen during no-flow tests performed before the beginning of a test day was removed from the signals of heated runs. This process was calculated from a modification to equation 15. Generally, this had small effect on the results.

$$Tu_q = \frac{\sqrt{q'^2_{RMS} - q'^2_{RMS(No-Flow)}}}{h(T_{AW} - T_{SUR})} \tag{19}$$

Turbulence intensity measurements based on heat flux were examined for 20 seconds of 1 kHz sampled run data. Specifically, Tu_q, was measured with the leading edge line gage for the grid 1 and no grid case. Figures 46 and 47 show how the RMS of the heat flux raw voltage signal stays relatively constant over the length of the run and does not scale with the mean heat flux as might be expected.

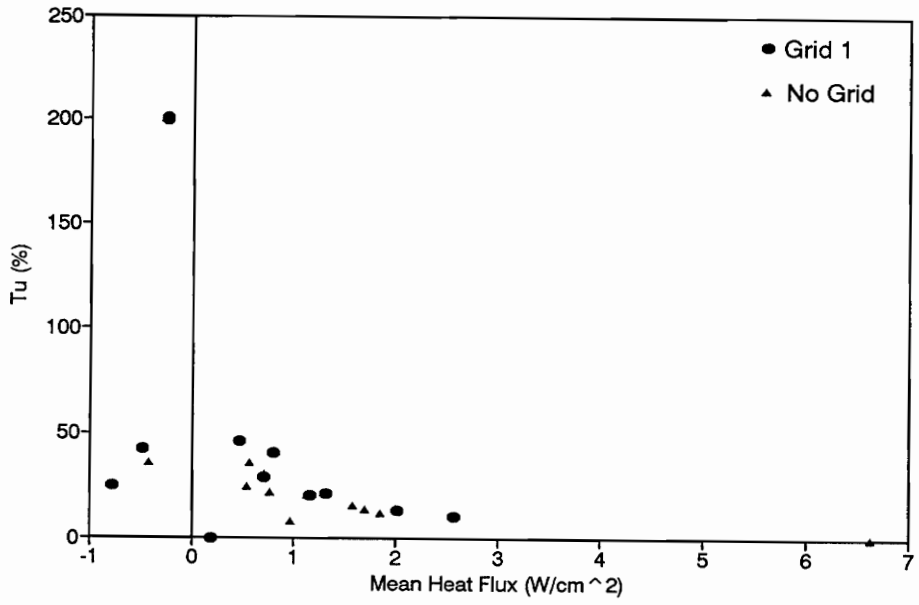

Figure 44. Mean vs. Tu_q for all HFM Leading Edge Runs.

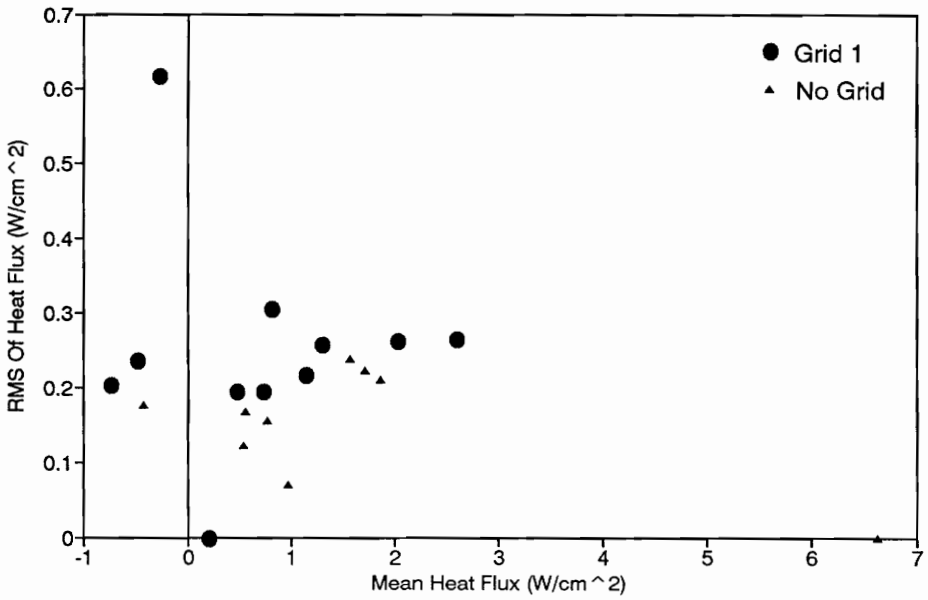

Figure 45. Mean vs. RMS for all HFM Leading Edge Runs.

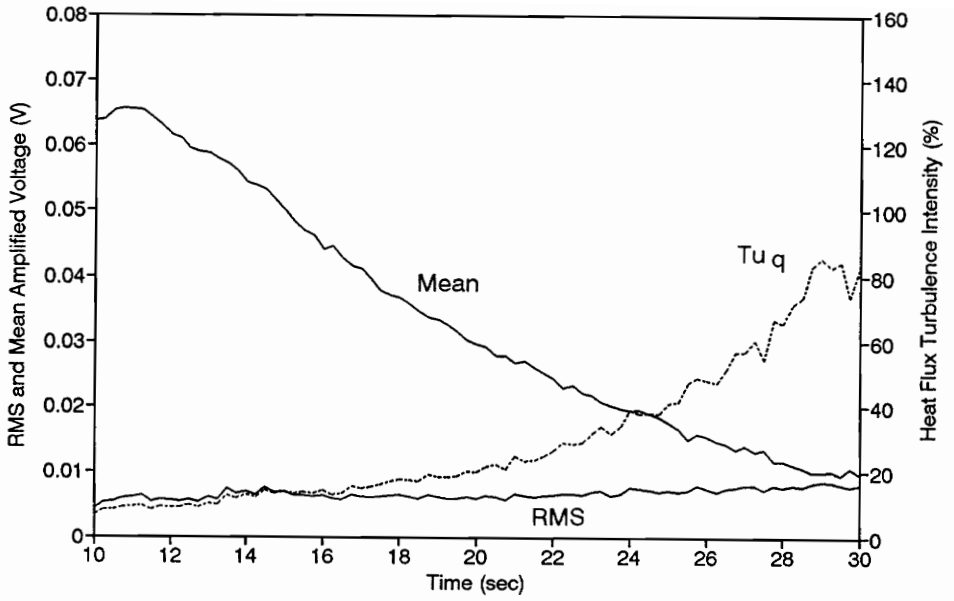

Figure 46. Mean vs. RMS Over 20 Seconds for No Grid Line Gage at 1 kHz.

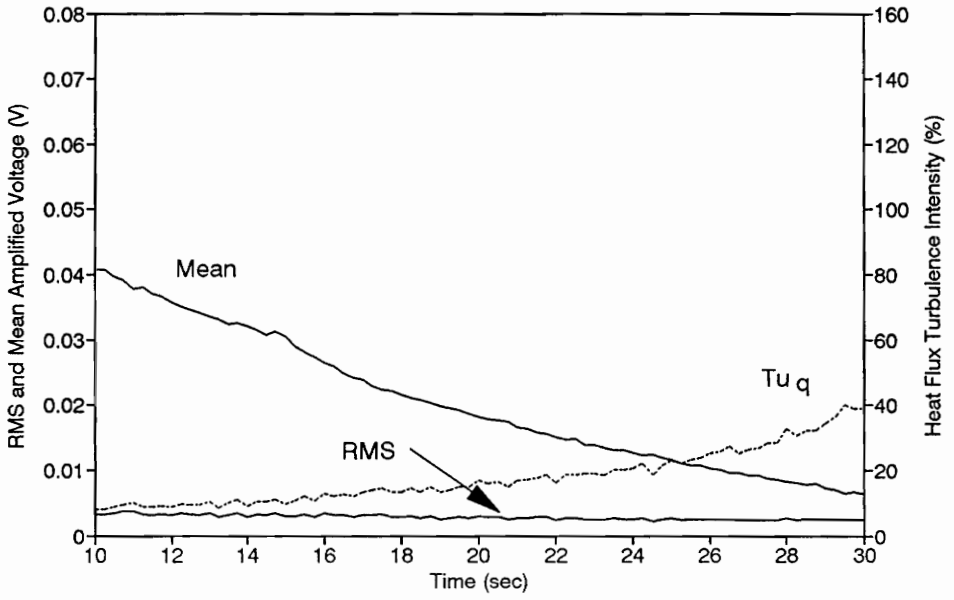

Figure 47. Mean vs. RMS Over 20 Seconds for Grid 1 Line Gage at 1 kHz.

Comparisons can be made between the spectra of the freestream velocity signal and the heat flux signal. Both indicate a difference of ~ 10 dB over the 0 - 10 kHz range. Figures 48 and 49 compare the hot wire signal with the HFM-6 signal for 1.0% Tu and 7.5% Tu, respectively. The HFM-6 signal closely matches the trends of the hot wire signal.

The HFM-6 insert gage and the HFM line gage at the leading edge are different gages physically. Whereas the HFM-6 insert gage averages heat flux over a small circular area on the blade, the HFM line gage averages heat flux across a narrow lengthwise span on the blade. These differences may have some effect on the time averaged heat flux and surface temperature values measured by each gage. These discrepancies might also be the result of the different effects of the turbulence length scale on each gage. More shadowgraphs of the leading edge with the HFM-6 gage may resolve the effects of the HFM-6 gage on the boundary layer.

Finally, an attempt was made to correlate the freestream turbulence intensity effects on the surface heat transfer at the leading edge of a turbine blade with the effects of freestream turbulence at the stagnation point on a circular cylinder. This comparison was made in order to determine an estimate of freestream turbulence effects on surface heat transfer using turbine blades compared with documented effects for circular cylinders. The comparison is made using a Frossling number ($Nu/Re^{0.5}$) ratio of 7.5% Tu over 1.0% Tu based on an equivalent radius of curvature estimate of the turbine blade as a circular cylinder. Note that the Reynold's number is the same for either turbulence intensity value and when a ratio comparison is made, only the Nusselt number is

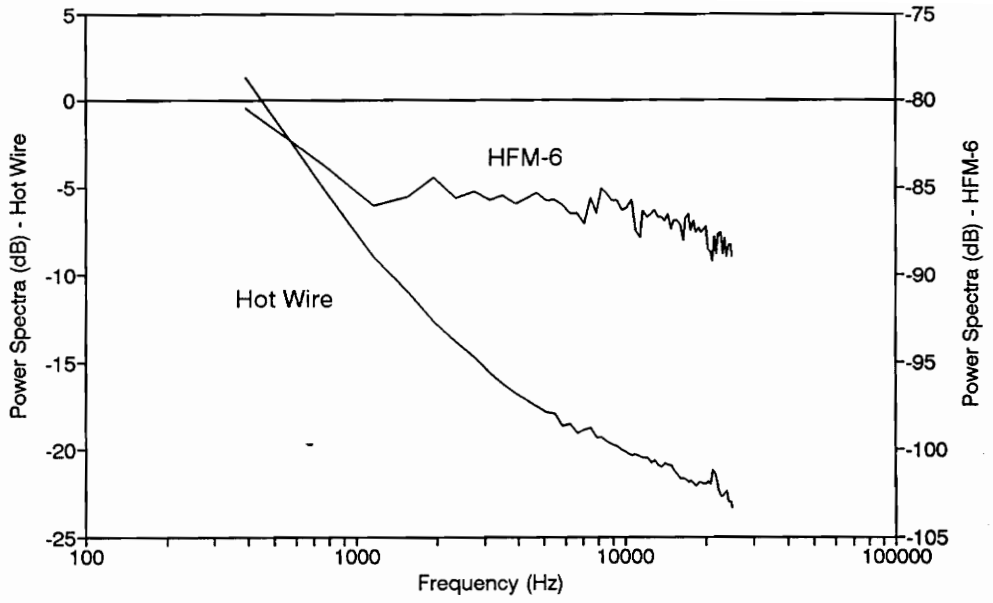

Figure 48. Comparison Between Hot Wire Power Spectra and HFM-6 Power Spectra for 1.0% Tu.

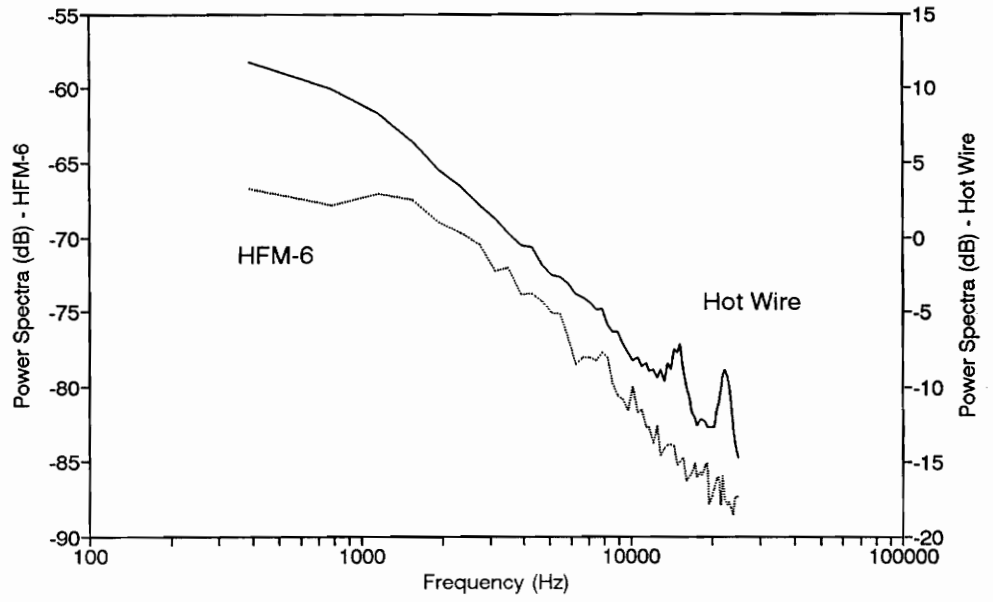

Figure 49. Comparison of Power Spectra for 7.5% Tu.

necessary to determine the experimental ratio. The experimental Nusselt ratio for 7.5% Tu over 1.0% Tu was 1.21 whereas the ratio from Kestin's formula with a Reynold's number based on equivalent radius of curvature

$$Fr = \frac{Nu}{\mathrm{Re}^{1/2}} = 0.945 + 3.48\left(\frac{Tu\,\mathrm{Re}^{1/2}}{100}\right) - 4.0\left(\frac{Tu\,\mathrm{Re}^{1/2}}{100}\right)^2 \qquad [7]$$

was 1.54 at the same turbulence intensity values (Table 5.6)

Table 5.6 Experimental data vs. Kestin's formula

Tu Ratio	Experimental Nusselt ratio	Kestin ratio
7.5/1.0	1.21	1.54

Remember that the leading edge gage was 1.0 cm from the blade stagnation point on the turbine blade. This might suggest that freestream turbulence has less effect on the heat transfer farther downstream of the stagnation point. It may also suggest a length scale effect relative to the boundary layer size. Although, Gundappa [1991] did show [fig. 2, pg. 767] with the same grids and similar turbulence intensity values for low speed flow over a cylinder, a constant 45% increase in the Frossling number from the stagnation point to 90° past the stagnation point on the front of the cylinder.

Chapter 6.0

Conclusions and Recommendations

6.1 Conclusions

Several conclusions can be made about the effects of freestream turbulence on turbine blade surface heat transfer.

(1) A major accomplishment with this project was the successful measurements of time average and unsteady heat flux with a HFM directly deposited on the aluminum blade. This was a first step at measuring RTS and HFS signals at two different locations on the blade; the trailing edge and the leading edge, both on the suction side of an aluminum turbine blade.

(2) The trailing edge measurements were conducted before the use of passive turbulence grids. Shadowgraphs showed the gage was near the trailing edge shock and that the boundary layer was going turbulent. The average heat transfer coefficient found at Mach 1.26 was 765 W/(m^2 °C) matched well with a predicted value of 738 W/(m^2 °C).

(3) The results at the leading edge due to freestream turbulence with the HFM line gage show an increase in the heat transfer coefficient by 15% when the freestream turbulence increased from 0.9% Tu to 7.5% Tu. The HFM-6 showed no increase in the average heat transfer coefficient due to changes in freestream turbulence.

(4) The fast response time of the HFM gages allowed for spectral density analysis and showed a definite increase in energy at the 0 -10 kHz range due to freestream turbulence. This evidence was also apparent in the raw heat flux signals, which showed an increase in signal fluctuations due to increased freestream intensity. Results using turbulence intensity based on heat flux, Tu_q, showed a higher Tu_q value for higher freestream turbulence. When compared to Kestin's formula [equation 7] on the effects of freestream turbulence at a stagnation point on a cylinder, the experimentally determined ratio of 8% Tu to 1% Tu was less than predicted.

6.2 Recommendations

Recommendations for future research include the following ideas.

(1) Manipulate length scales and turbulence intensities to closely match actual engine parameters. This study used passive grids to create freestream turbulence and a more suitable method must be found to decrease the length scales while maintaining high freestream turbulence levels. If higher turbulence is generated, then a method to use similar length scales is important for understanding how intensity or length scales separately effect surface heat transfer.

(2) Measure heat flux signals on the pressure side of the turbine blade and compare with computer predictions for various turbulence intensities. Much more study must be conducted in order to piece together the "complete" heat transfer process along the entire blade profile. Presently, for this project, the

heat flux measurements have been made at two positions on the suction side of the blade.

(3) Simultaneously measure heat flux and velocity at surface of blade to compare signals and power spectra during heated tunnel runs. By measuring velocity and heat flux together, a strong coherence relationship may exist. A direct correlation may exist between freestream turbulence, Tu, and turbulence intensity based on heat flux , Tu_q . This should also help piece together a more complete picture of how the RMS heat flux signal varies with the mean heat flux signal due to increased freestream turbulence.

References

ATMIO-16 User Manual - Multifunction I/O board for PC/AT, October 1993 ed., Part # 320476-01, copyright 1992, 1993.

Baker, Karen, "Unsteady Surface Heat Flux and Temperature Measurements", M.S. thesis, Virginia Tech, Blacksburg, 1993.

Bertsch, R., "An Experimental Examination of the Influence of Trailing-Edge Cooling Ejection on Blade Losses in Transonic Turbine Cascades", M.S. thesis, Virginia Tech, Blacksburg, 1990.

Crawford, M.E., and Kays, W.N., "STAN5 - A Program for Numerical Computation of 2-D Internal and External Boundary Layer Flows", NASA CR-2742, 1976

Corrsin, S., "Turbulence: Experimental Methods", Encyclopedia of Physics, Ed. S. Flugge, Vol. VIII/2. Fluid Dynamics II., pp. 524-590, 1963.

Diller, T.E., "Advances in Heat Flux Measurements", Advances in Heat Transfer, Vol. 23, Academic Press, NY, pp. 279-368, 1993.

Doorly, J.E., and Oldfield, M.L.G., "New Heat Transfer Gages for Use on Multilayered Substrates", **ASME Journal of TurboMachinery**, Vol. 108, pp. 153-160, July 1986.

Doorly, J.E., and Oldfield, M.L.G., "The Theory of Advanced Multi-Layer Thin Film Heat Transfer Gauges", **International Journal of Heat Mass Transfer**, Vol. 30, No. 6, pp. 1159-1168, 1987.

Glezer, B., Moon, H.K., Zhang, L., and Camci, C., "Application of a Heat Flux/Calorimeter-Based Method to Asses the Effect of Turbulence on Turbine Airfoil Heat Transfer," **International Gas Turbine and Aeroengine Congress and Exposition**, The Hague, Netherlands, June 1994.

Gundappa, M., and Diller, T.E., "The Effects of Freestream Turbulence and Flow Pulsation on Heat Transfer From a Cylinder in Crossflow," **ASME Journal of Heat Transfer**, Vol. 113, pp. 766-769, 1991.

Gundappa, M., and Diller, T.E., "The Effects of Freestream Turbulence and Flow Pulsation on Heat Transfer From a Cylinder in Cross-flow," in **Augmentation of Heat Transfer in Energy Systems**, Ed. P.J. Bishop, **ASME**, HTD Vol 52, pp. 29-36., 1985.

Hager, J.M., Simmons, S., Smith, D., Onishi, S., Langley, L.W., and Diller, T.E., "Experimental Performance of a Heat Flux Microsensor," **AMSE Journal of Engineering for Gas Turbines and Power**, Vol. 113, pp. 246-250, 1991a

Hager, J.M., Terrell, J.P., Langley, L.W., Onishi, S., and Diller, T.E., "Measurements with the Heat Flux Microsensor," Proceedings of the 37th International Instrumentation Symposium, ISA, Research Triangle Park, pp. 551-561, 1992b

Holmberg, D.G., Reid, T., Kiss, T., Moses, H.L., Ng, W.F., and Diller, T.E., "Effects of Shock Wave Passage on Heat Transfer in a Transonic Turbine Cascade," **International Gas Turbine and Aeroengine Congress and Exposition**, The Hague, Netherlands, June 1994.

Holmberg, Dave G, Modified Labview VI's - SWITCH.VI, LORENHFM.VI, DGHSPCTM.VI, LORENHW.VI

Holmberg, D.G, and Diller, T.E., "High Frequency Heat Flux Sensor Calibrations and Modeling", **ASME Unsteady Flow in Aeropropulsion** AD-Vol.40, pg. 27-35, 1994.

IFA 100 Intelligent Flow Analyzer Instruction Manual, Revision A. P/N 1990237, copyrigth 1983 by TSI, Inc.

Kestin, J., "The Effect of Freestream Turbulence on Heat Transfer Rates," Advanced Heat Transfer, Vol. 3, Academic Press, NY, pp. 1-32, 1966.

Kestin, J. and Wood, R., "The Influence of Turbulence on Mass Transfer from Cylinders," **Journal Heat Transfer**, vol. 93, pp. 321-327, 1971.

Lowery, G.W., and Vachon, R.I., "The Effect of Turbulence on Heat Transfer from Heated Cylinders," **International Journal Heat Mass Transfer**, Vol. 18, pp. 1229-1242, 1975.

Manual on the use of thermocouples in temperature measurement, 4th ed., ASTM Committee on temperature measurement, ASTM Manual Series: MNL12, Revision of special technical publication STP-470B, ASTM Pub. Code no. 28-012093-40, pg. 209, Table 10.21 Type K

Moss, R.W., and Oldfield, M.L.G., "Effect of Freestream Turbulence on Flat-Plate Heat Flux Signals: Spectra & Eddy Transport Velocities," **International Gas Turbine and Aeroengine Congress and Exposition**, The Hague, Netherlands, June 1994.

O'Brien, J.E., and Vanfossen, Jr., G.J., "The Influence of Jet Grid Turbulence on Heat Transfer from the Stagnation Region of a Cylinder in Crossflow," National Heat Transfer Conference, Denver Colorado, August 4-7, 1985.

Simmons, S.G., Hager, J.M., and Diller, T.E., "Simultaneous Measurements of Time-Resolved Surface Heat Flux and Freestream Turbulence at a Stagnation Point," pp. 375-380, 1990.

Sohn, K.H., O'Brien, J.E., and Reshotko, E., "Some Characteristics of Bypass Transition in a Heated Boundary Layer," **Seventh Symposium on Turbulent Shear Flows**, pp 2.4.1-2.5.6, Stanford University, August 21-23, 1989

Swisher, S.E., Diller, T.E., and Pierce, F.J.,"Time-Resolved Heat Flux Measurements in a Turbulent Junction," Topics in Heat Transfer Volume 1, HTD-Vol. 206-1, pp. 55-63, ASME 1992.

Tan-Atichat, J., Nagib, H.M., and Loehrke, R.I., "Interaction of Freestream Turbulence with Screens and Grids: A Balance Between Turbulence Scales," **Journal of Fluid Mechanics**, Vol. 114, pp. 501-528, 1982.

Uberoi, M.S., and Wallis, S., "Spectra of Grid Turbulence," The Physics of Fluids, Vol. 12, No. 7, pp. 1355-1358, July 1969.

Van Fossen, Jr., G.J., and Simoneau, R.J., "A Study of the Relationship Between Freestream Turbulence and Stagnation Region Heat Transfer," **Journal of Heat Transfer**, Vol. 109, pp. 10- 15, February 1987.

Wesner, Angela L., Personal Communication, September 27, 1994, Virginia Tech, Blacksburg, Virginia.

Young, C.D., and Han, J.C., "Effect of Jet Grid Turbulence on Turbulent Boundary Layer Heat Transfer," **ASME Winter Annual Meeting**, Chicago, Illinois, November 1988.

Zerkle, R.D., and Lounsbury, R.J., "The Influence of Freestream Turbulence and Pressure Gradient on Heat Transfer to Gas Turbine Airfoils," **AIAA** Paper No. 87-1917, 1987.

Appendix A
Data Runs

Table A.1 - Trailing Edge Line Gage

Figure	Run #	Exit Mach #	$P_{NITROGEN}$ (psi)	Ttot/(Tinterior) (3 Tint points averaged)	Comments
A1,A2	1	1.16	---	---	No cooling
A3,A4	2	1.16	200	1.62	5 s delay
A5,A6	3	1.16	180	1.57	5 s delay
A7,A8	4	1.16	180	1.54	10 s delay
A9,A10	5	1.16	180	1.51	10 s delay
A11,A12	6	1.16	180	1.40	No delay
A13,A14	7	1.26	180	1.35	No delay
A15.A16	8	1.22	180	1.31	No delay
A17,A18	9	1.12	150	1.34	No delay
A19,A20	10	1.16	---	1.11	No cooling

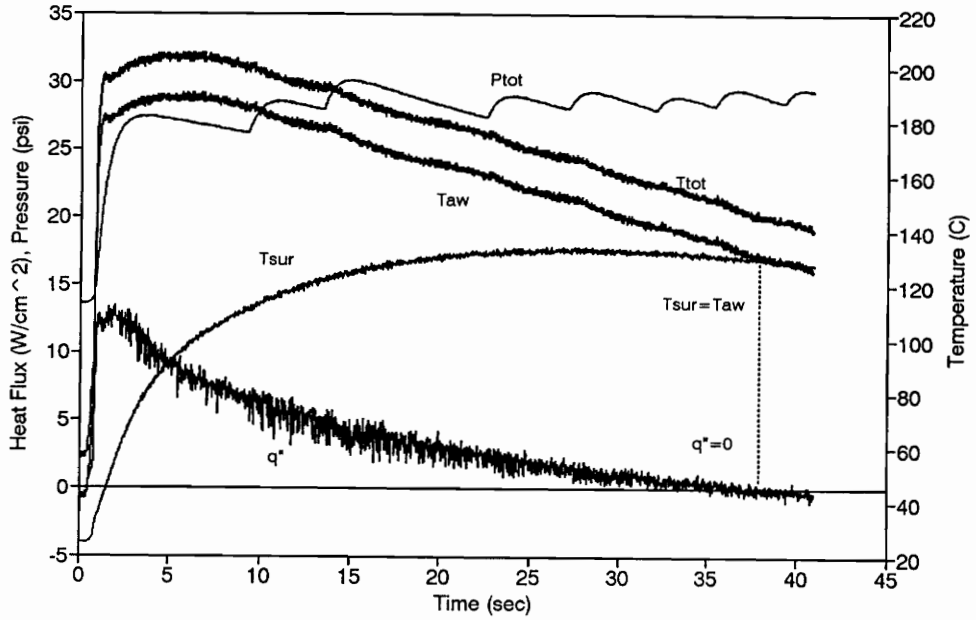

Figure A1. Trailing Edge Gage Run 1.

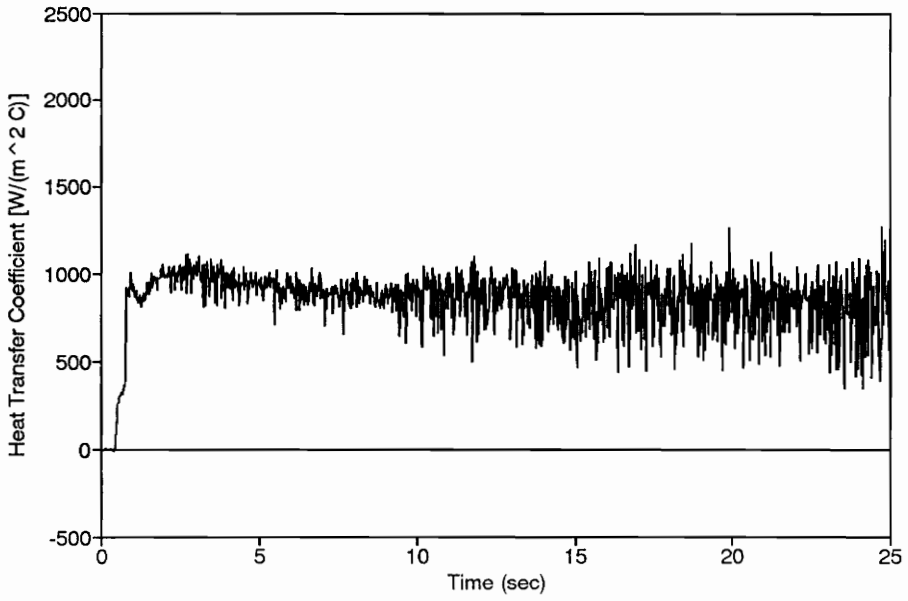

Figure A2. HTC Calculated from Trailing Edge Run 1.

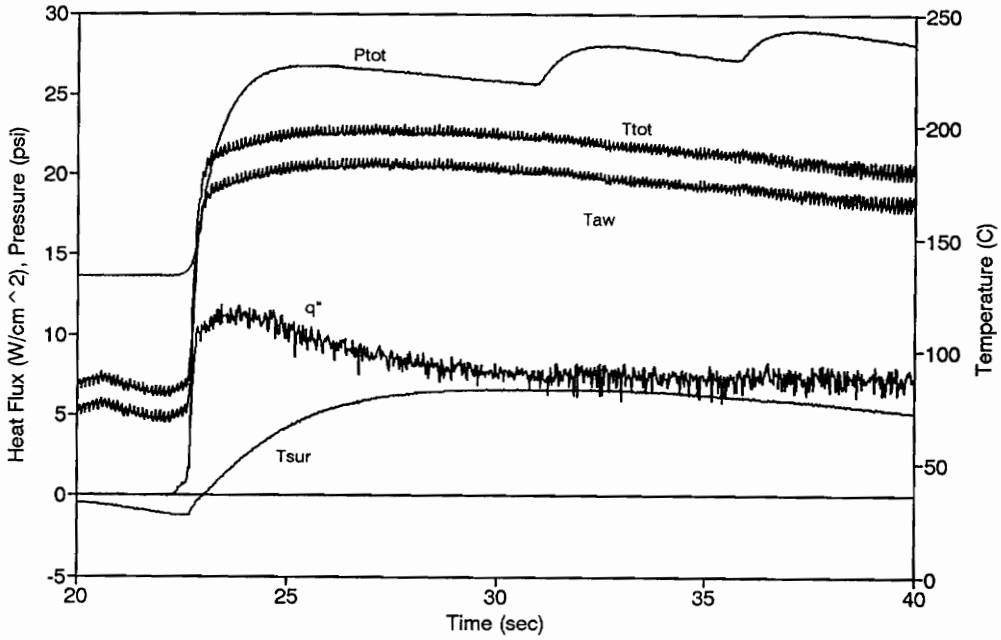

Figure A3. Trailing Edge Gage Run 2.

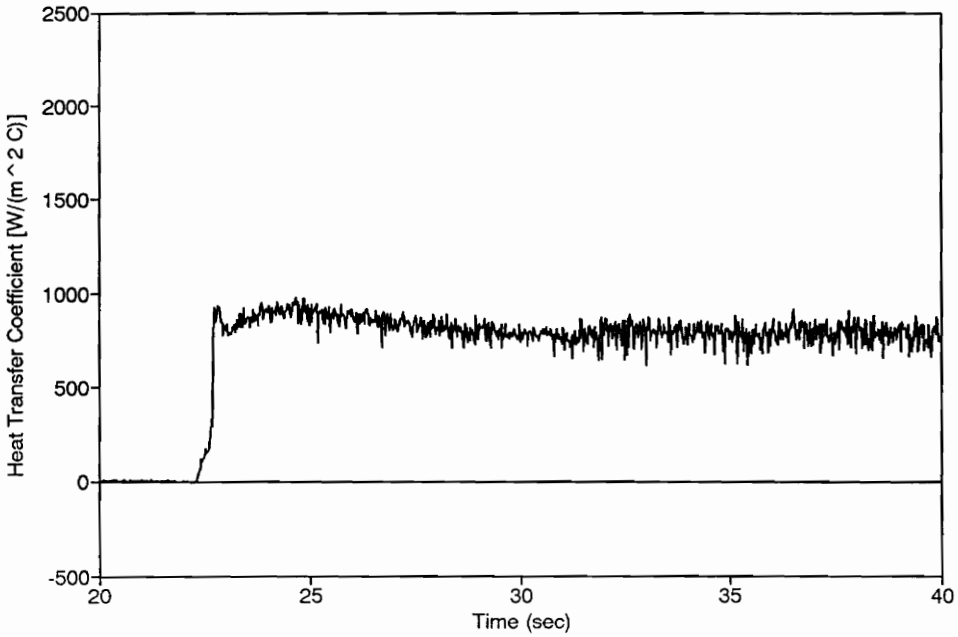

Figure A4. HTC Calculated from Trailing Edge Run 2.

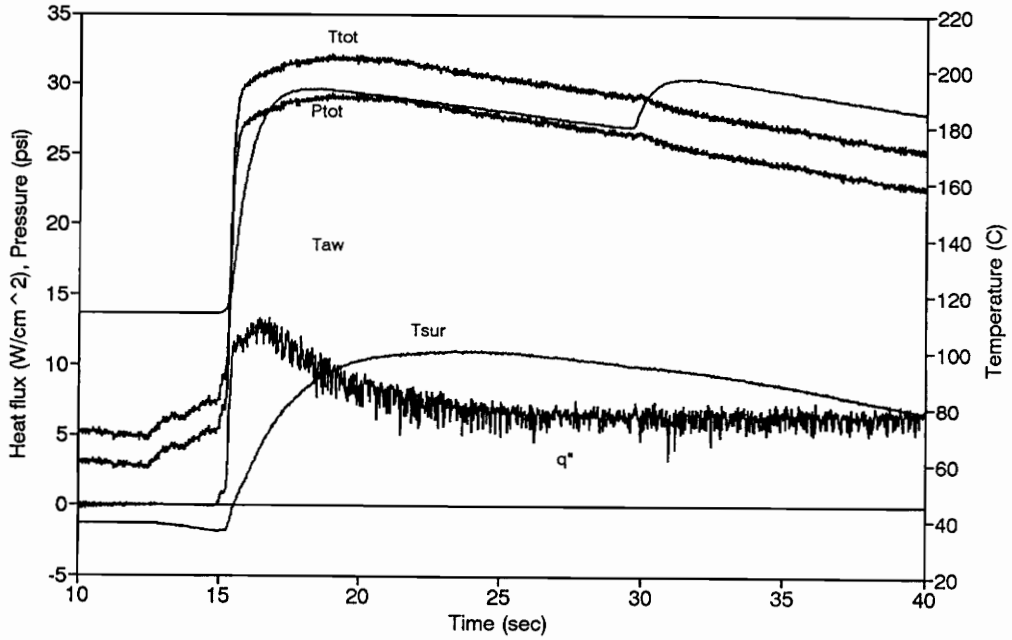

Figure A5. Trailing Edge Gage Run 3.

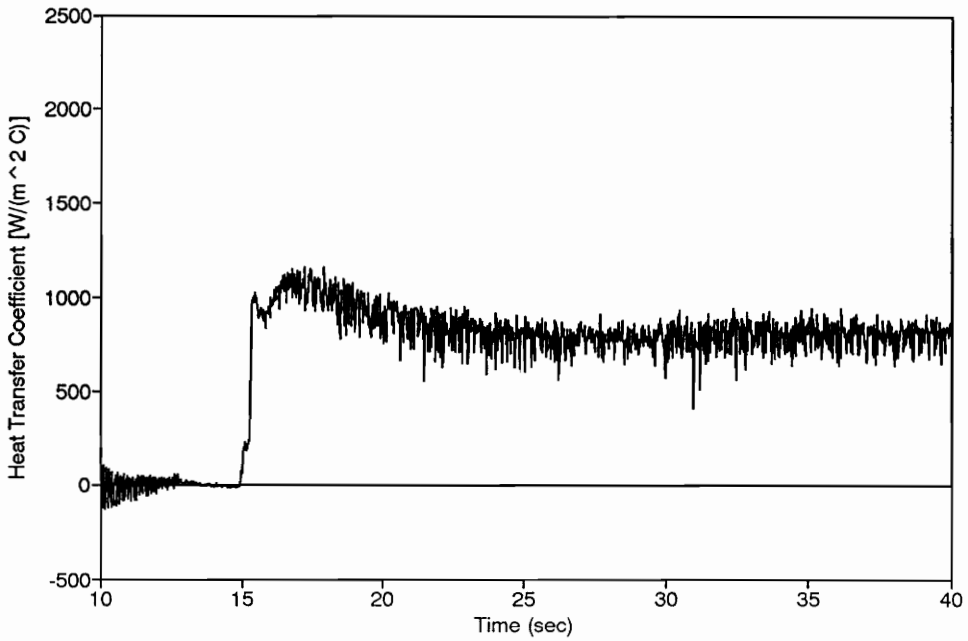

Figure A6. HTC Calculated from Trailing Edge Run 3.

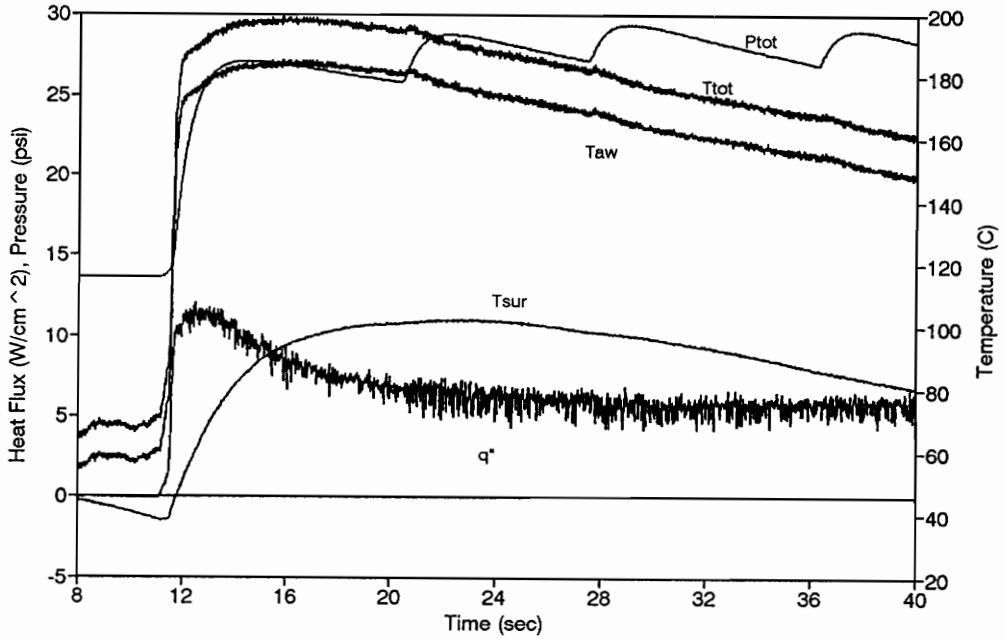

Figure A7. Trailing Edge Gage Run 4.

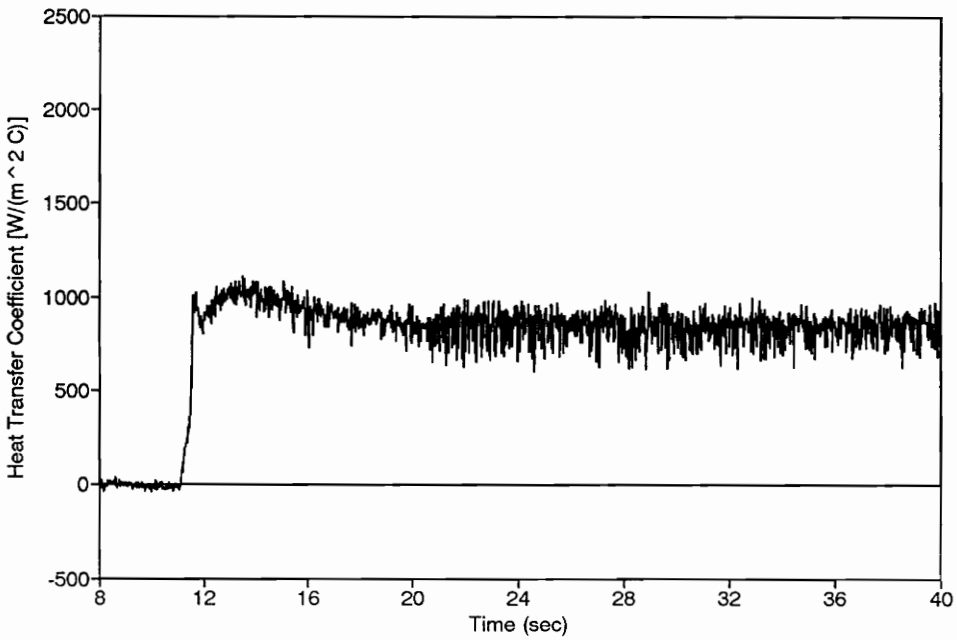

Figure A8. HTC Calculated from Trailing Edge Run 4.

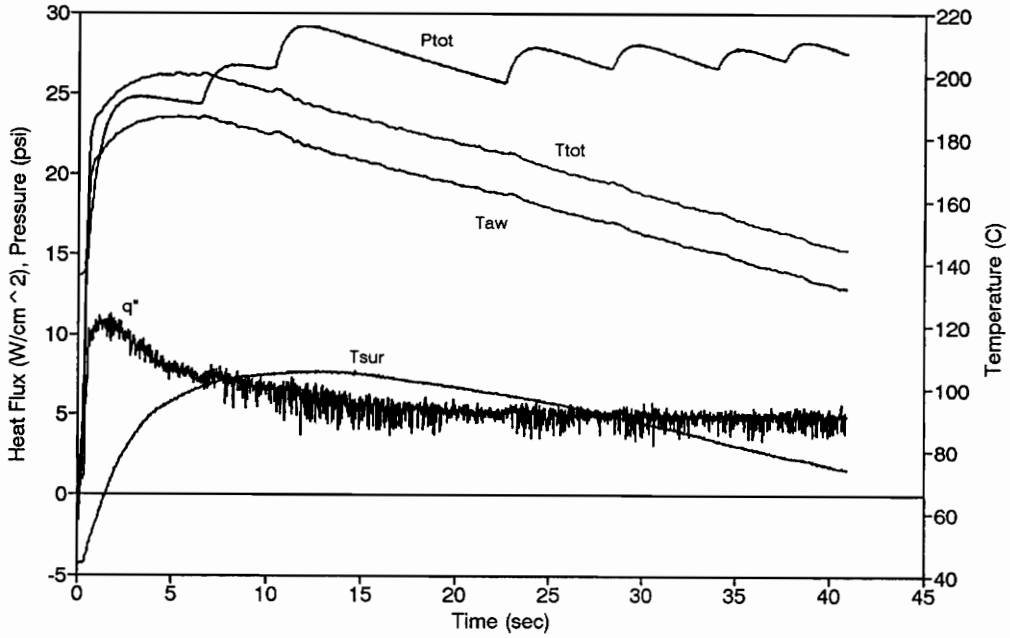

Figure A9. Trailing Edge Gage Run 5.

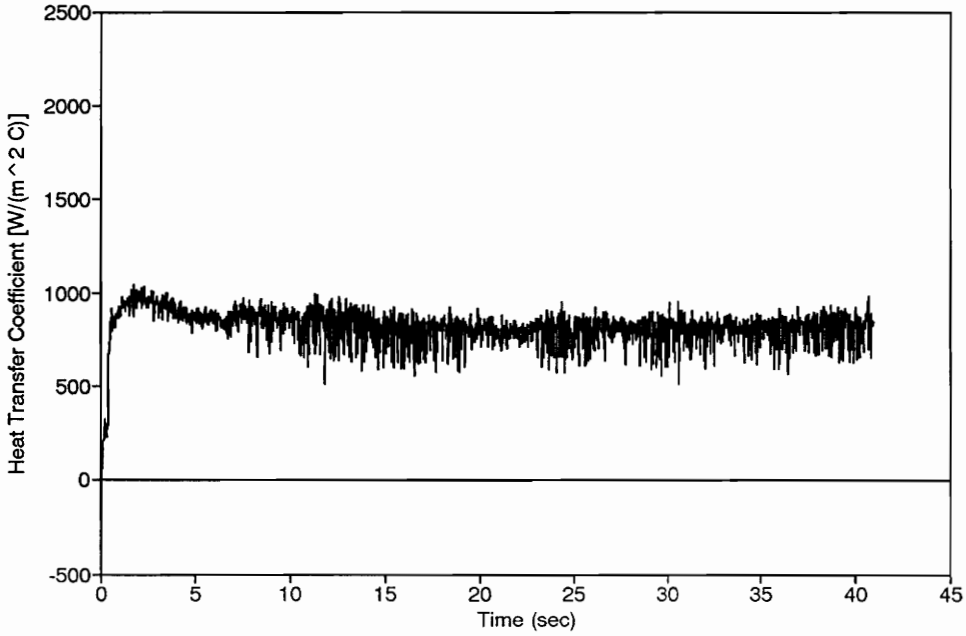

Figure A10. HTC Calculated from Trailing Edge Run 5.

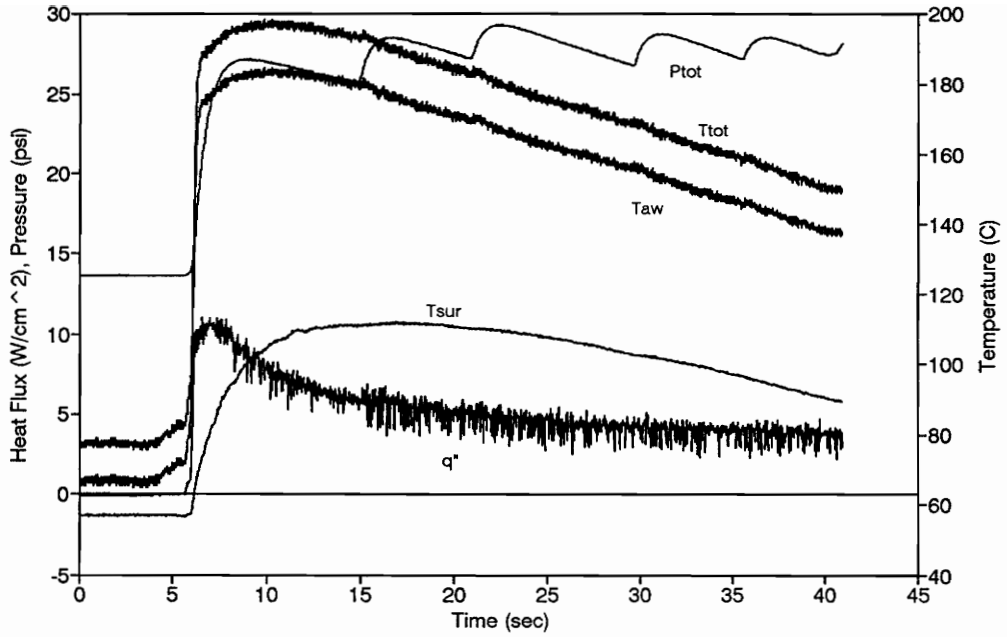

Figure A11. Trailing Edge Gage Run 6.

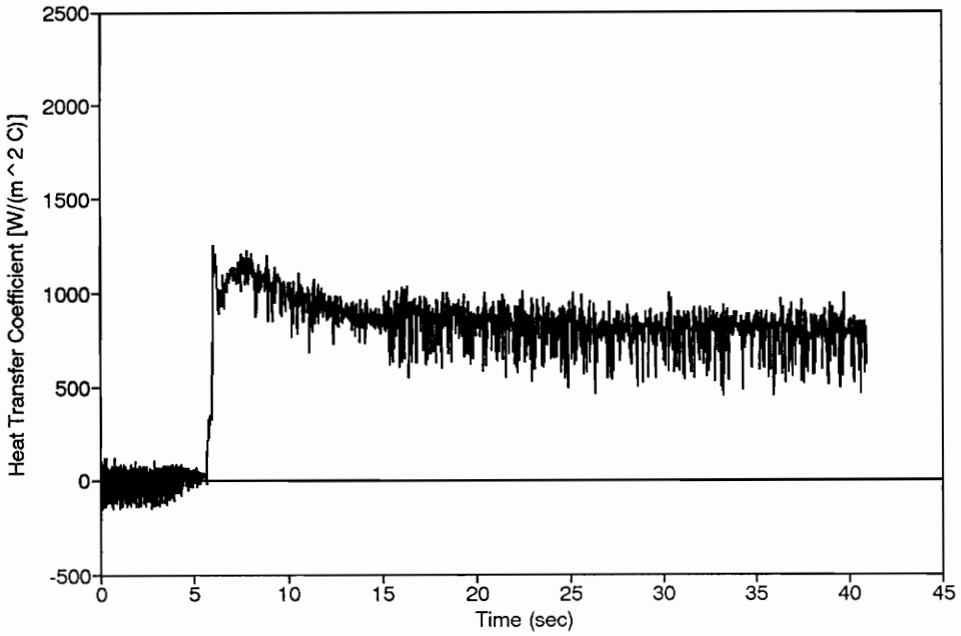

Figure A12. HTC Calculated from Trailing Edge Run 6.

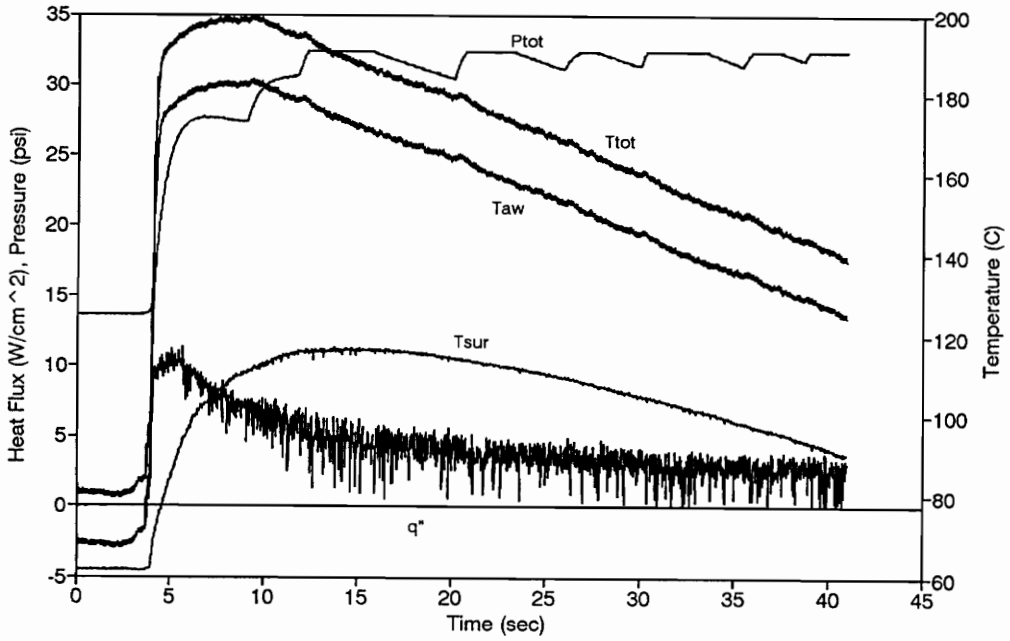

Figure A13. Trailing Edge Gage Run 7.

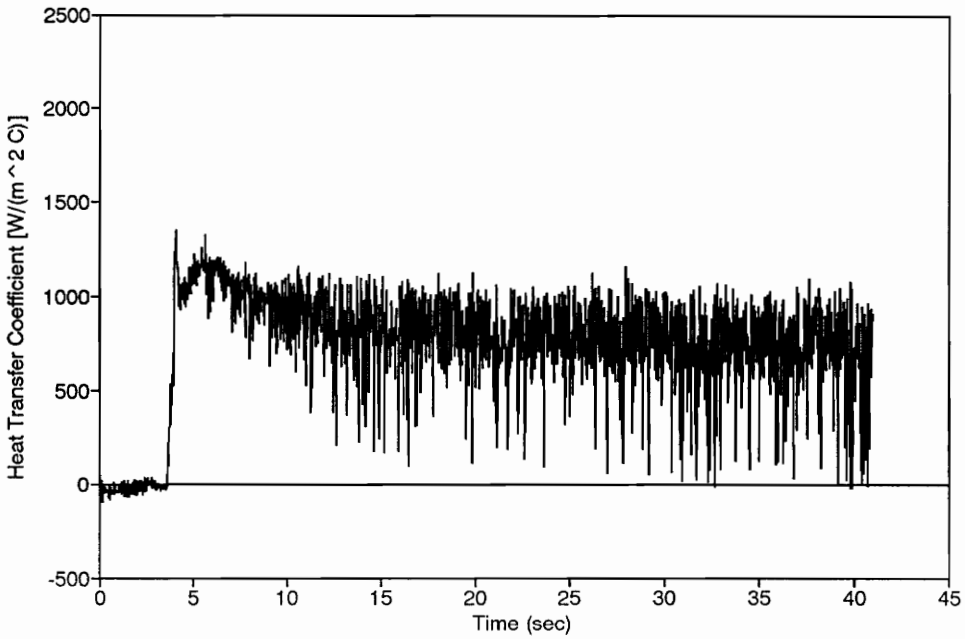

Figure A14. HTC Calculated from Trailing Edge Run 7.

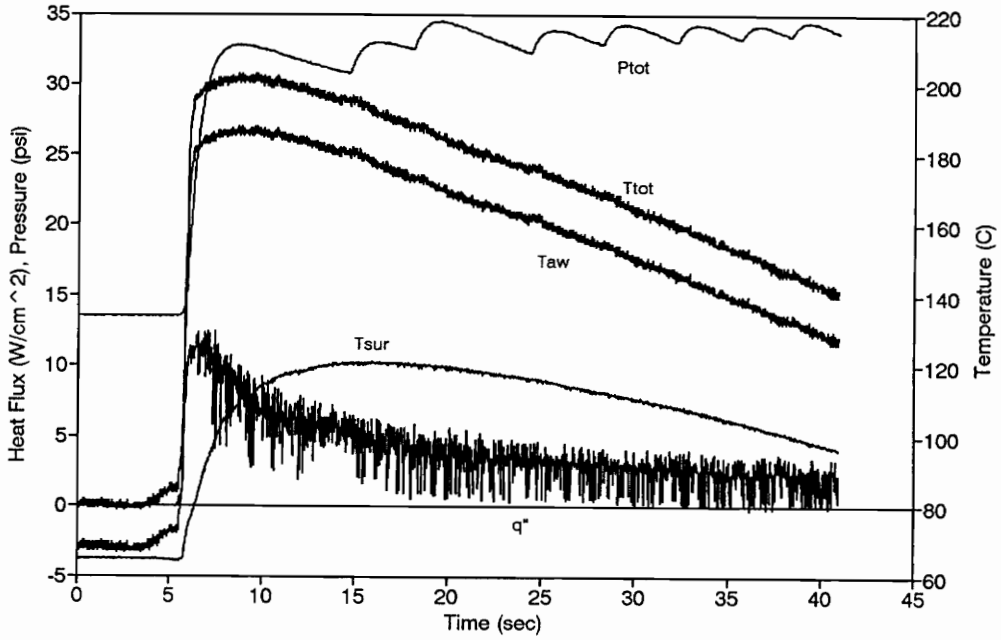

Figure A15. Trailing Edge Gage Run 8.

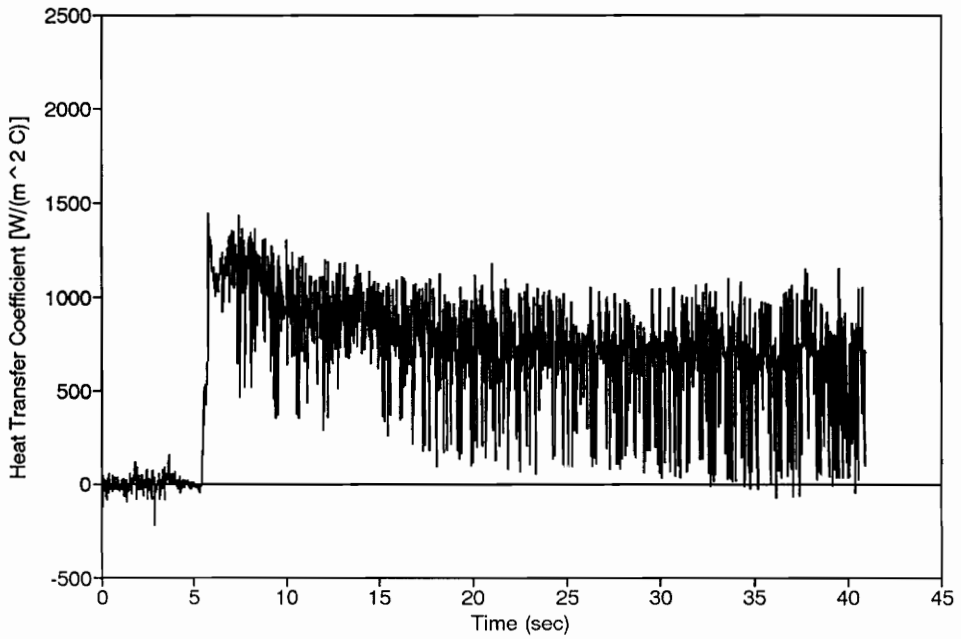

Figure A16. HTC Calculated from Trailing Edge Run 8.

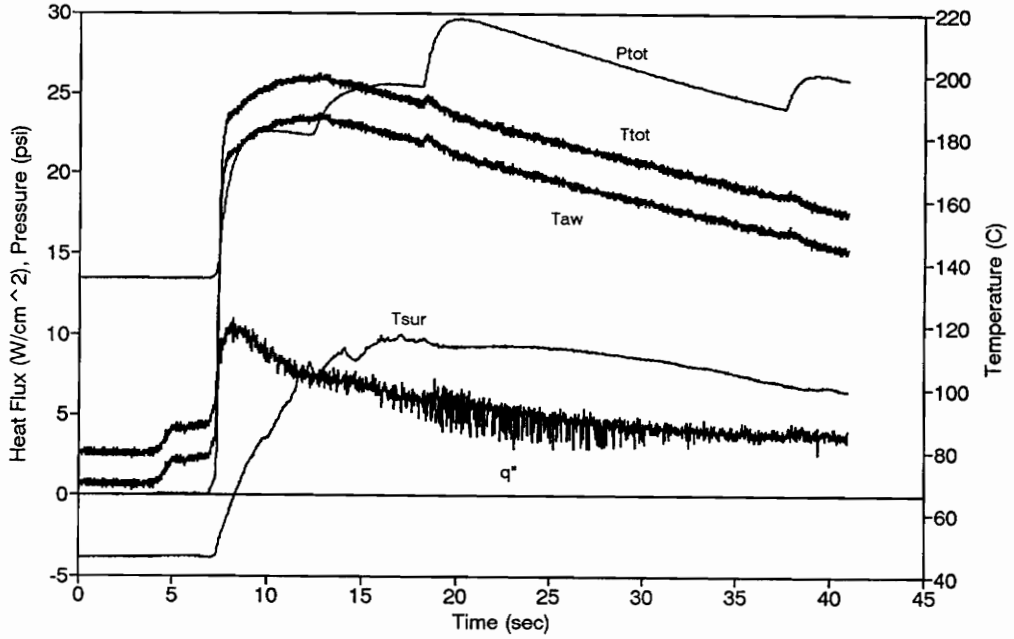

Figure A17. Trailing Edge Gage Run 9.

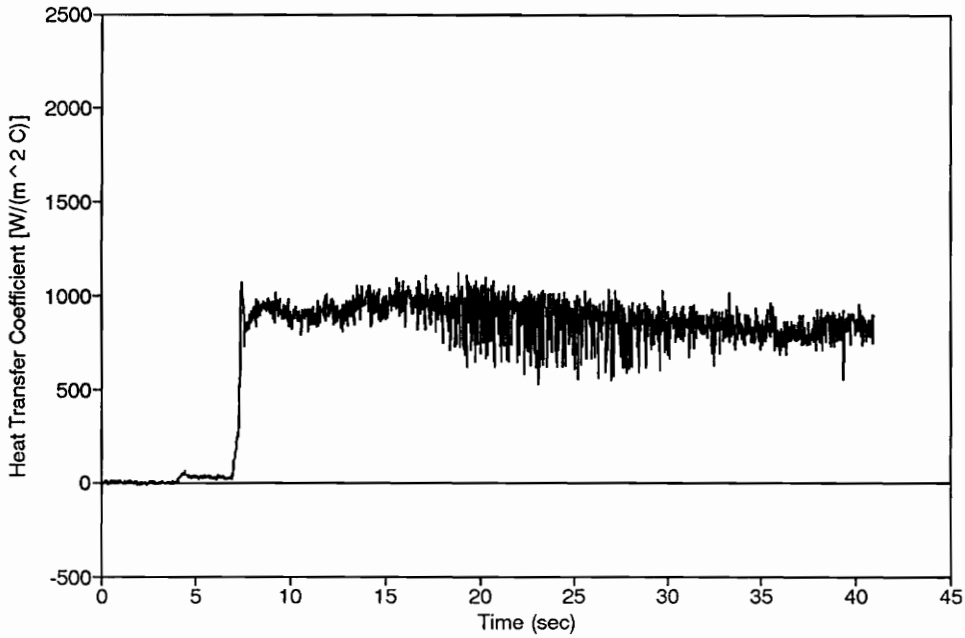

Figure A18. HTC Calculated from Trailing Edge Run 9.

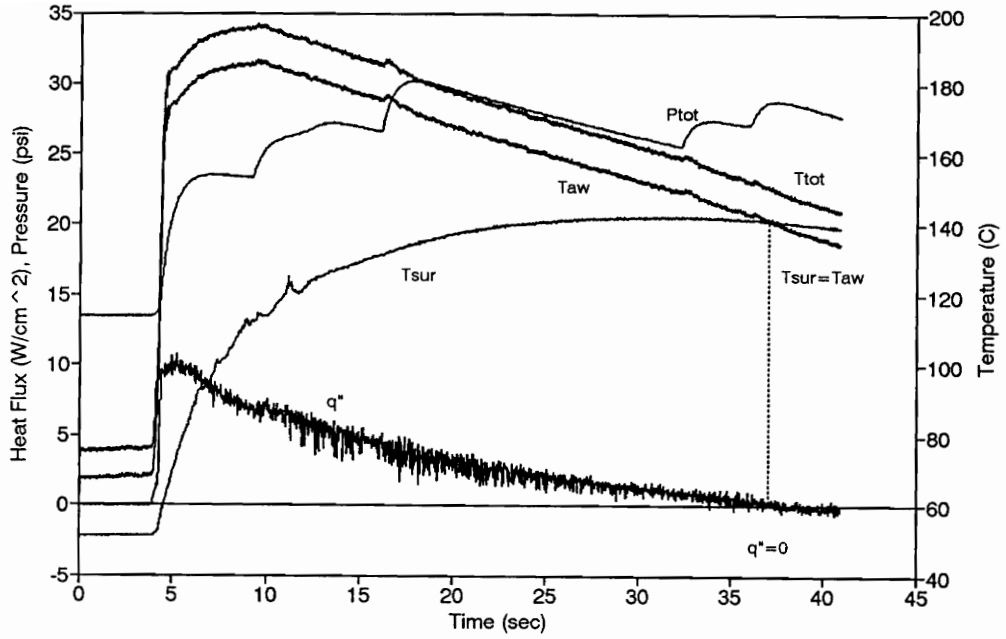

Figure A19. Trailing Edge Gage Run 10.

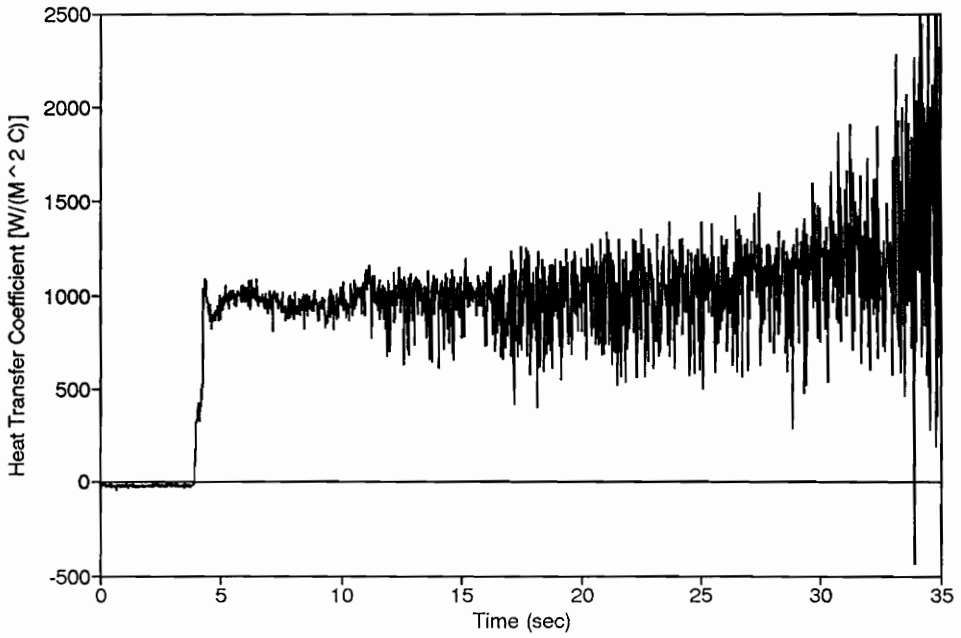

Figure A20. HTC Calculated from Trailing Edge Run 10.

Table A.2a - HFM-6 Leading Edge Gage (No Grid)

Figure	Run Number	Exit Mach #	Ttubes (C)	Humidity (%)
A21,A22	1	1.25	93	8.92
A23,A24	2	1.25	93	6.11
A25,A26	3	1.29	93	3.82
A27,A28	4	1.27	93	3.52
A29,A30	5	1.30	96	3.16
A31,A32	6	1.27	93	3.76
A33,A34	7	1.3	93	N/A
A35,A36	8	1.26	93	6.04
A37,A38	9	1.27	93	5.52

Table A.2b - HFM-6 Leading Edge Gage (Grid 1)

Figure	Run Number	Exit Mach #	Ttubes (C)	Humidity (%)
A39,A40	10	1.29	93	4.05
A41,A42	11	1.29	93	3.86
A43,A44	12	1.28	93	4.69
A45,A46	13	1.24	93	5.91
A47,A48	14	1.26	93	3.75
A49,A50	15	1.29	93	5.48
A51,A52	16	1.30	93	4.78
A53,A54	17	1.29	93	4.28
A55,A56	18	1.30	93	3.90
A57,A58	19	1.29	93	3.76
A59,A60	20	1.20	93	6.70
A61,A62	21	1.24	93	6.30
A63,A64	22	1.25	93	5.64

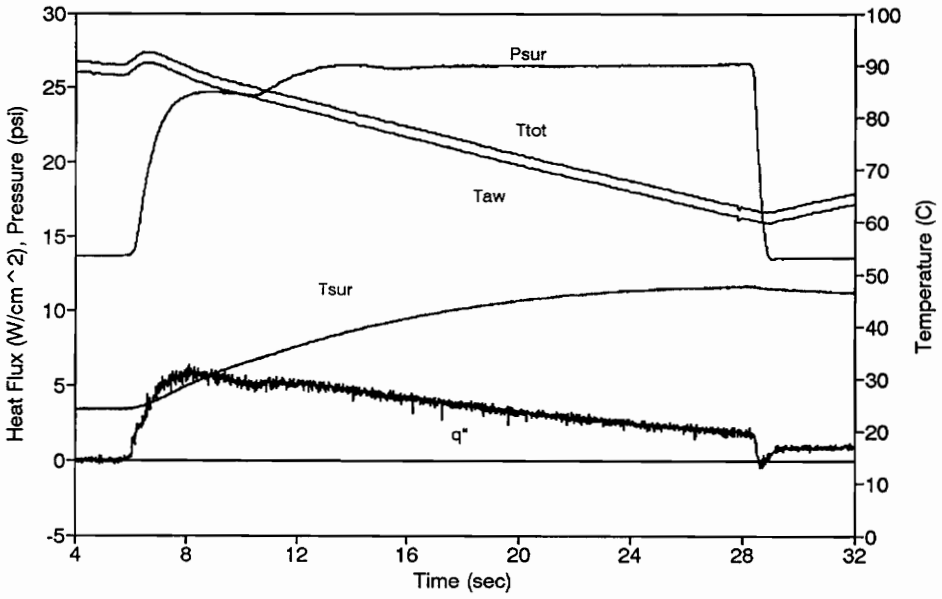

Figure A21. HFM-6 Leading Edge Gage Run 1 - No Grid.

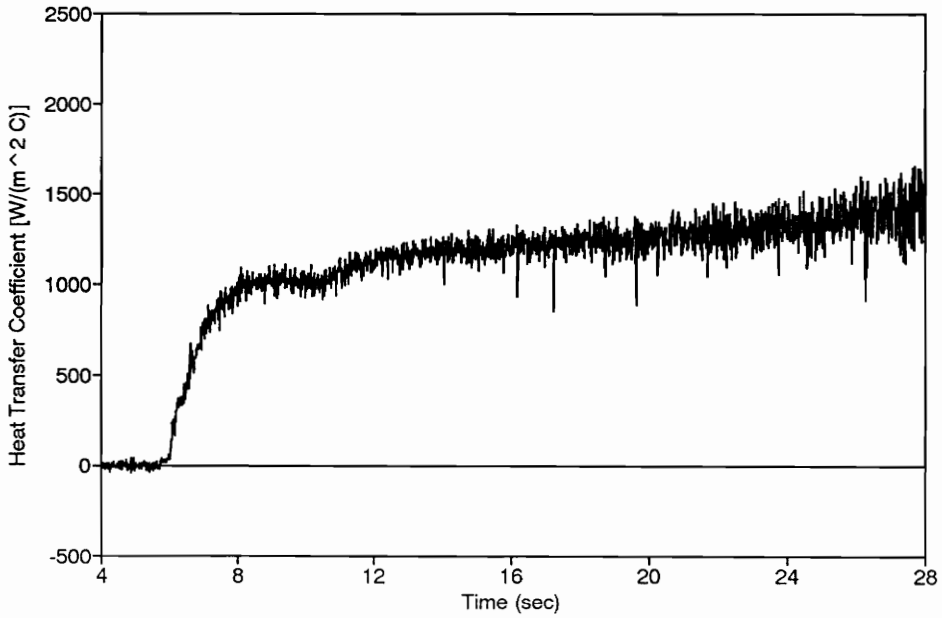

Figure A22. HTC Calculated from HFM-6 Leading Edge Gage Run 1 - No Grid.

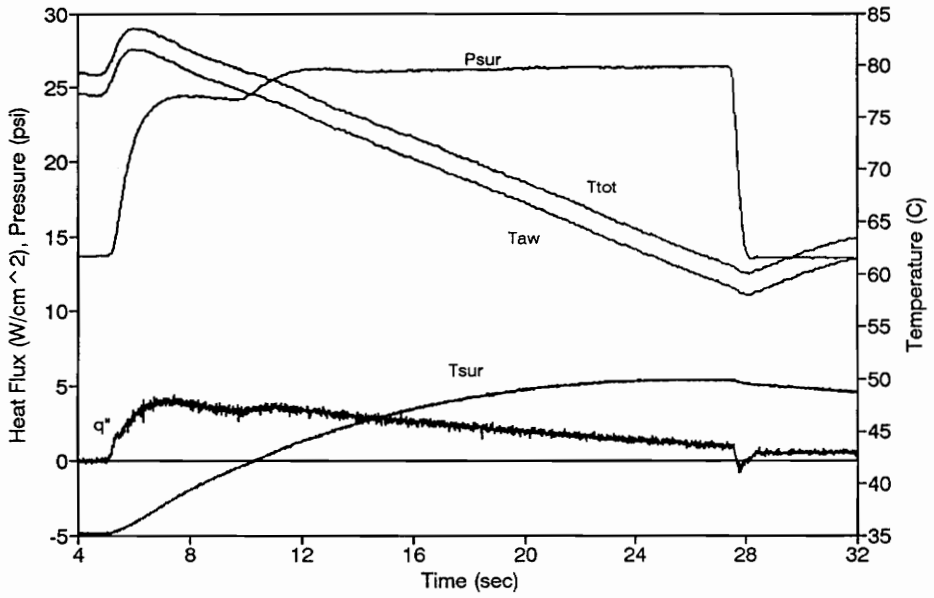

Figure A23. HFM-6 Leading Edge Gage Run 2 - No Grid.

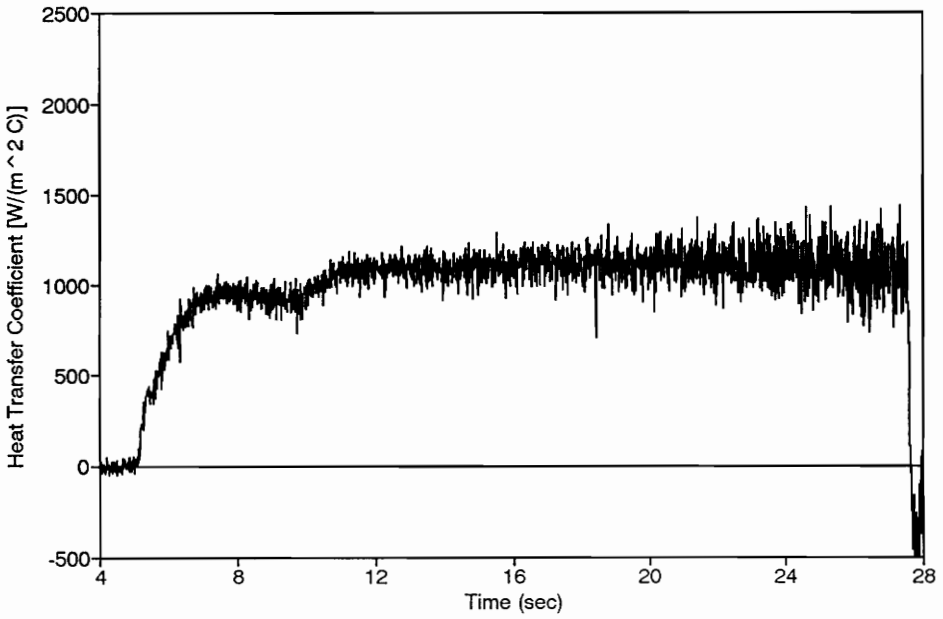

Figure A24. HTC Calculated from HFM-6 Leading Edge Gage Run 2 - No Grid.

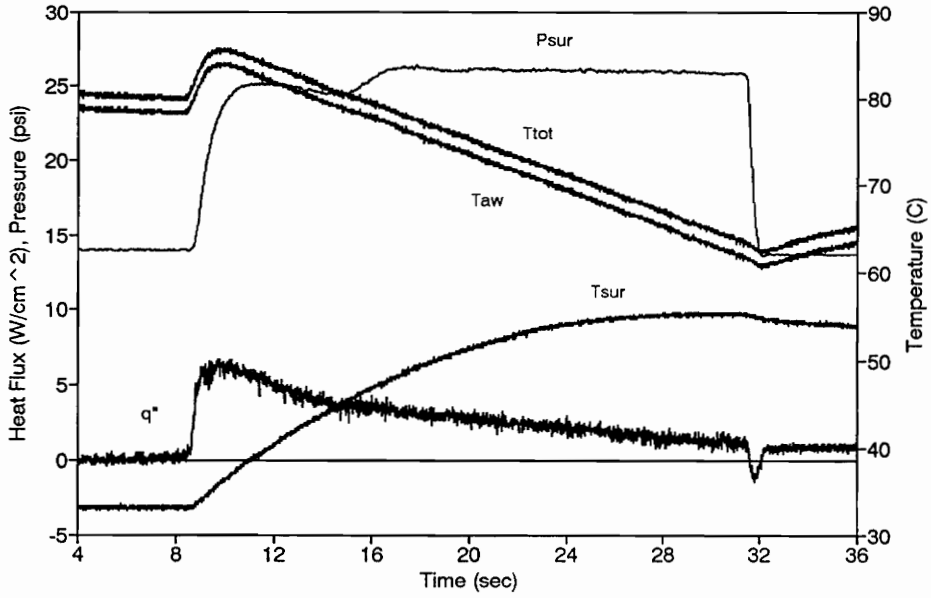

Figure A25. HFM-6 Leading Edge Gage Run 3 - No Grid.

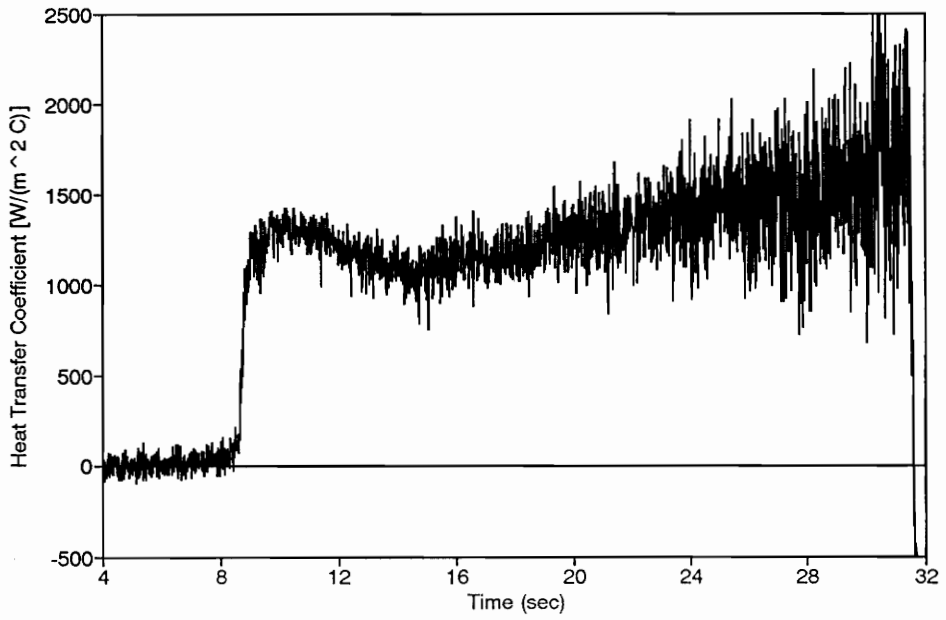

Figure A26. HTC Calculated from HFM-6 Leading Edge Gage Run 3 - No Grid.

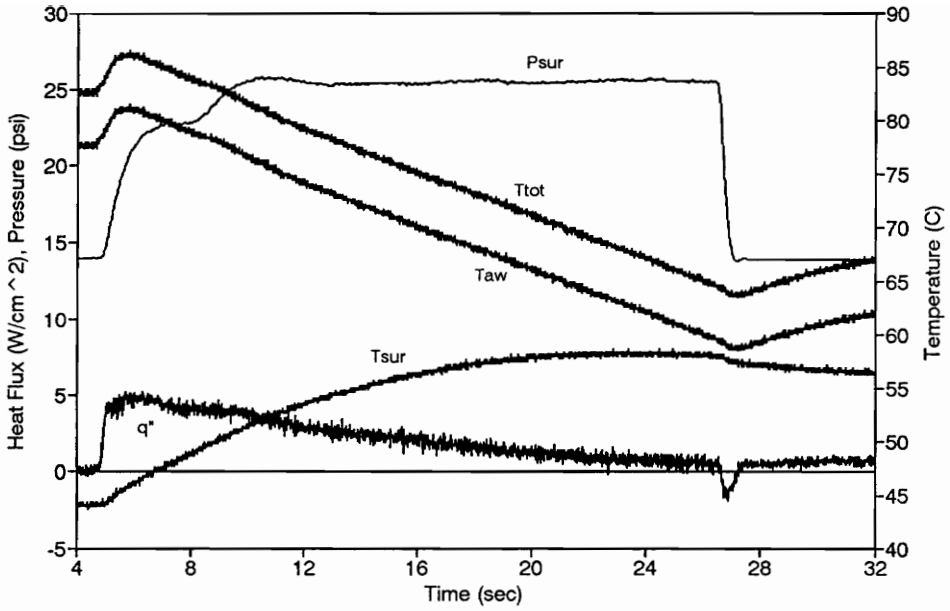

Figure A27. HFM-6 Leading Edge Gage Run 4 - No Grid.

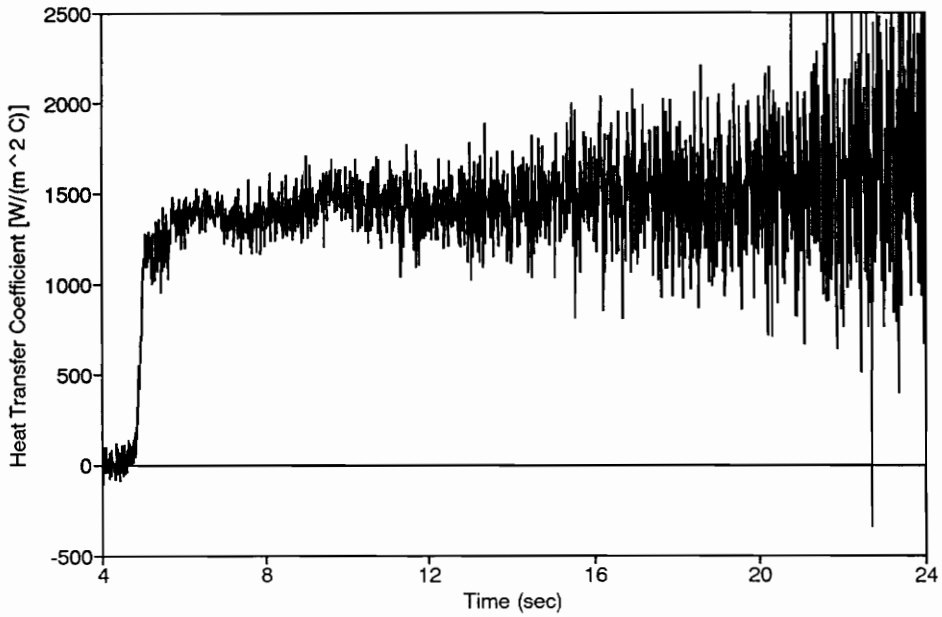

Figure A28. HTC Calculated from HFM-6 Leading Edge Gage Run 4 - No Grid.

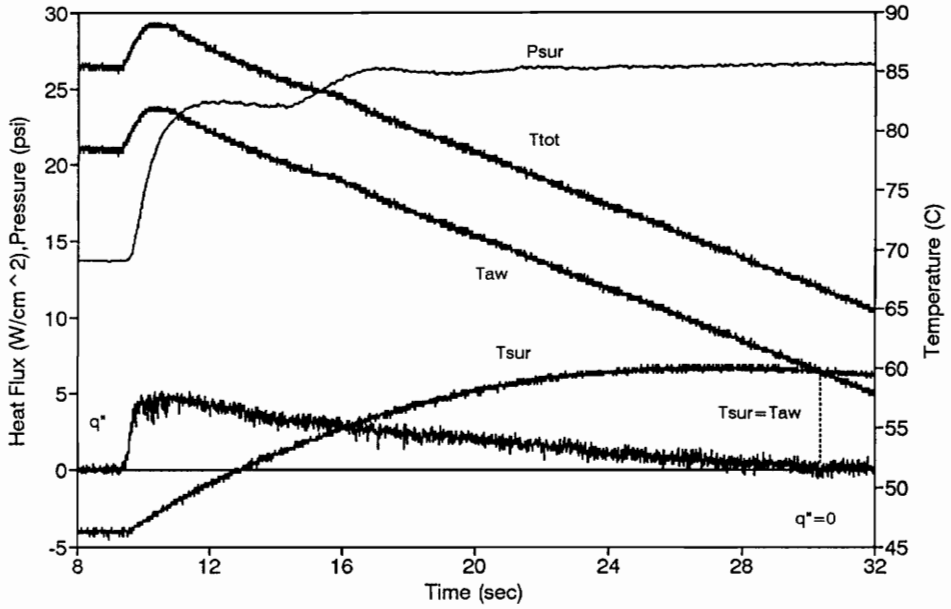

Figure A29. HFM-6 Leading Edge Gage Run 5 - No Grid.

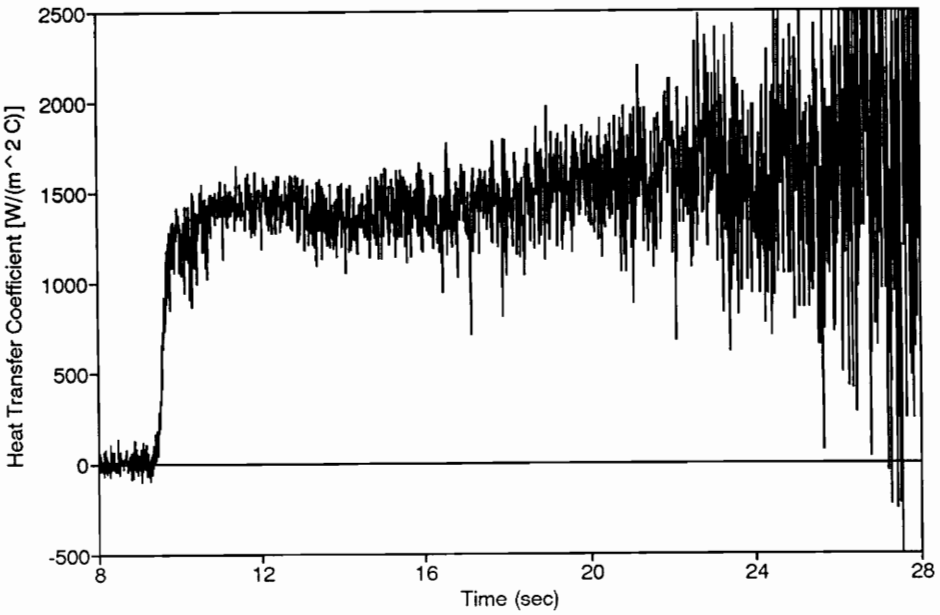

Figure A30. HTC Calculated from HFM-6 Leading Edge Gage Run 5 - No Grid.

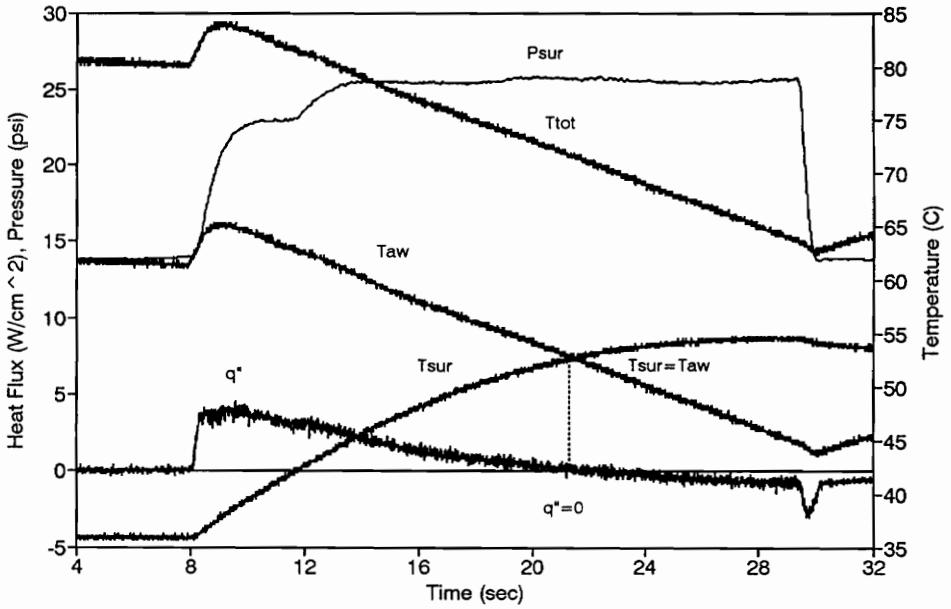

Figure A31. HFM-6 Leading Edge Gage Run 6 - No Grid.

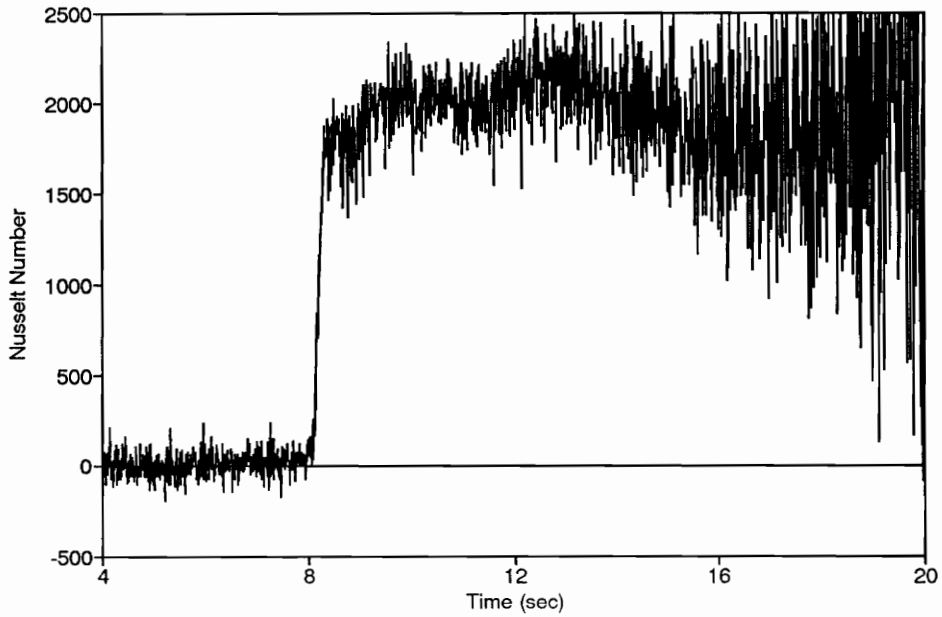

Figure A32. HTC Calculated from HFM-6 Leading Edge Gage Run 6 - No Grid.

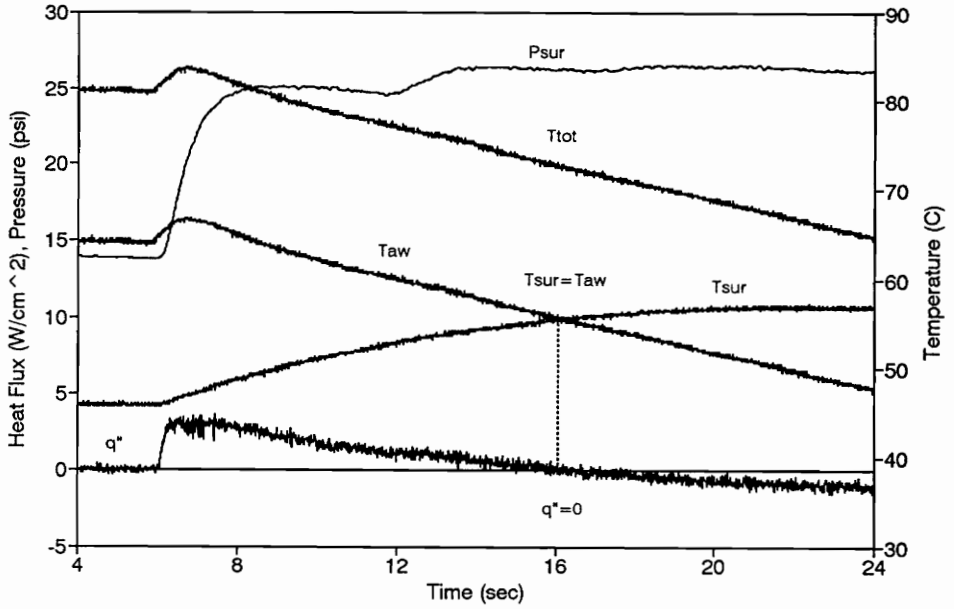

Figure A33. HFM-6 Leading Edge Gage Run 7 - No Grid.

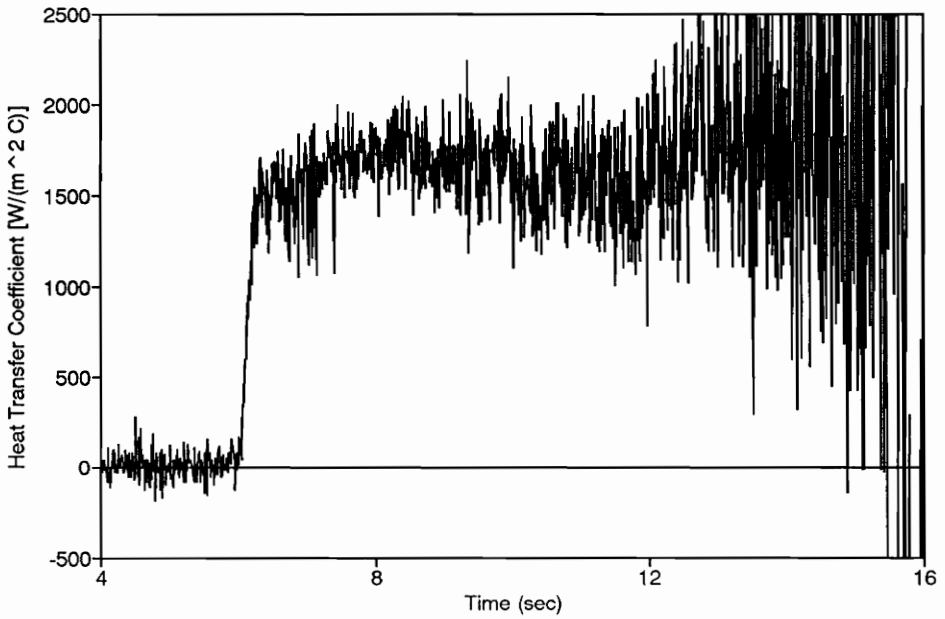

Figure A34. HTC Calculated from HFM-6 Leading Edge Gage Run 7 - No Grid.

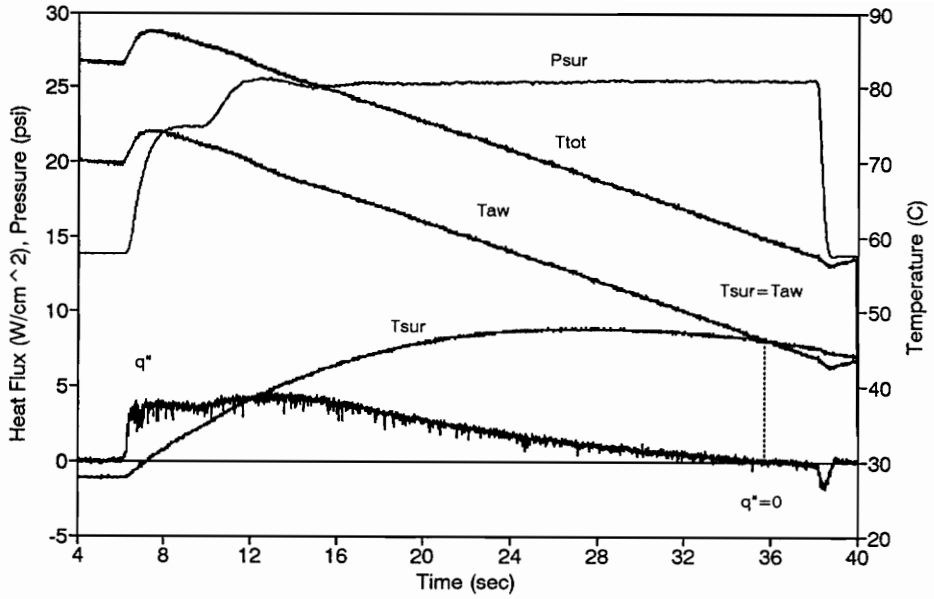

Figure A35. HFM-6 Leading Edge Gage Run 8 - No Grid.

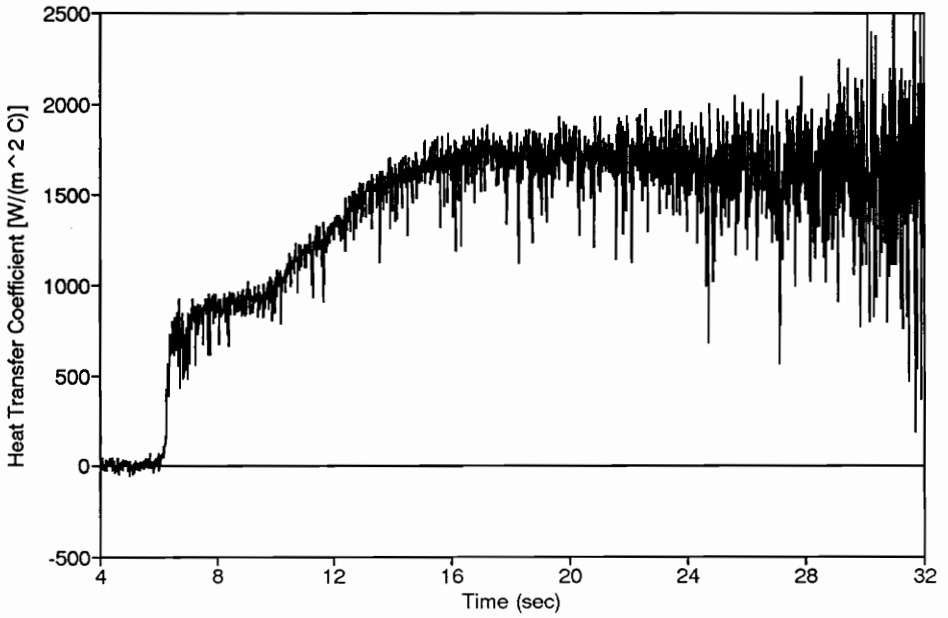

Figure A36. HTC Calculated from HFM-6 Leading Edge Gage Run 8 - No Grid.

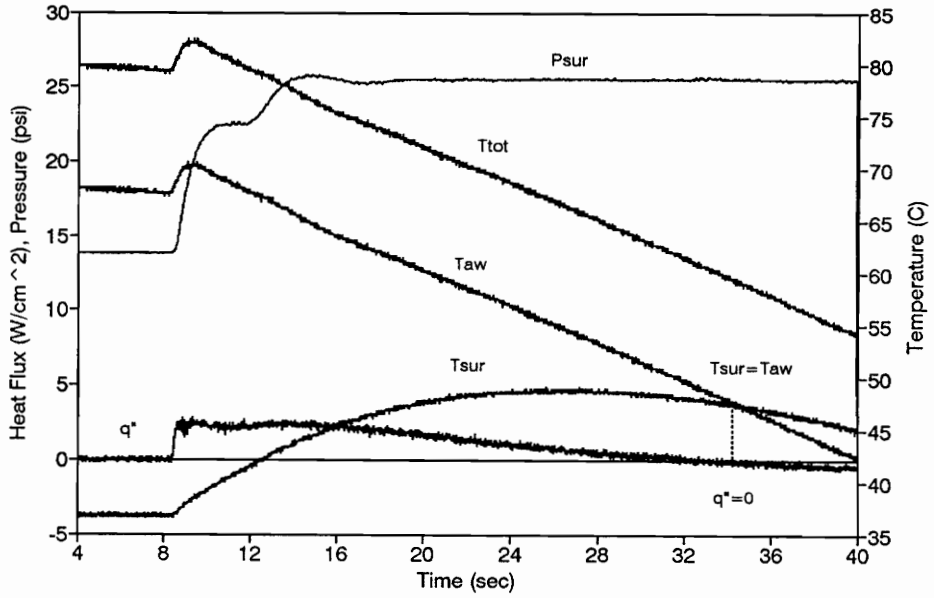

Figure A37. HFM-6 Leading Edge Gage Run 9 - No Grid.

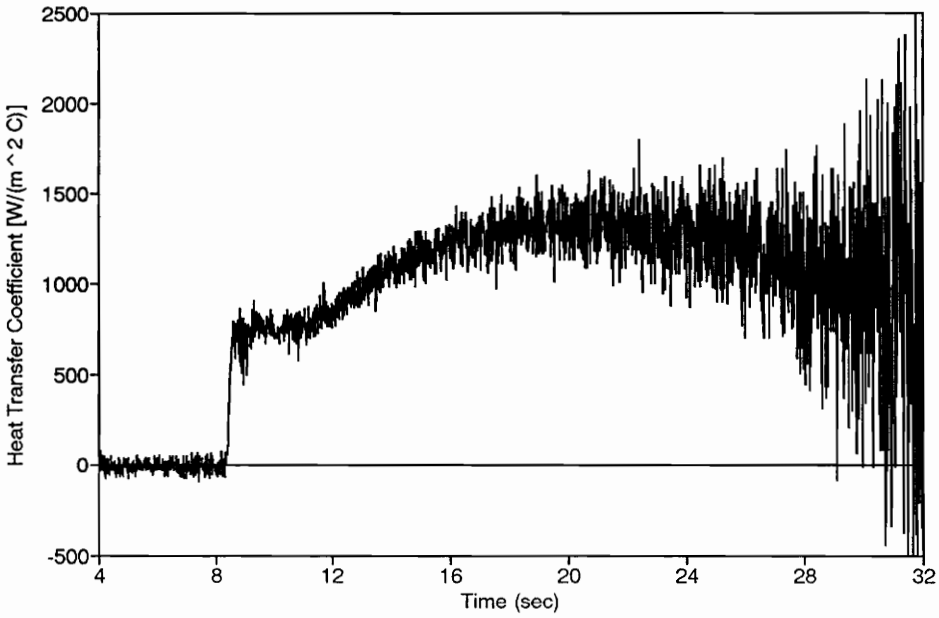

Figure A38. HTC Calculated from HFM-6 Leading Edge Gage Run 9 - No Grid.

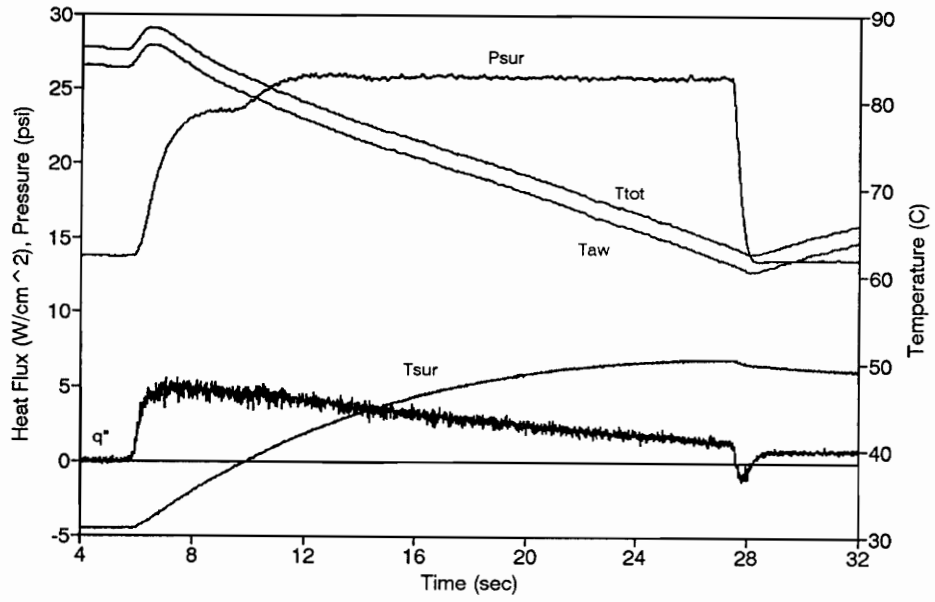

Figure A39. HFM-6 Leading Edge Gage Run 10 - Grid 1.

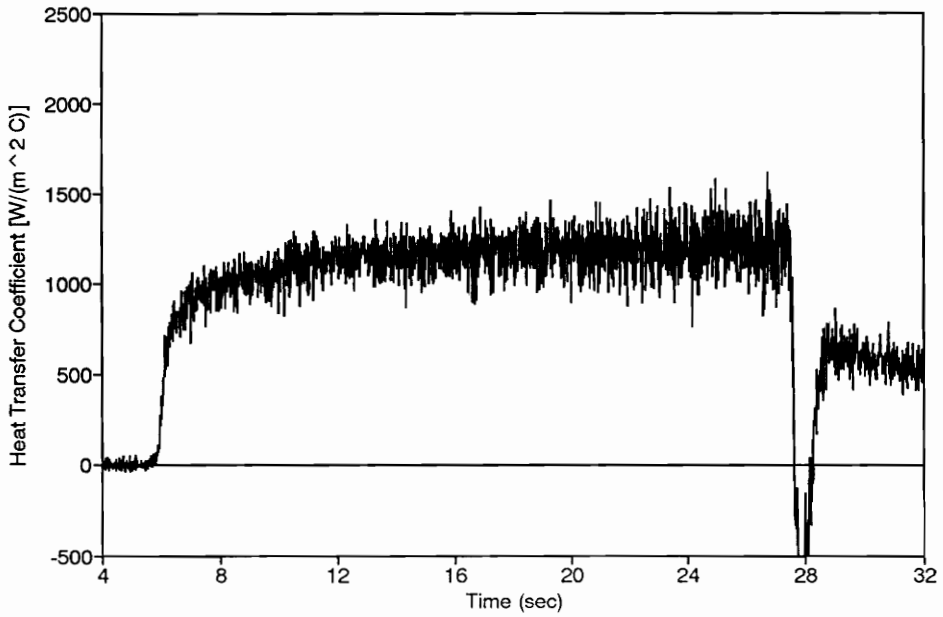

Figure A40. HTC Calculated from HFM-6 Leading Edge Gage Run 10.

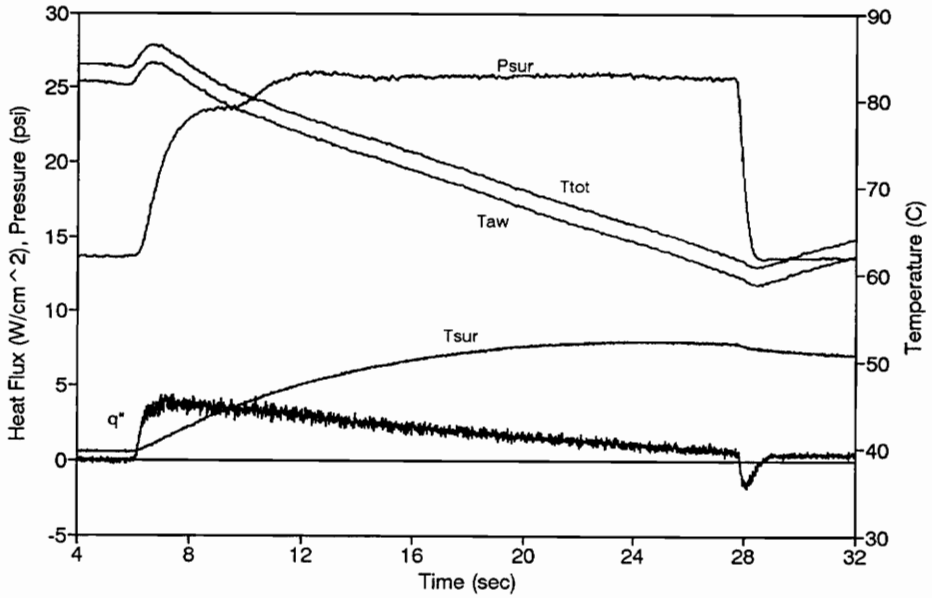

Figure A41. HFM-6 Leading Edge Gage Run 11 - Grid 1.

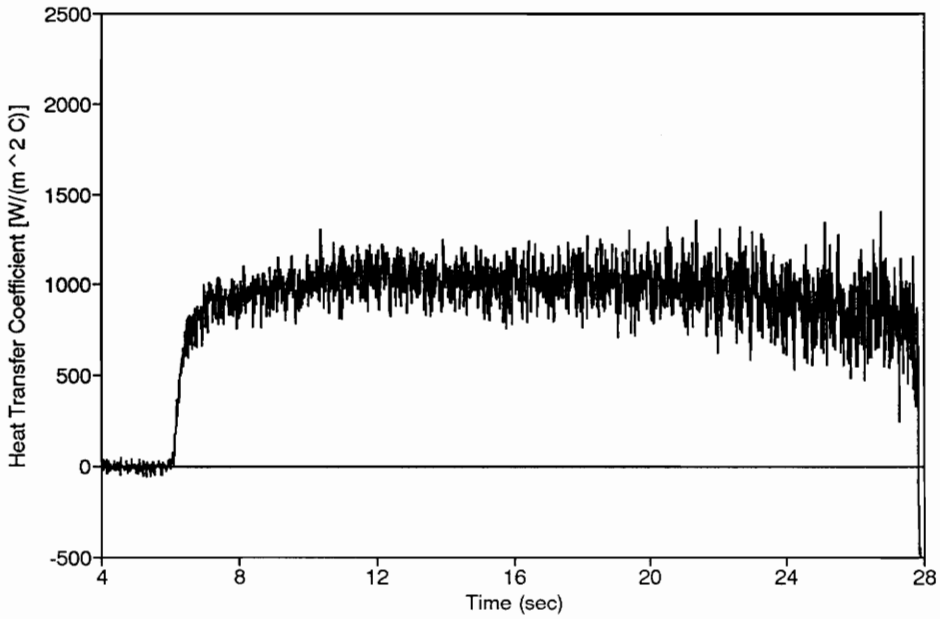

Figure A42. HTC Calculated from HFM-6 Leading Edge Gage Run 11 - Grid 1.

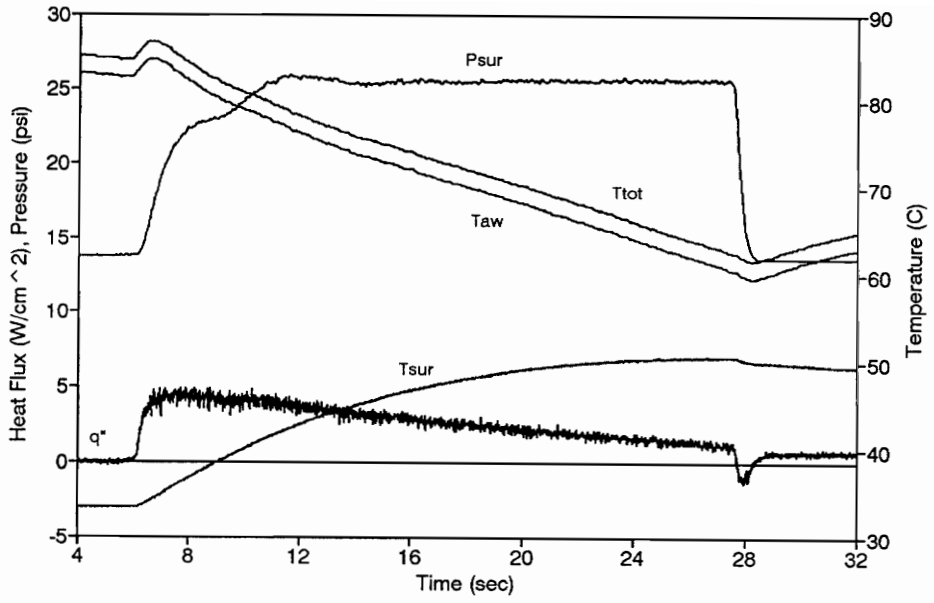

Figure A43. HFM-6 Leading Edge Gage Run 12 - Grid 1.

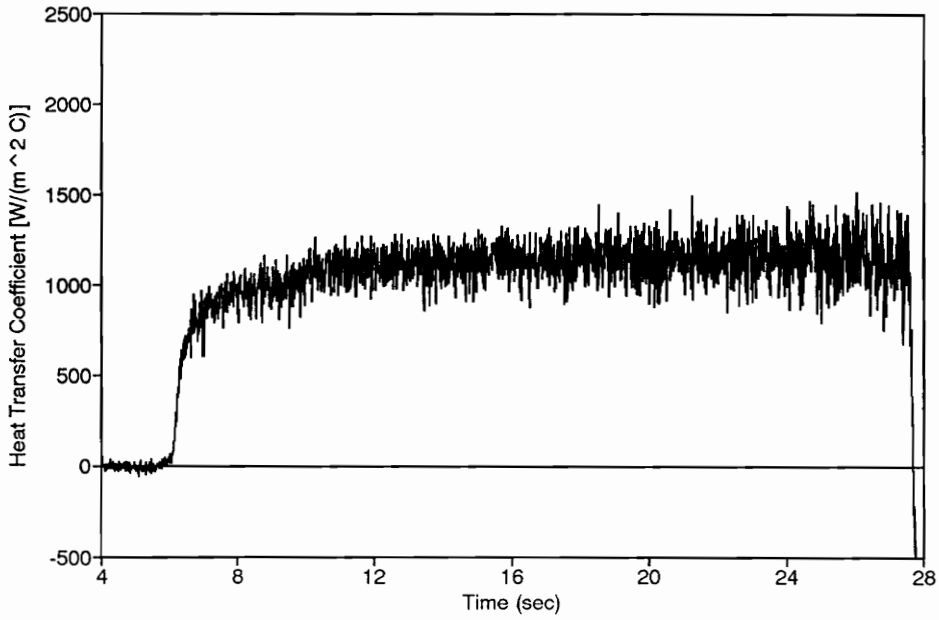

Figure A44. HTC Calculated from HFM-6 Leading Edge Gage Run 12 - Grid 1.

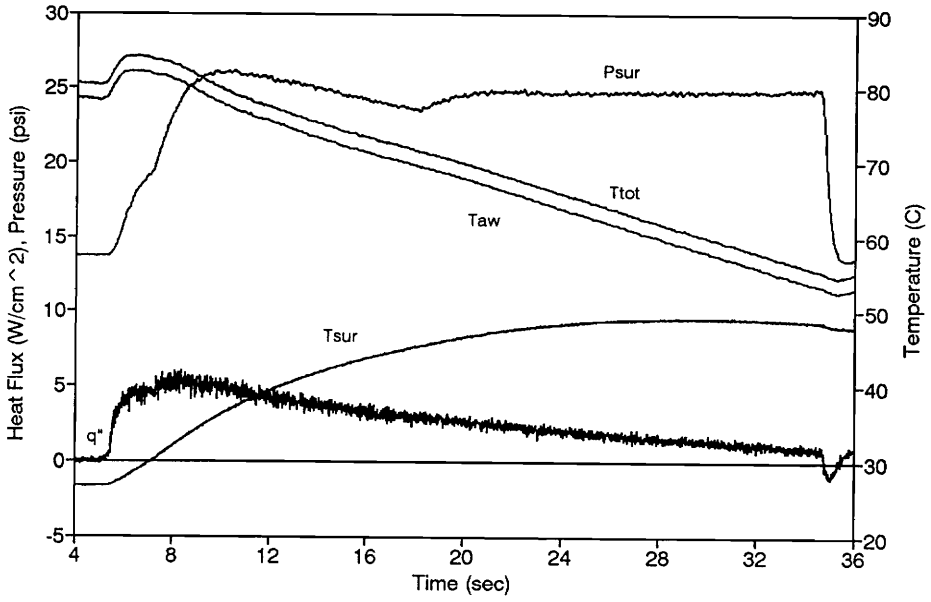

Figure A45. HFM-6 Leading Edge Gage Run 13 - Grid 1.

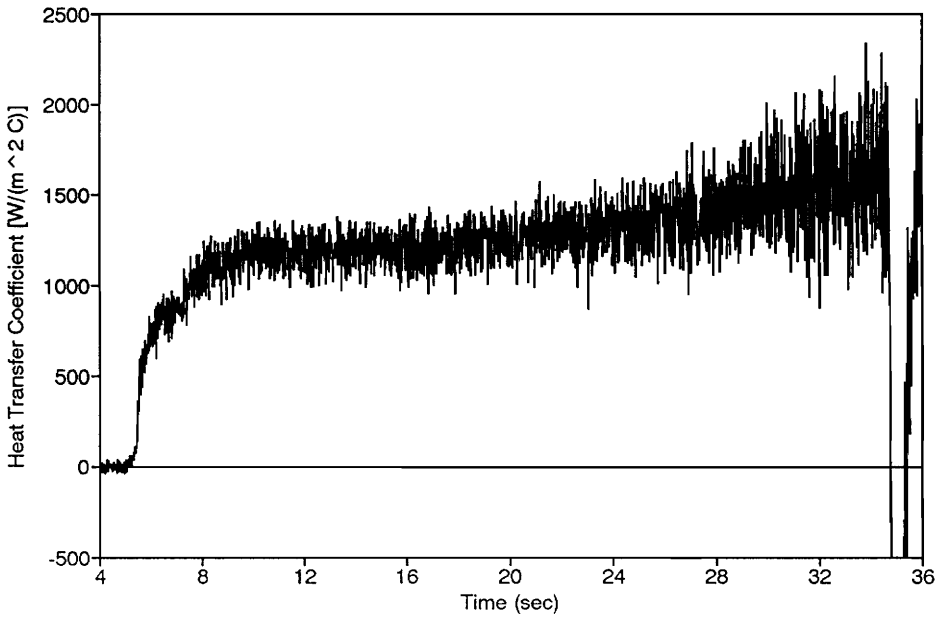

Figure A46. HTC Calculated from HFM-6 Leading Edge Gage Run 13 - Grid 1.

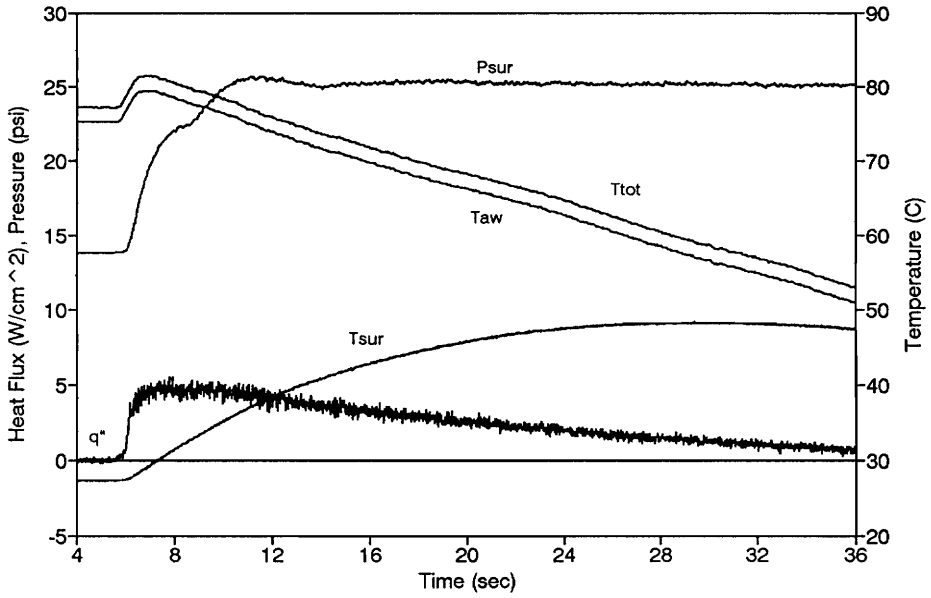

Figure A47. HFM-6 Leading Edge Gage Run 14 - Grid 1.

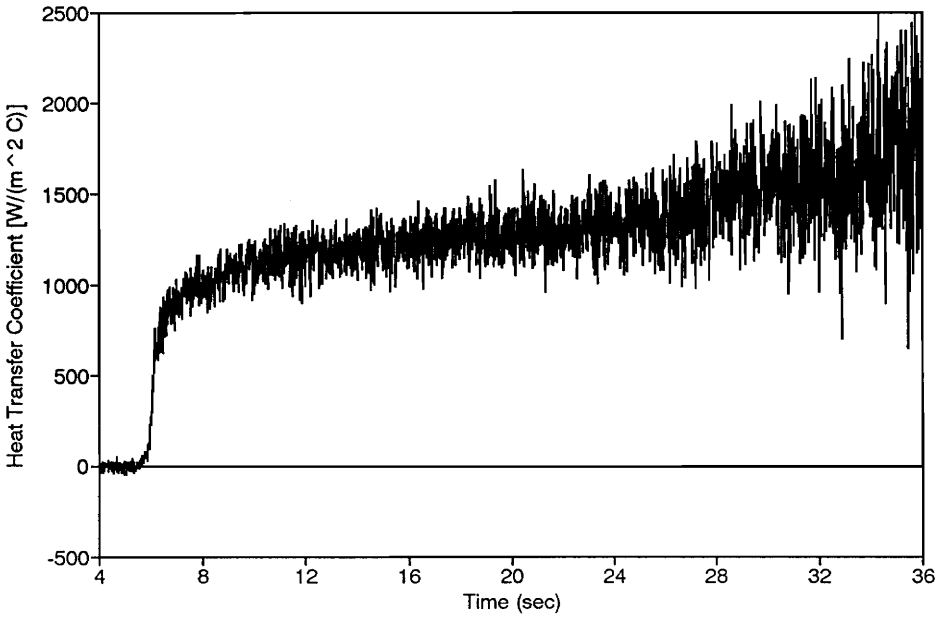

Figure A48. HTC Calculated from HFM-6 Leading Edge Gage Run 14 - Grid 1.

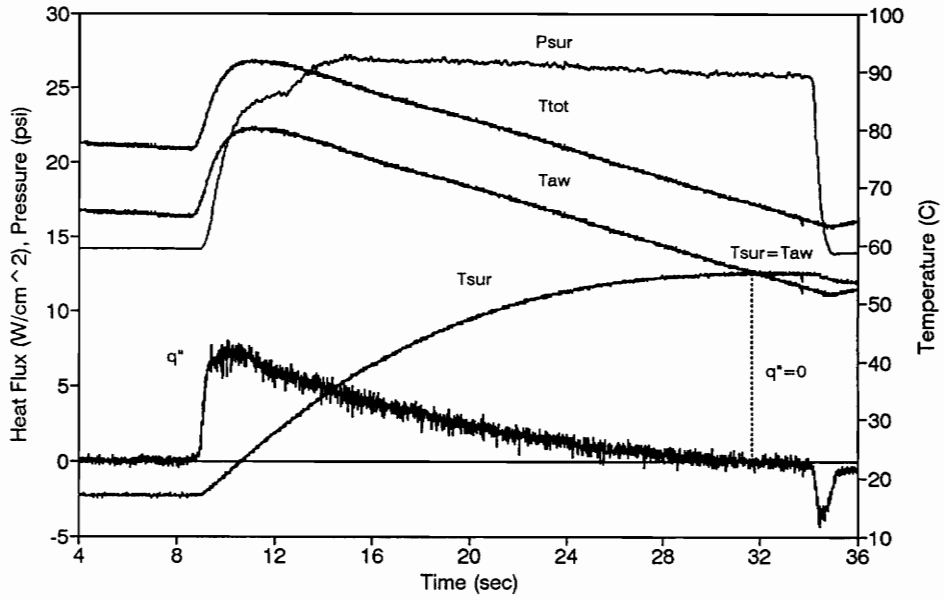

Figure A49. HFM-6 Leading Edge Gage Run 15 - Grid 1.

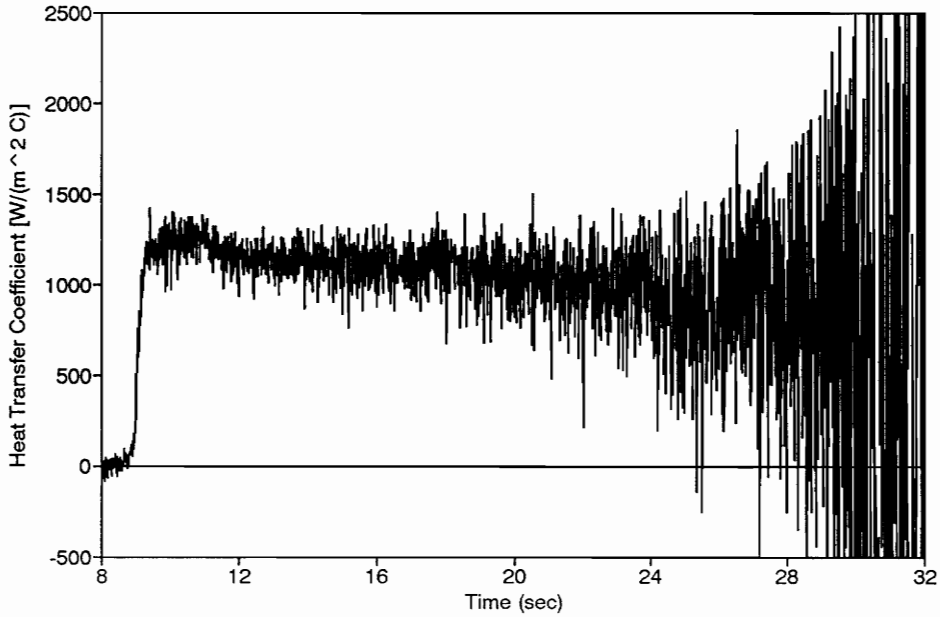

Figure A50. HTC Calculated from HFM-6 Leading Edge Gage Run 15 - Grid 1.

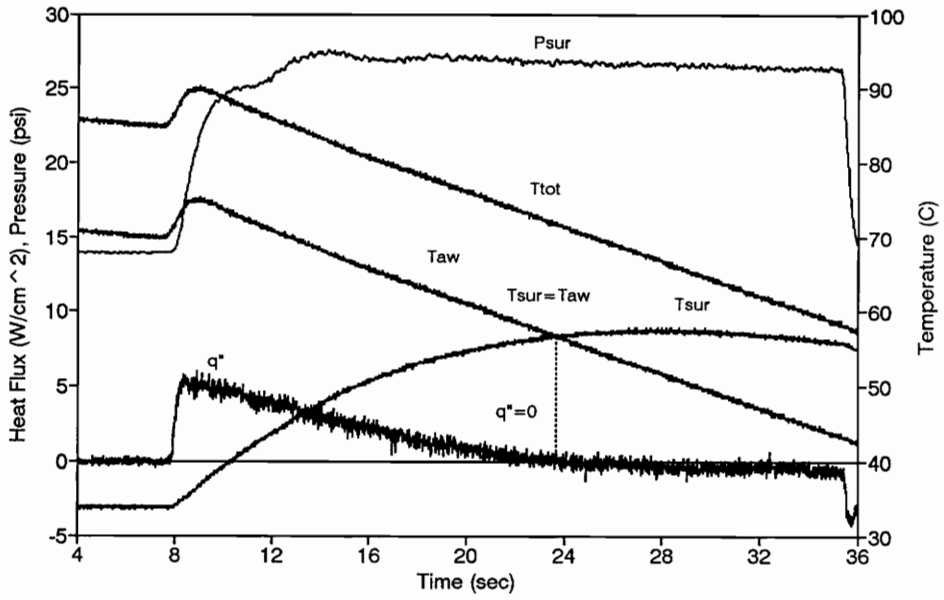

Figure A51. HFM-6 Leading Edge Gage Run 16 - Grid 1.

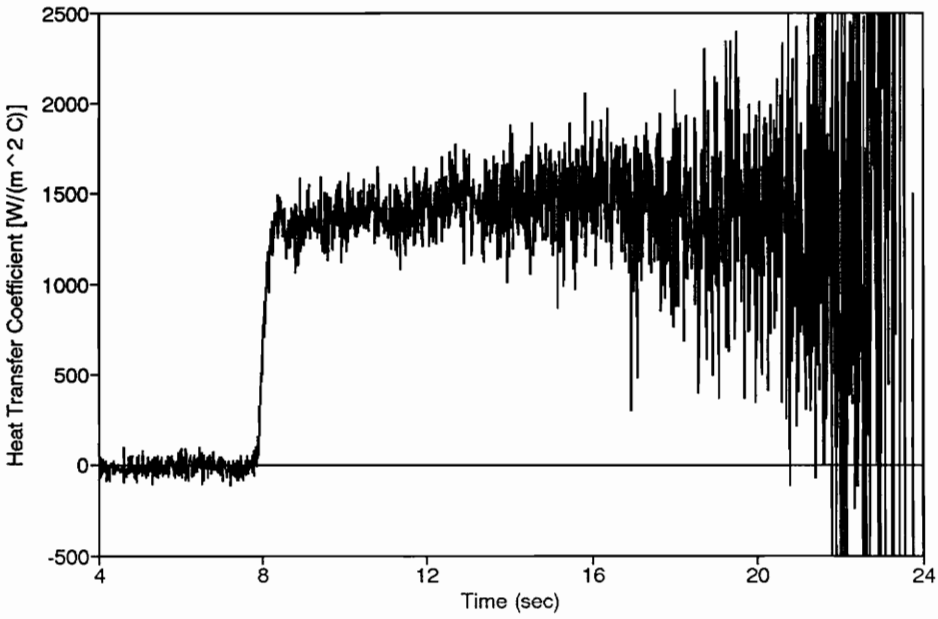

Figure A52. HTC Calculated from HFM-6 Leading Edge Gage Run 16 - Grid 1.

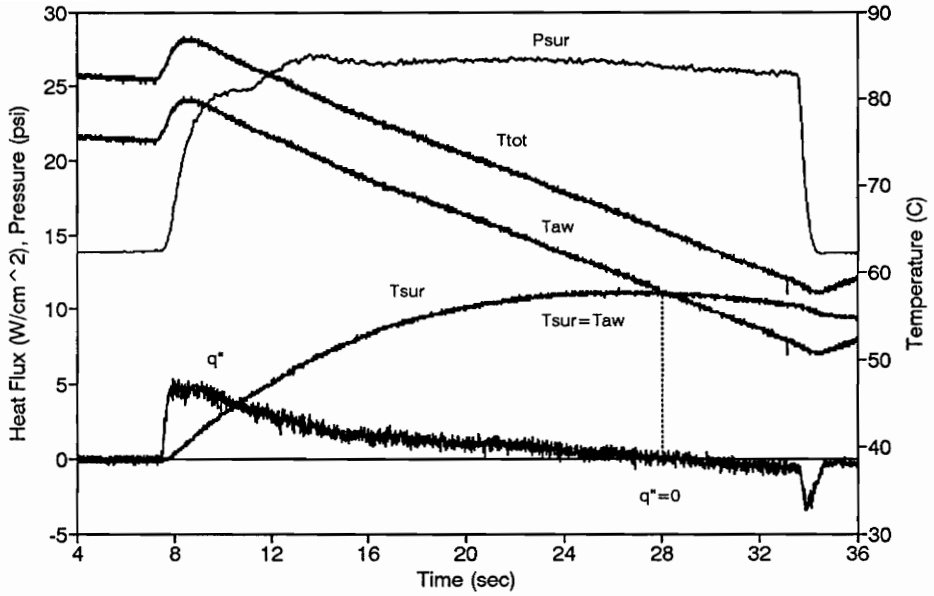

Figure A53. HFM-6 Leading Edge Gage Run 17 - Grid 1.

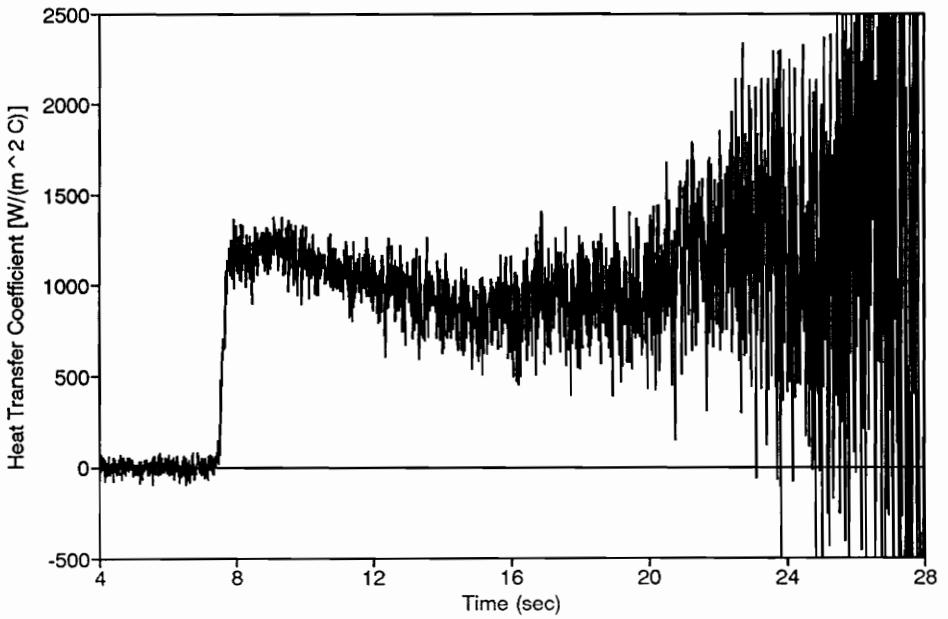

Figure A54. HTC Calculated from HFM-6 Leading Edge Gage Run 17 - Grid 1.

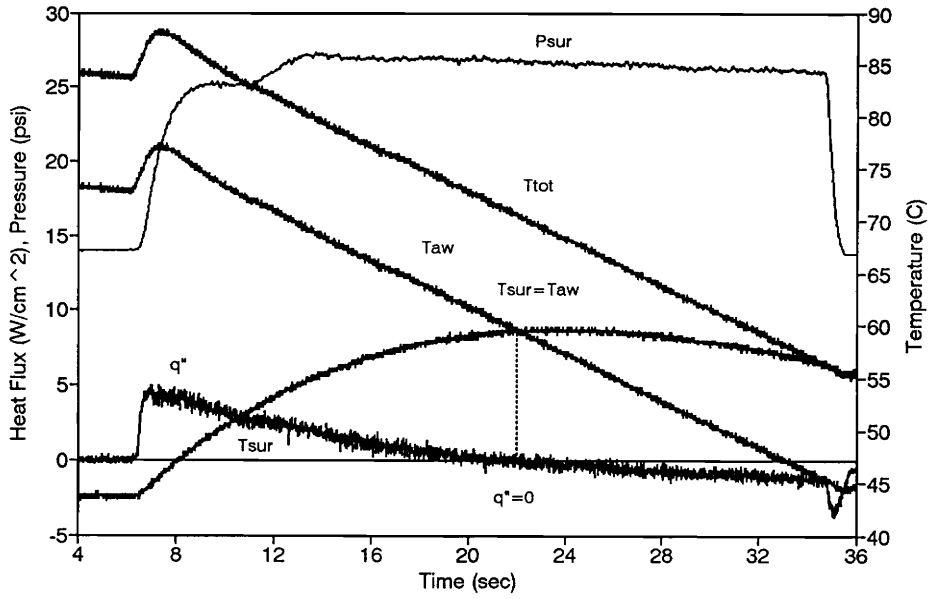

Figure A55. HFM-6 Leading Edge Gage Run 18 - Grid 1.

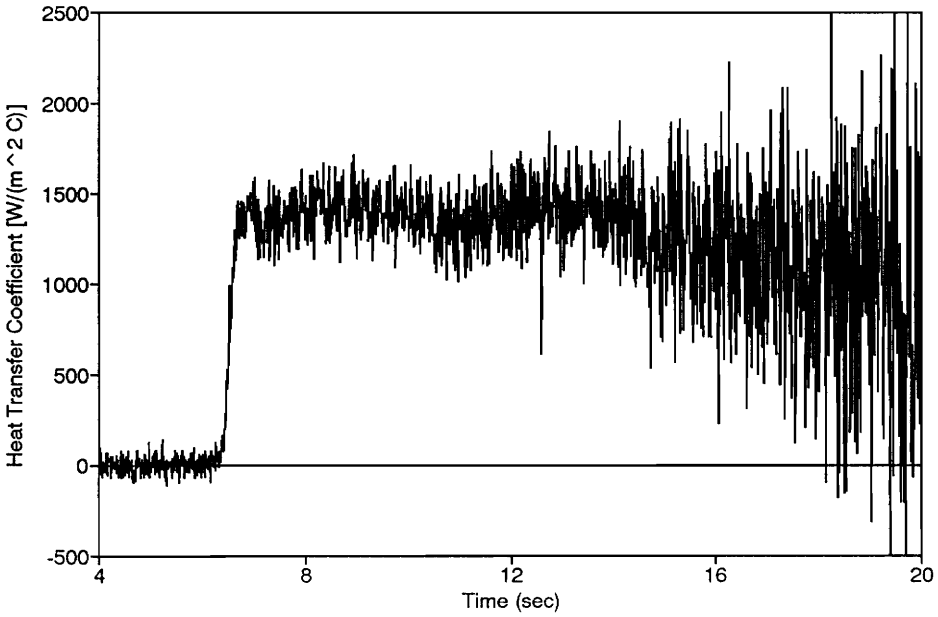

Figure A56. HTC Calculated from HFM-6 Leading Edge Gage Run 18 - Grid 1.

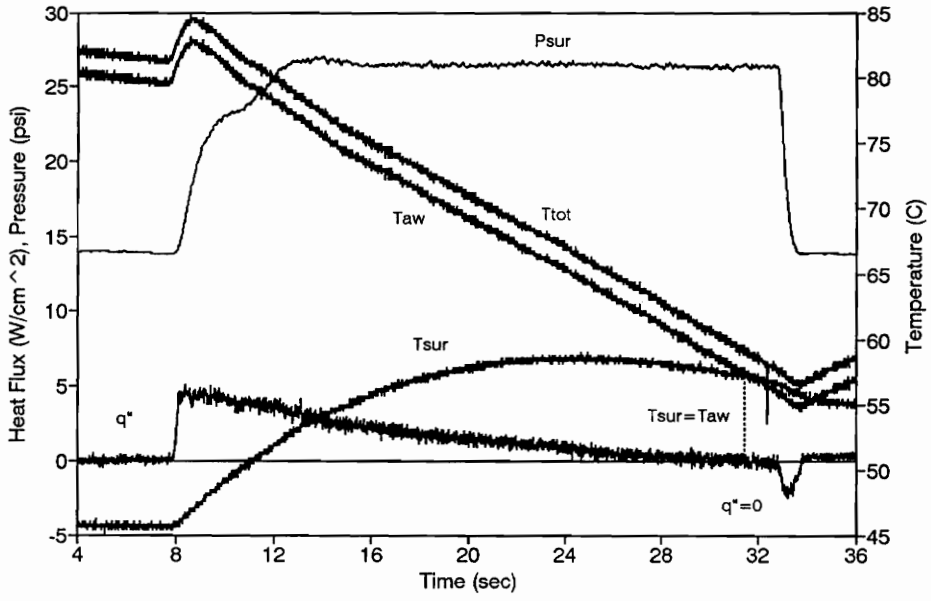

Figure A57. HFM-6 Leading Edge Gage Run 19 - Grid 1.

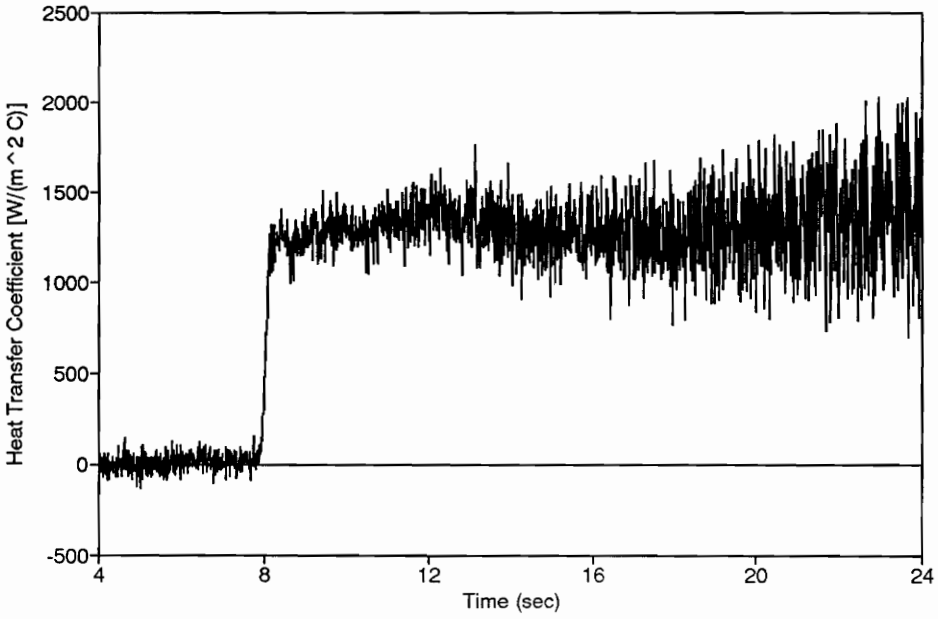

Figure A58. HTC Calculated from HFM-6 Leading Edge Gage Run 19 - Grid 1.

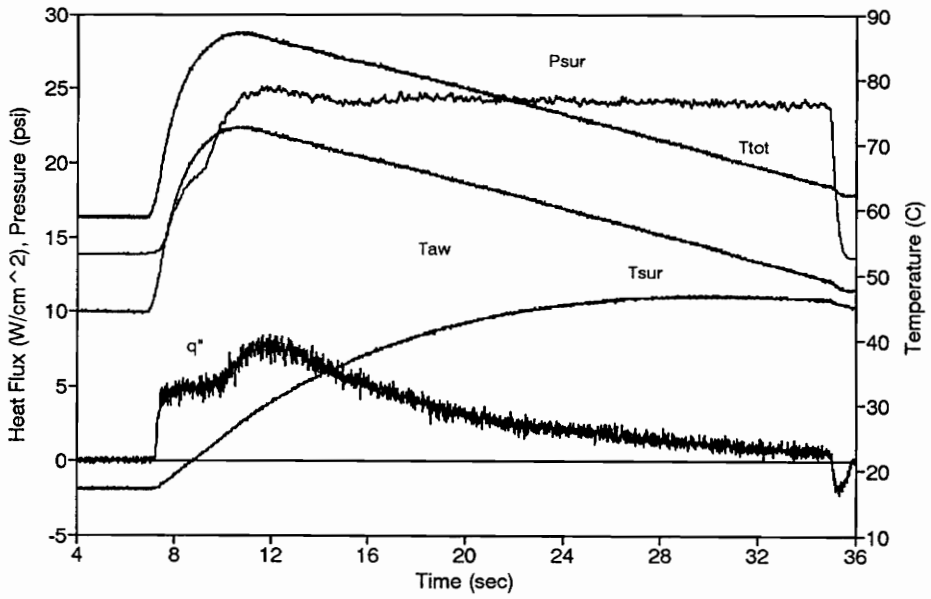

Figure A59. HFM-6 Leading Edge Gage Run 20 - Grid 1.

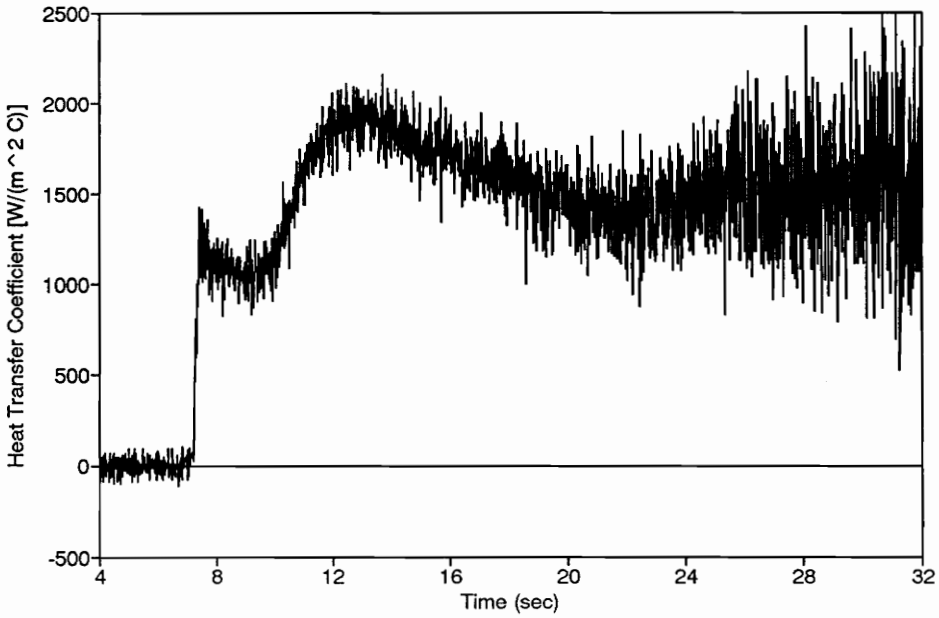

Figure A60. HTC Calculated from HFM-6 Leading Edge Gage Run 20 - Grid 1.

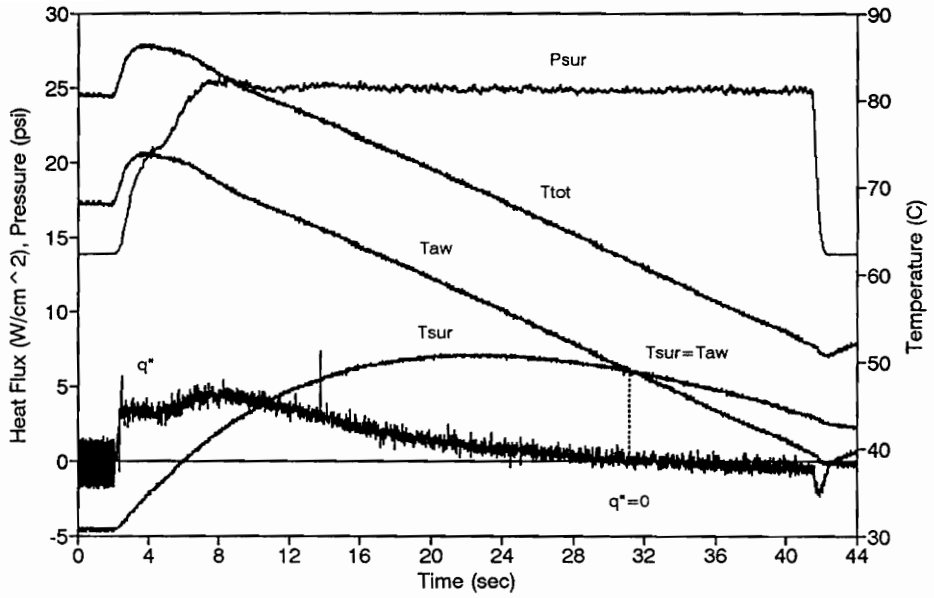

Figure A61. HFM-6 Leading Edge Gage Run 21 - Grid 1.

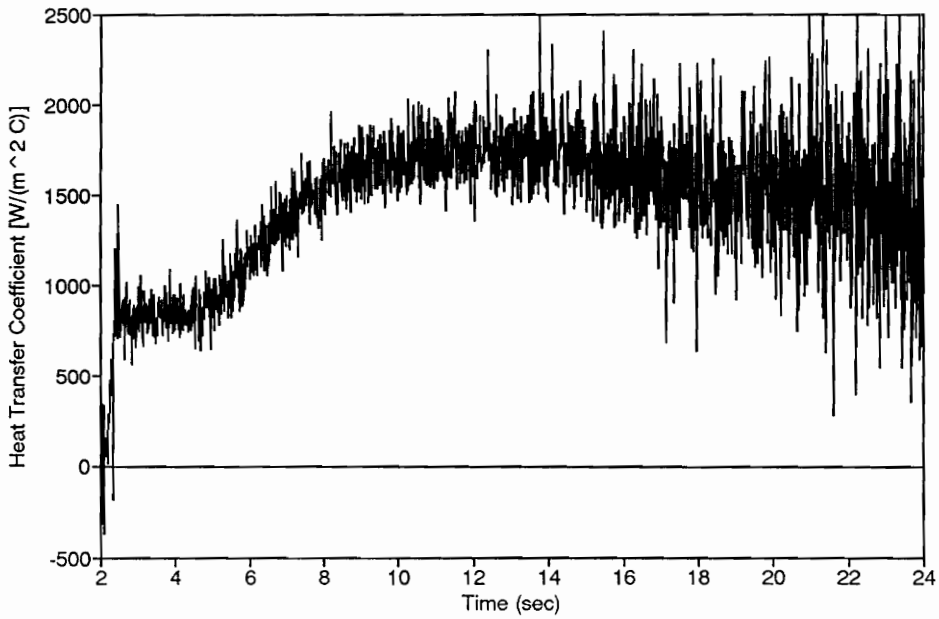

Figure A62. HTC Calculated from HFM-6 Leading Edge Gage Run 21 - Grid 1.

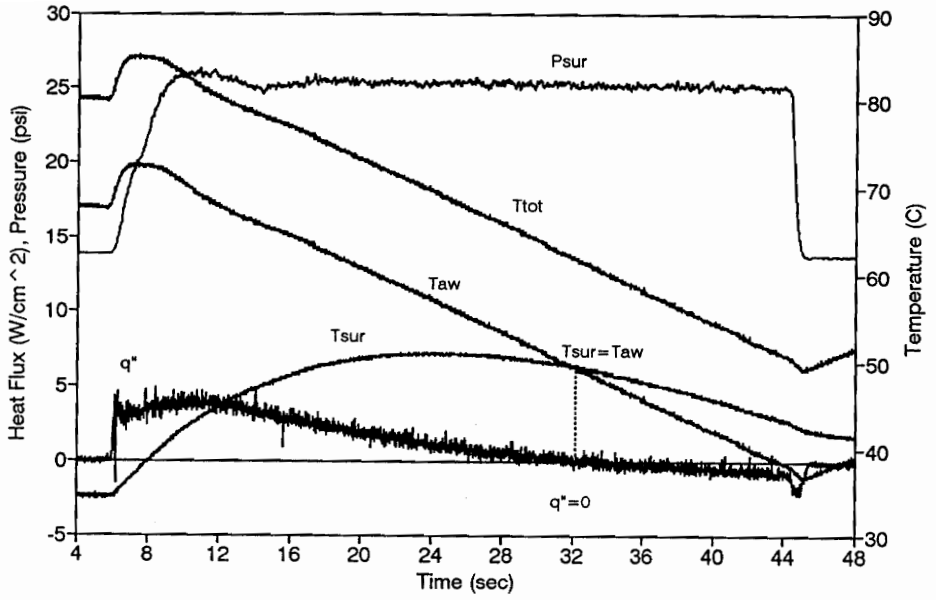

Figure A63. HFM-6 Leading Edge Gage Run 22 - Grid 1.

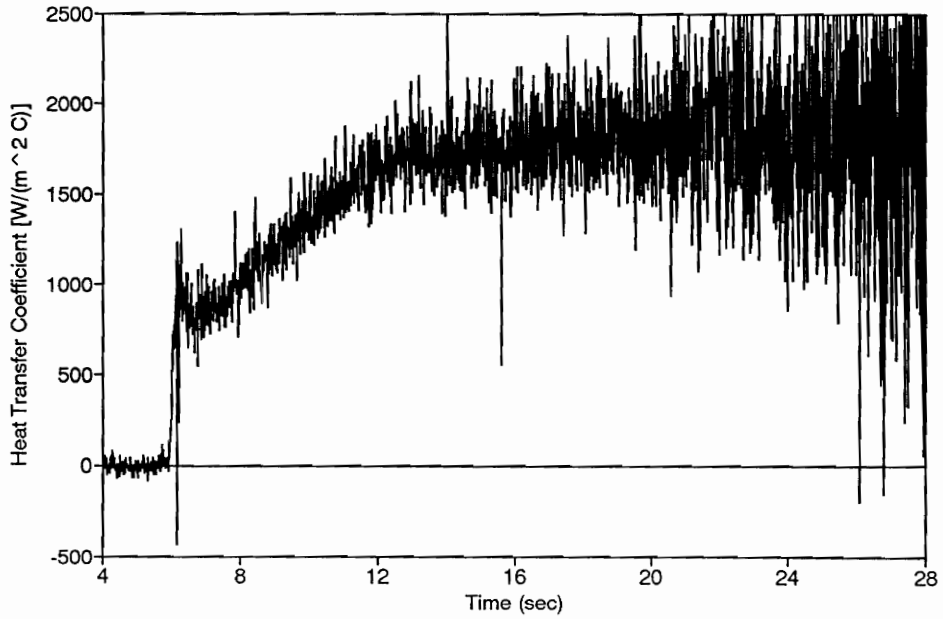

Figure A64. HTC Calculated from HFM-6 Leading Edge Gage Run 22 - Grid 1.

Table A.3 - Leading Edge Line Gage

Figure	Run #	Exit Mach #	Ttubes(C)	Humidity(%)
A65,A66	1 - Grid1	1.25	94.4	5.1
A67,A68	2 - Grid 1	1.18	96.1	4.4
A69,A70	3 - Grid 1	1.15	96.1	3.8
A71,A72	4 - No grid	1.22	94.4	5.0
A73,A74	5 - No grid	1.20	94.4	4.4
A75,A76	6 - No grid	1.26	96.1	4.1

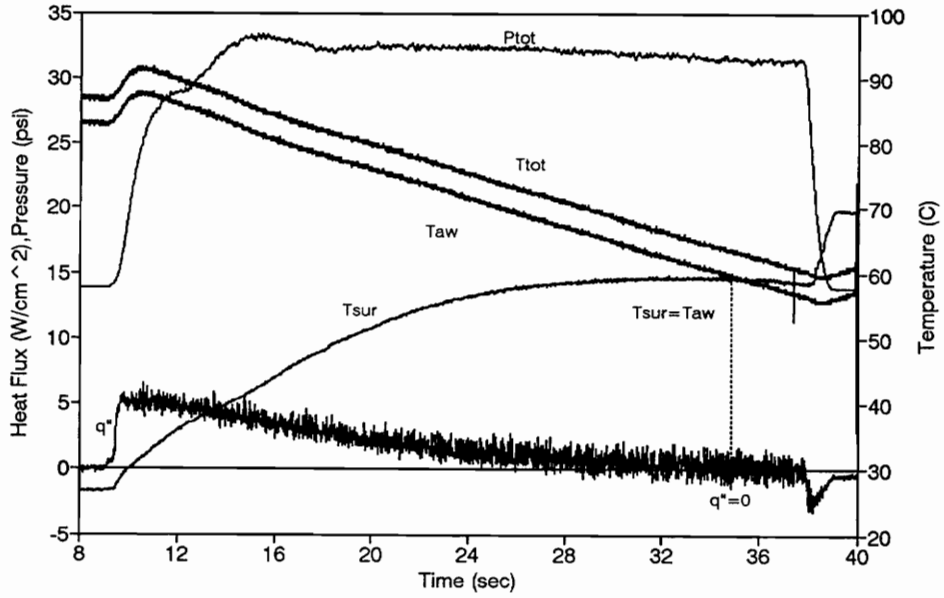

Figure A65. Leading Edge Line Gage Run 1 - No Grid.

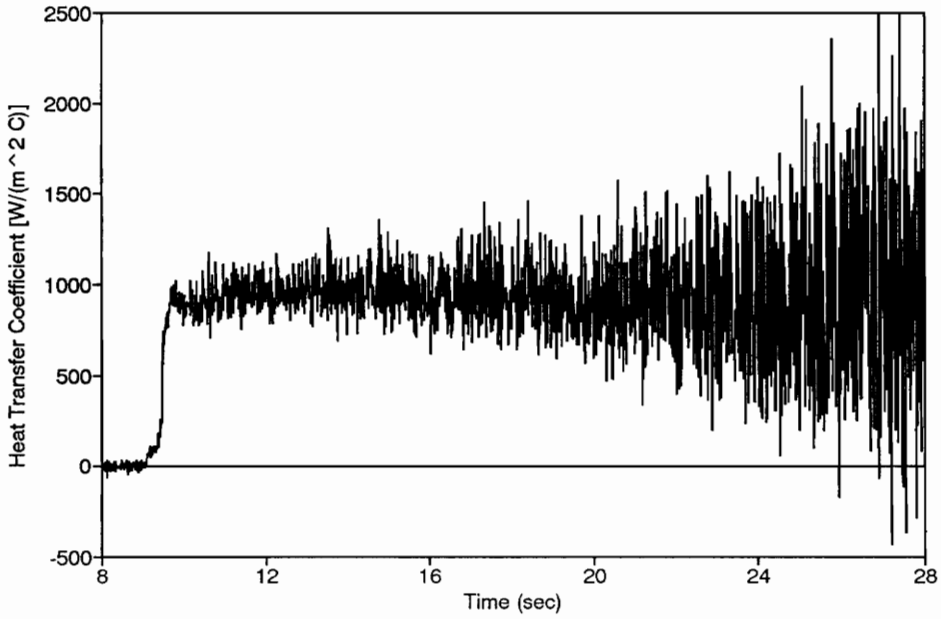

Figure A66. HTC Calculated from Leading Edge Line Gage Run 1 - No Grid.

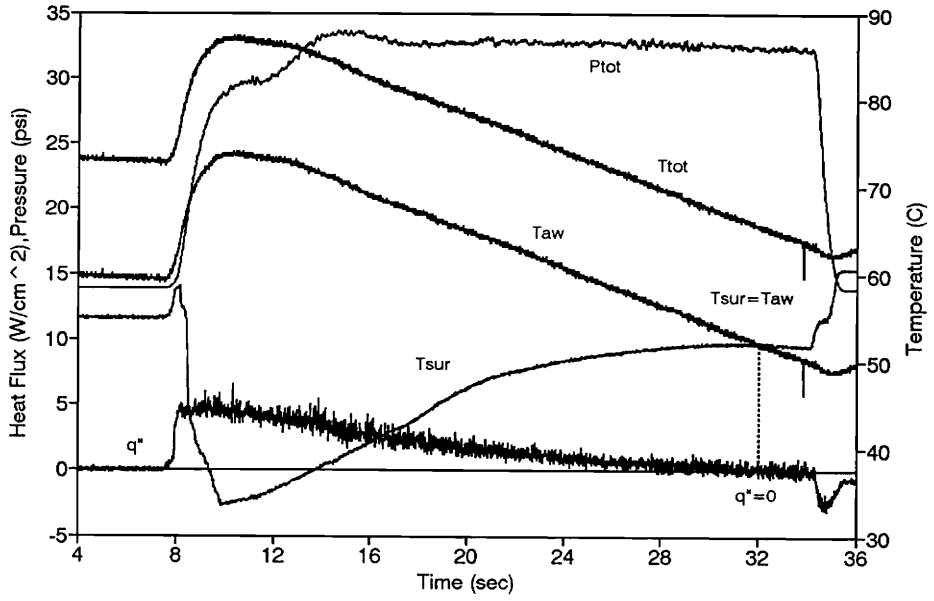

Figure A67. Leading Edge Line Gage Run 2 - No Grid.

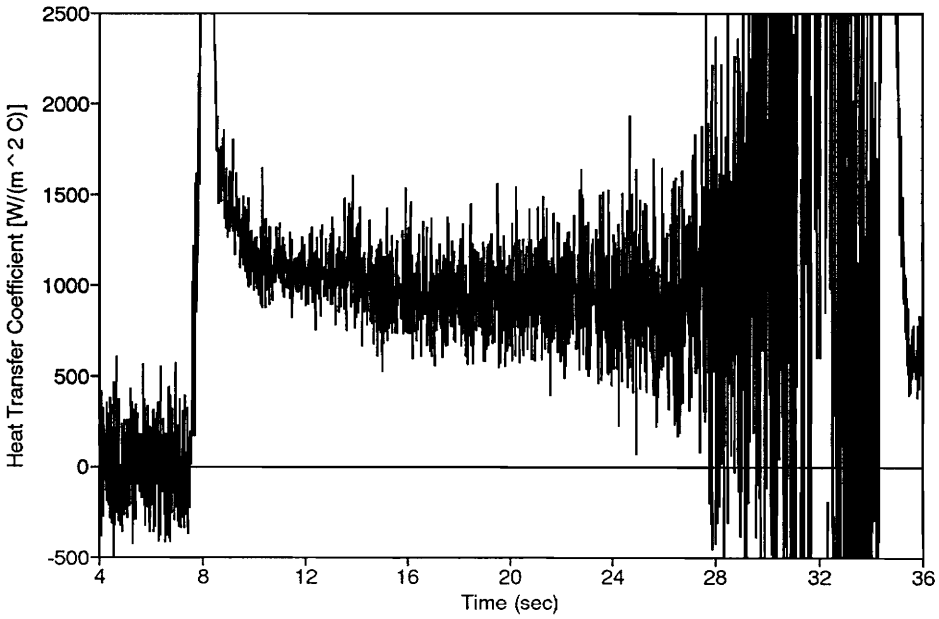

Figure A68. HTC Calculated from Leading Edge Line Gage Run 2 - No Grid.

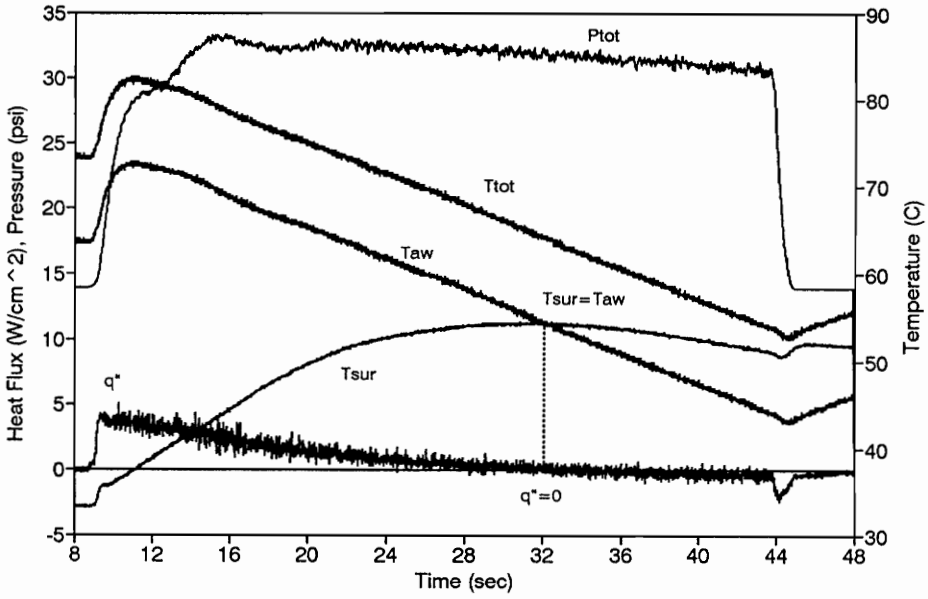

Figure A69. Leading Edge Line Gage Run 3 - No Grid.

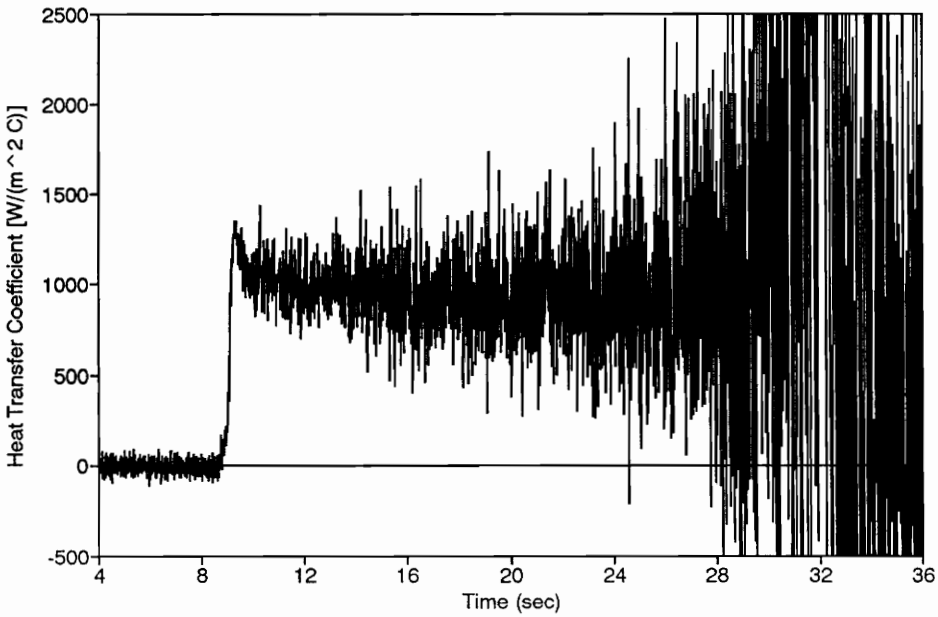

Figure A70. HTC Calculated from Leading Edge Line Gage Run 3 - No Grid.

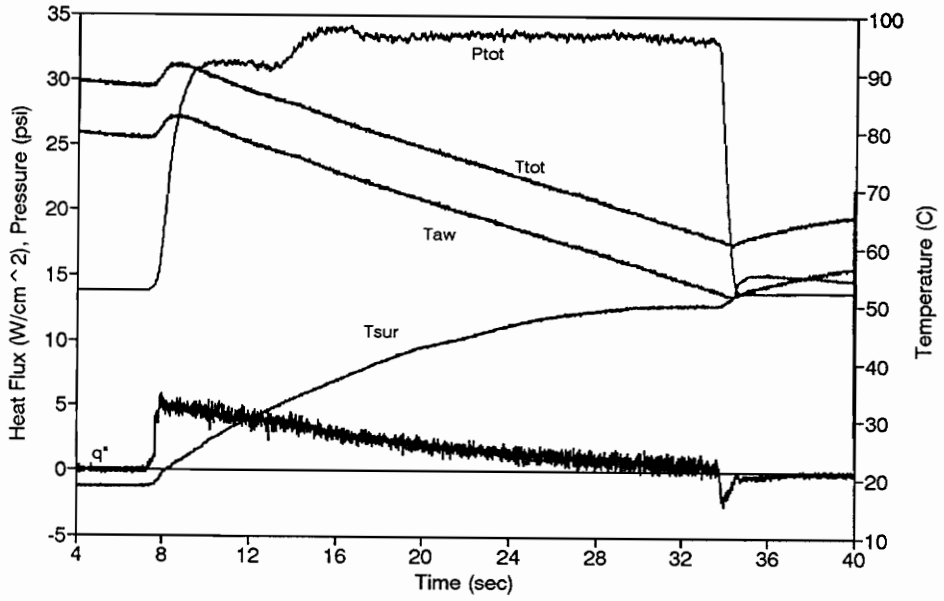

Figure A71. Leading Edge Line Gage Run 4 - Grid 1.

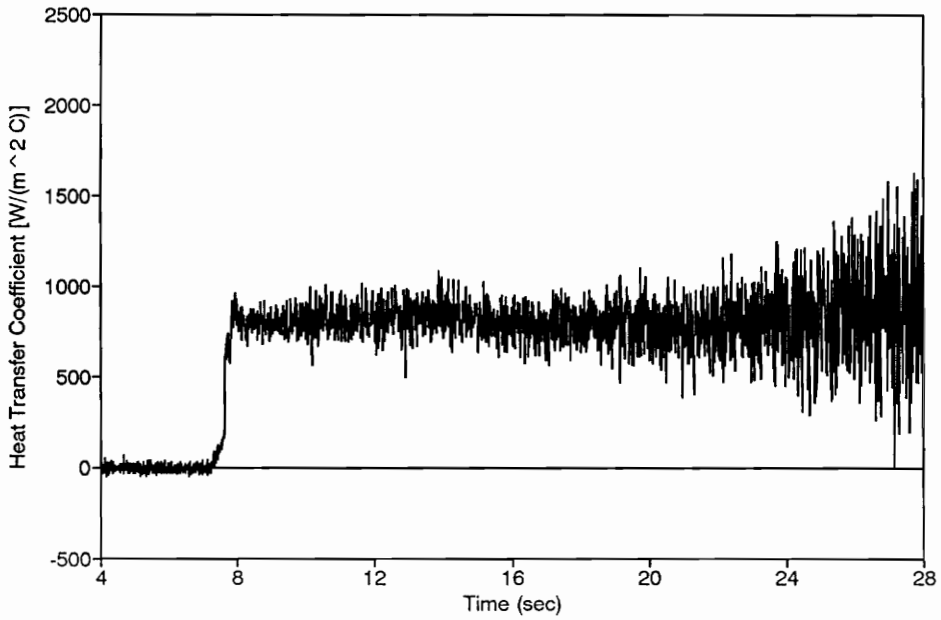

Figure A72. HTC Calculated from Leading Edge Line Gage Run 4 - Grid 1.

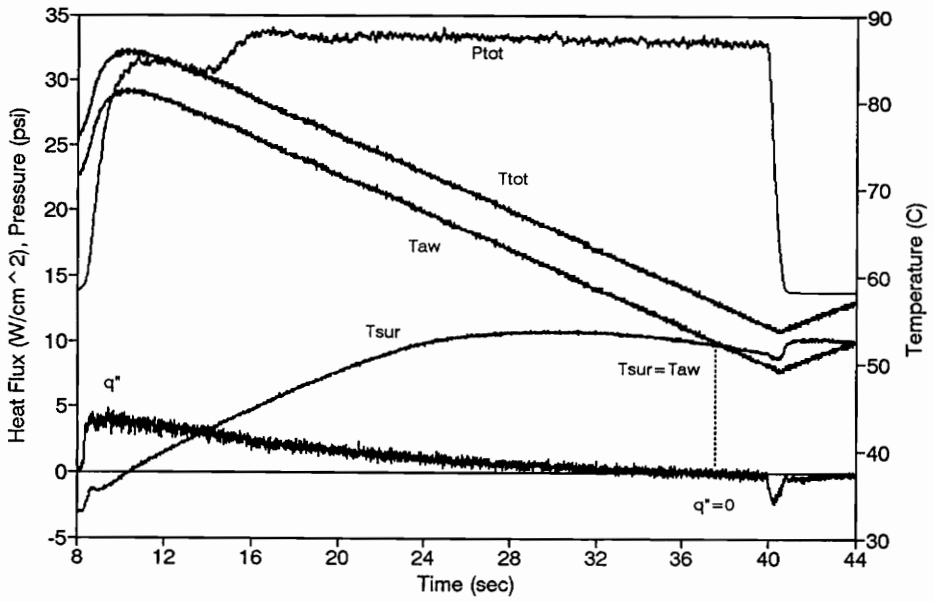

Figure A73. Leading Edge Line Gage Run 5 - Grid 1.

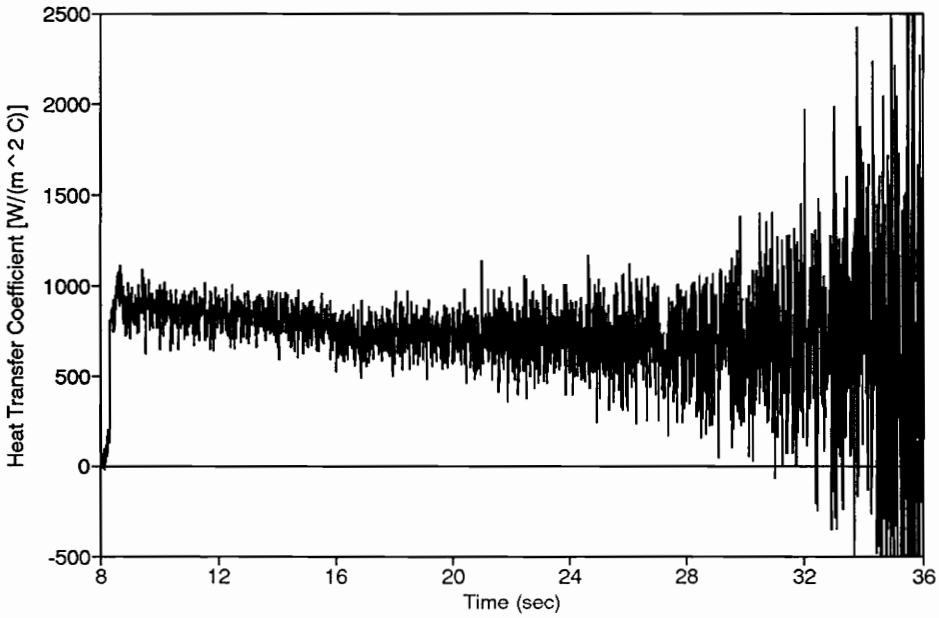

Figure A74. HTC Calculated from Leading Edge Line Gage Run 5 - Grid 1.

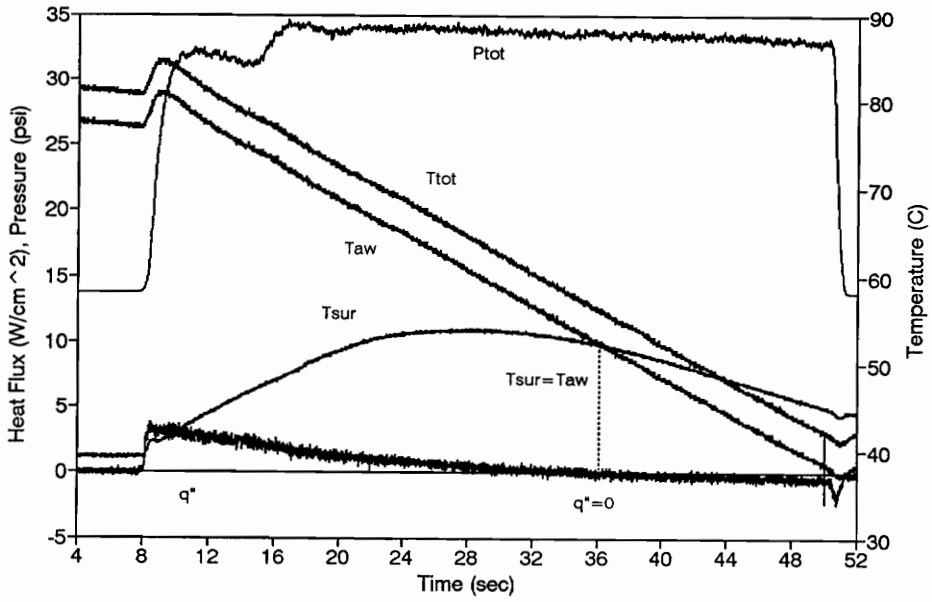

Figure A75. Leading Edge Line Gage Run 6 - Grid 1.

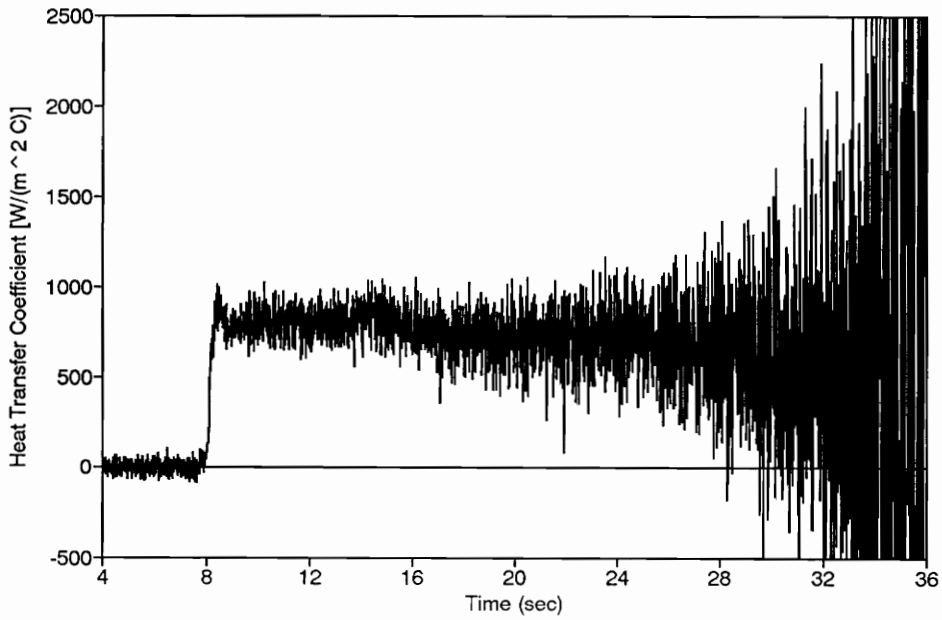

Figure A76. HTC Calculated from Leading Edge Line Gage Run 6 - Grid 1.

Appendix B
Signal Conversion Equations

Note: All voltages are unamplified. Calibrations were performed on all devices.

P_{TOT} (psi) = 5.34×10^{-3}(E)-1.79×10^{-2}+P_{ATM} (psi)

Kulite pressure signal (psi) = 14.89(E)+ P_{ATM} (psi)

Thermocouple temperature measurements such as T_{TOT}, T_{SUR}.
E is unamplified voltage and has units of millivolts (mV).

$$T(^{O}C) = C_0 + C_1E + C_2E^2 + C_3E^3 + C_4E^4 + C_5E^5 + C_6E^6 + C_7E^7 + C_8E^8 + C_9E^9$$

where C_0=	0	[from "Manual on the use
C_1=	2.508355	of Thermocouples in
C_2=	0.07860106	Temperature Measurement"
C_3=	-0.2503131	0°-500°C
C_4=	0.0831527	0.0mV - 20.644 mV]
C_5=	-0.01228034	
C_6=	9.804036×10^{-4}	
C_7=	-4.41303×10^{-5}	
C_8=	1.057734×10^{-6}	
C_9=	-1.052755×10^{-8}	

Heat Flux Signals - From manufacturer ±10%

HFM-6	$S(T) = \frac{E_q}{q''} = 8.54\,\mu V/W/cm^2 + 0.02T_{SUR}(^{\circ}C)$	(10a)
HFM-2a Trailing Edge	$S = 106.28\,\mu V/W/cm^2$	(10b)
HFM-2a Leading Edge	$S(T) = 11.86\,\mu V/W/cm^2 + 0.02T_{SUR}(^{\circ}C)$	(10c)

RTS Signals - From manufacturer ±10%

HFM-6	T_{SUR}(°C)=(35710°C/V)E_T+Ti(°C)	(11a)
HFM-2a Trailing Edge	T_{SUR}(°C)=(54800°C/V)E_T+Ti(°C)	(11b)
HFM-2a Leading Edge	T_{SUR}(°C)=(37630°C/V)E_T+Ti(°C)	(11c)

Appendix C

HOT WIRE CALIBRATION

HOT WIRE CALIBRATION

Before placing the hot wires into the tunnel, the hot wires were tuned according to the IFA 100 Manual. First, the cable resistance was entered (0.370 Ω). The operating resistance was given by the manufacturer as 7.21 Ω and was verified using an overheat ratio of 1.8. Generally, the hot wires are then placed into a known velocity jet flow and the signal adjusted by bridge and frequency compensation knobs to achieve a test square wave on an oscilloscope screen. Instead, the calibration test was performed in the wind tunnel since flow into the test section had a higher inlet velocity (>100 m/s) approaching compressible conditions. The wind tunnel was run at $Ma_{exit} = 1.26$ and the hot wire signals adjusted on the oscilloscope until a steady 1 kHz square wave was achieved.

Next the voltage of the hot wire had to be calibrated with a known inlet velocity. This could be determined from the inlet static tap and the inlet Pitot tap to calculate velocity and correspond with the hot wire voltage.

The Lecroy sampled at 20 Hz and recorded the two hot wire voltages plus the total temperature and total upstream pressure. The PSI sampled at 0.2 Hz and recorded the total upstream pressure and static wall pressure. Both the PSI and Lecroy were triggered simultaneously to match time histories. A 30 kHz low pass filter was programmed into the IFA Anemometer.

DATA REDUCTION

From chapter 2.0, the turbulence intensity equation is

$$Tu = \frac{\sqrt{\overline{u'^2}}}{U_\infty} \qquad (5)$$

which is the RMS value of velocity divided by the mean velocity. For the tunnel calibration, a correlation for hot wire voltage to tunnel velocity was established with a velocity-voltage curve fit approximation. This curve-fit was calculated using LABVIEW (Tunnel Single HW Cal.vi) with four variables for input (T_{TOT}), hot wire voltage (V), upstream pressure(P_{TOT}), and the static wall pressure (P_S). First, a static temperature was calculated

$$T_S = \frac{T_{TOT}}{\left(P_{TOT}/P_S\right)^{\left(\frac{\gamma-1}{\gamma}\right)}} \qquad (C1)$$

and then a Nusselt, Reynolds^0.45 curve was created from the four variable input array. Nusselt number is defined as

$$Nu = \frac{\frac{V^2(R_W)}{(R_W+10)^2}\left(\frac{T_M}{T_S}\right)^{Tx}(\mathrm{Pr}^{-\frac{1}{3}})}{\Pi(L_W)(k)(T_W - T_S)} \qquad (C2)$$

where V is the hot wire voltage, R_W is the operating resistance, T_M is the mean film temperature, T_S is the static temperature, Pr is the Prandtl number, L_W is the wire length, k is the thermal conductivity and T_W is the wire temperature. The Reynolds number is defined as

$$\mathrm{Re} = \sqrt{2Cp(T_{TOT} - T_S)}\,\frac{\rho * L_W}{\mu} \qquad (C3)$$

and from this curve, a linear curve fit equation is produced with a constant D and an offset C.

$$Nu_{FIT} = D * \mathrm{Re}^{0.45} + C \qquad (C4)$$

Now that a calibration curve fit has been generated, the hot wire voltage can be correlated to velocity with the following equation

$$Velocity(V) = \frac{\left(\frac{\left(\frac{V^2(R_W)}{(R_W+10)^2}\left(\frac{T_M}{T_S}\right)^{Tx}(\mathrm{Pr}^{-\frac{1}{3}})\right)}{\frac{\Pi(L_W)(k)(T_W-T_S)}{D}} - C \right)^{1/0.45}}{\frac{(\rho * d_W)}{\mu}} \qquad \text{(C5)}$$

Air properties were taken as

MW = 28.8149 kg/kmol	Pr = 0.7143
u = 332.5724 m/s	γ = 1.4023
R = 288.5418 J/(kg K)	Tx = 0.51
Cp = 1005.8 J/(kg K)	ρ = 1.28 kg/m
k = 24.29E-3 W/(m K)	μ = 17.251E-6 (Ns/m^2)

and the wire properties as

L_W = 0.00127 m	R_W = 7.21 Ω
d_W = 3.81E-6 m	

Table C.1 shows the four input variables of total temperature (T_{TOT}), hot wire voltage (V), difference in total pressure (P_{TOT}) and static pressure(P_S), and total upstream pressure (P_{TOT}) necessary to establish a voltage to velocity correlation for the hot wire.

Table C.1 - Hot Wire Calibration Variables

Data Point Number	Ttot (°C)	Hot Wire Voltage (V)	delta P (kPa)	Total Upstream Pressure (kPa)
1	12.28694	2.35778	17.37617	200.5478
2	11.4058	2.35889	17.84432	205.8361
3	10.68376	2.36301	17.95671	206.5677
4	9.790406	2.36564	17.94361	205.9747
5	8.737928	2.36763	17.89948	204.9922
6	7.532489	2.36997	17.69264	203.9297
7	5.996628	2.37478	17.5182	201.8309
8	4.222106	2.38553	17.31895	200.703
9	2.208961	2.38565	17.3803	199.9879
10	-0.10402	2.35687	16.82183	194.1288
11	-2.3191	2.29279	15.35945	176.8125
12	-3.76318	2.21323	13.25724	152.2533
13	-4.55866	2.13093	10.81305	129.1627
14	-5.01146	2.04696	8.082035	114.4037
15	-5.18891	1.95828	5.568206	105.0103
16	-4.91967	1.78262	3.34051	100.0288

From LABVIEW (Tunnel Single HW Cal.vi), a straight line approximation was determined as

$$Nu_{FIT} = (1.17) * \mathrm{Re}^{0.45} - 0.13 . \qquad \text{(C6)}$$

and can be seen graphically in figure C1.

In order to calibrate the hot wires, several data sets were needed. The solution on how to record these data sets was to run the tunnel for approximately 120 - 180 seconds and record the stable drop in pressure over this time period and correlate freestream velocity to a hot wire voltage. Due to equipment limitations, the PSI pressure recorder could only read a maximum of 36 data sets over a 180 second interval meaning a sampling rate of 0.2 Hz. The PSI,

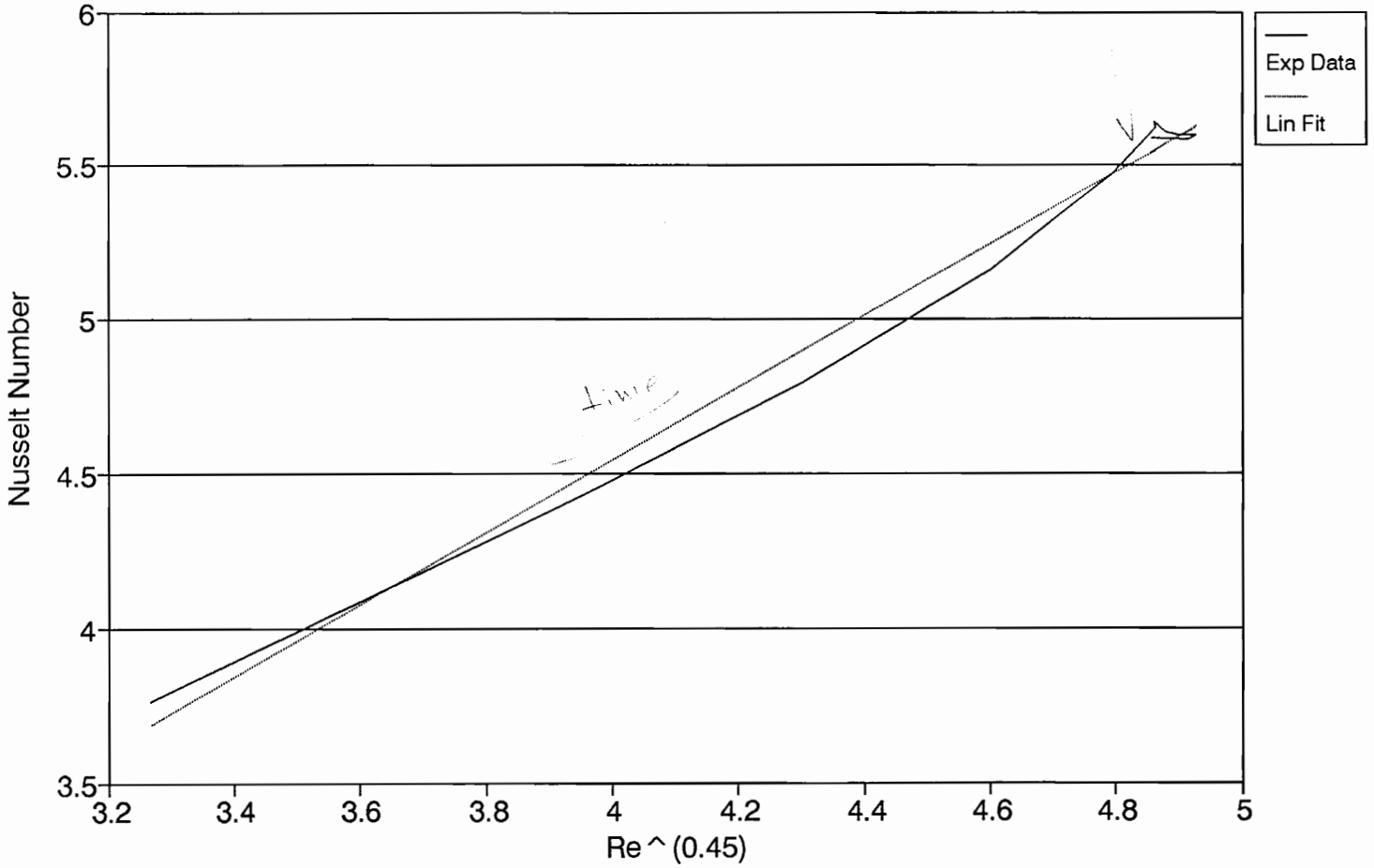

Figure C1 Nusselt - Reynolds Calibration Curve Fit for Hot Wire.

recording total and static pressure, triggered the Lecroy, which recorded voltage and total temperature, in order to match time histories. The minimum Lecroy sampling rate was 20 Hz and thus every 100^{TH} point on the Lecroy was matched to every PSI point of data. Several points were removed due to pressure instability both at the beginning and end of the calibration run. Therefore only 16 data points were used to determine the calibration curve fit to convert voltage to velocity (Table C.1).

The LABVIEW program [LORENHW.VI] converted voltage to velocity based on the Nu, $Re^{0.45}$ fit and information about the hot wires. Another LABVIEW program, [DGHSPCTM.VI] then performed the integral length scale, based on the autocorrelation function, and turbulence intensity calculations. The user had to input the sampling rate of the data (100 kHz).

Appendix D

SWITCH BOX SET-UP

With the failure of the RTS on the HFM-6 gage, a first attempt was made to make the HFS serve as both an RTS and a HFS. This dual role could be achieved if a multiplexing switch was implemented to pass current through the HFS and turn it into an RTS. The use of LABVIEW was essential in this process.

The switching box was designed by the mechanical engineering shop at VA Tech and operated on the principle of an electronic pulse to connect either the HFS circuit or RTS circuit. In the off (0) setting, the switch connected the HFS circuit and grounded the RTS circuit. In the on (1) position, the switch connected the RTS circuit, passing a 0.1 mA current through the HFS in order to read temperature. The sensor voltages were acquired with the Lecroy.

In order to calibrate the new RTS signal, the existing surface thermocouple acted as a reference signal. By matching the room temperature reference along with the start up of the tunnel, the RTS signal was calculated as

$$T_{SUR}(^{o}C)=(30120^{o}C\ /V)E_T+T_I(^{o}C) \qquad [D1]$$

LABVIEW sent out a 1 mA, 5 V signal to the switch box through an AT-MIO-16 board. LABVIEW (SWITCH.VI) software controlled the length of the pulse (duty cycle) and frequency of the pulse. Through experimentation, it was discovered that the RTS signal stabilized 20 ms after switching, and the HFS stabilized after 15 ms of switching. A duty cycle of 0.06 (0.03 s) allowed the RTS signal an extra 10 ms to stabilize. It was more efficient to obtain the HFS signal

than the RTS signal. The RTS signal could be reconstructed from fewer points. A frequency of 2 Hz (0.5 s) was chosen as a frequency the switch could safely maintain over 60 seconds of tunnel run time.

Figures D1 and D2 show an example of an actual data run and heat transfer coefficient for run 1. Notice that the RTS signal railed when the circuit was open while the HFS signal grounded to a 0 voltage level when its circuit was open. In order to clean the HFS signal, the three grounded points (0.03 s) were replaced with an average value of the neighboring points. Likewise, 0.97 seconds of the railed RTS signal was replaced with an average of the neighboring points and a curve fit estimate. Figures D3 and D4 show the results of a cleaned run 1. A summary of the three switch runs are in Table D.1.

Table D.1 - Average Heat Transfer Coefficients and Nusselt Numbers for HFM-6 Leading Edge Gage with Switch Set-up

Run Number	Heat Transfer Coefficient [W/(m^2 C)]	Nusselt Number
1 - no grid	1216±15	1619±20
2 - no grid	1676±13	2217±18
3 - no grid	882±14	1162±18

Table D.2 - HFM-6 Leading Edge Gage with Switch Set-up

Figure	Run #	Exit Mach #	Humidity(%)
D3,D4	1 - No grid	1.31	5.3
D5,D6	2 - No grid	1.28	4.5
D7,D8	3 - No grid	1.28	4.0

It should be noted that the switch box set-up that allows the HFS to act as an RTS during the course of a run has potential future benefit. Never before has a heat flux gage served a two-fold purpose during the same run. This was a first

attempt at this process and the results show that more research and experimentation must be carried out to validate this method. The set-up has the advantage of having only one sensor measure both heat flux and surface temperature. Problems arise in measuring high frequency sampled data, such as Tuq, since the switching and stabilization period may interfere with the results.

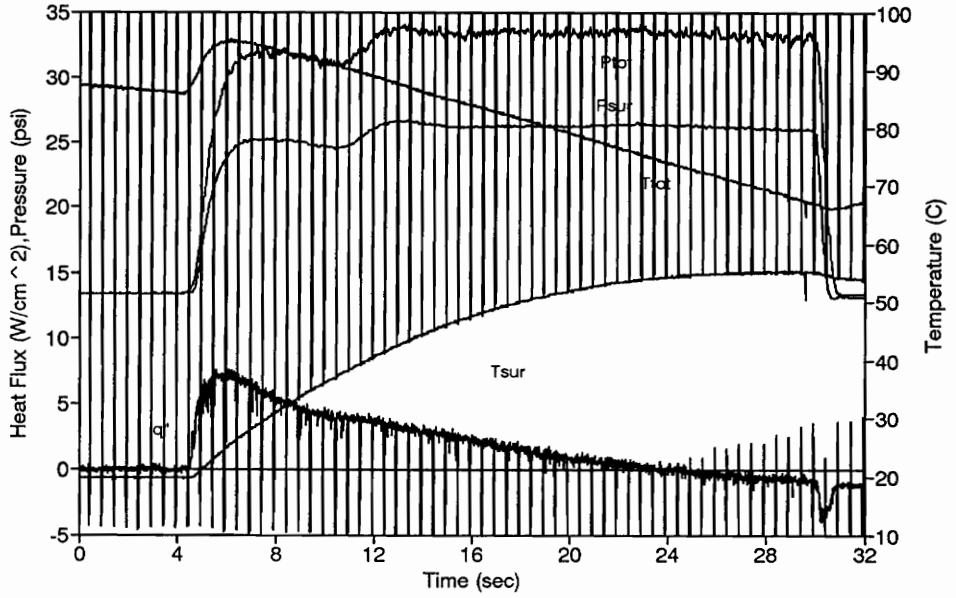

Figure D1. HFM-6 Leading Edge Gage with Switch Set-up - Run 1 - No Grid - Actual Signal.

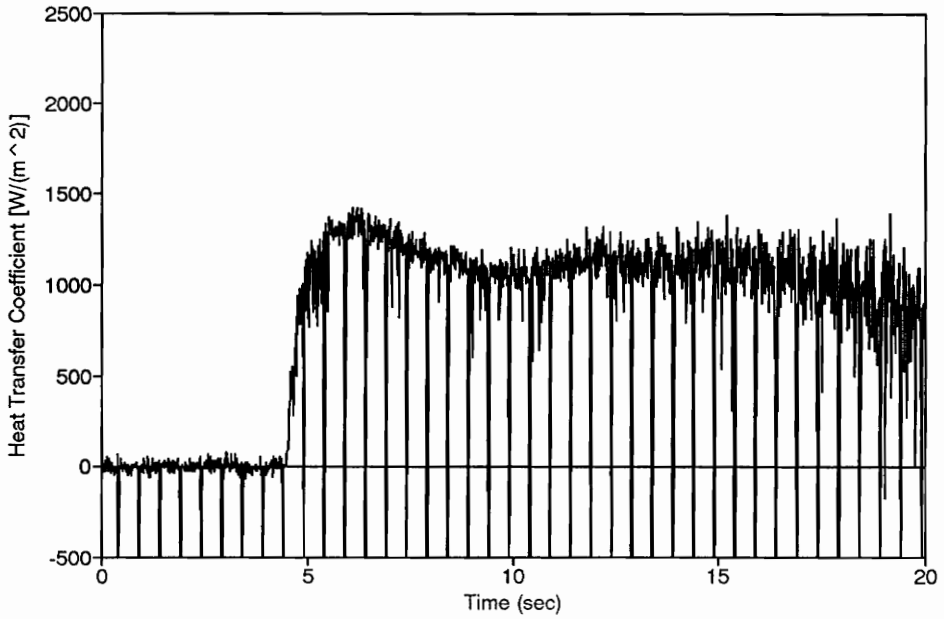

Figure D2. HTC from HFM-6 with Switch Set-up Run 1 - Actual Signal.

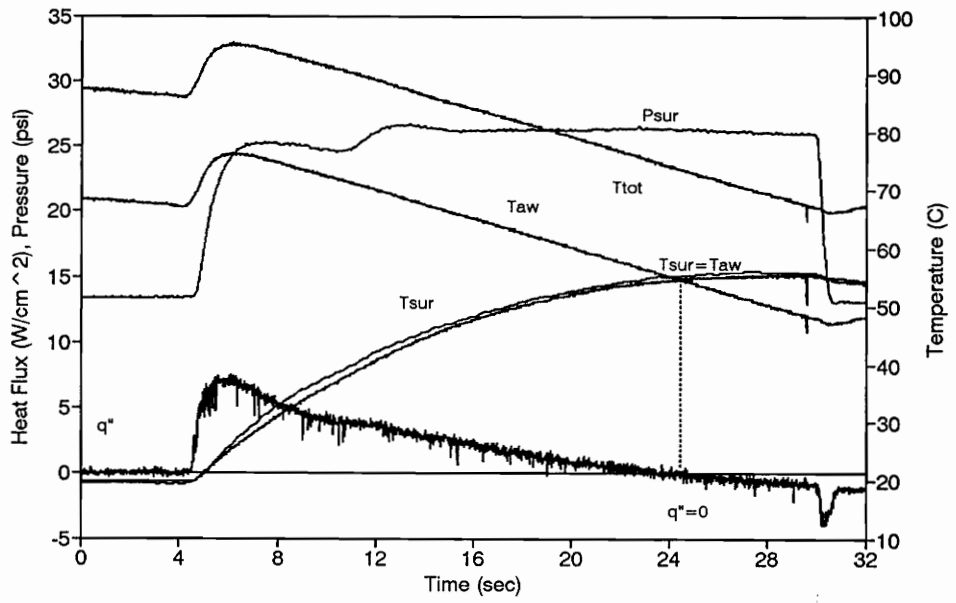

Figure D3. HFM-6 Leading Edge Gage with Switch Set-up - Run 1 - No Grid.

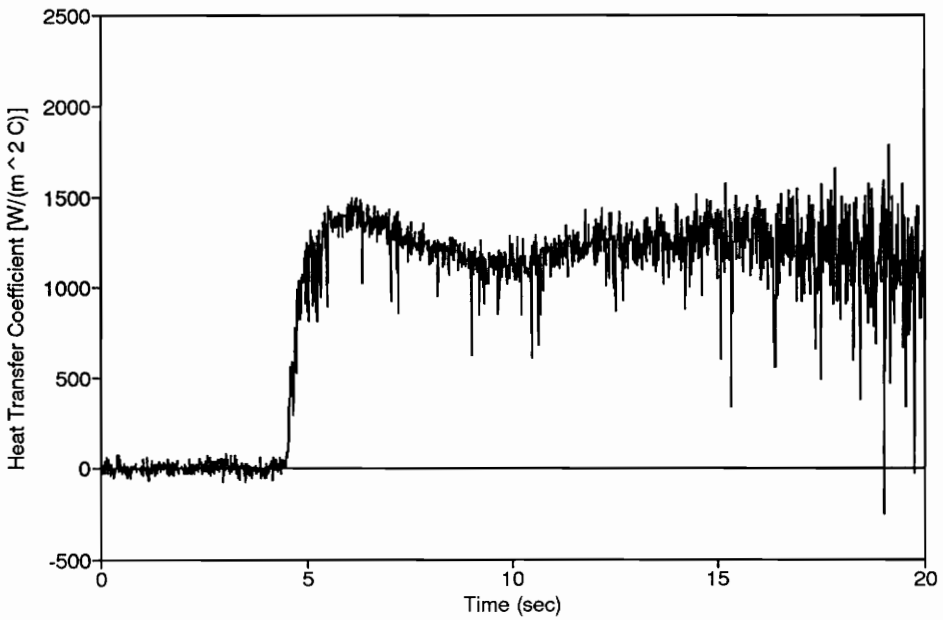

Figure D4. HTC from HFM-6 with Switch Set-up Run 1 - No Grid.

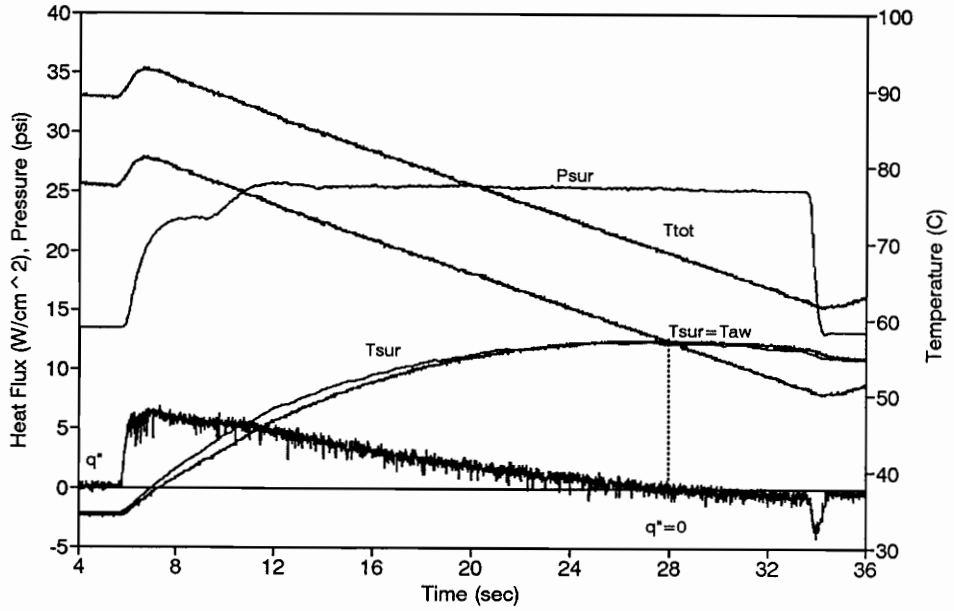

Figure D5. HFM-6 Leading Edge Gage with Switch Set-up - Run 2 - No Grid.

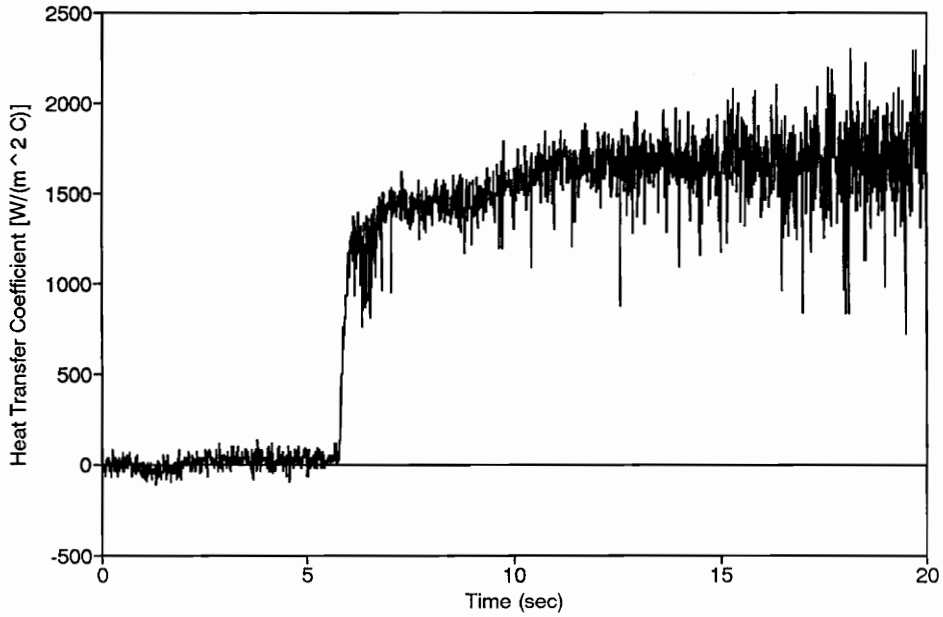

Figure D6. HTC from HFM-6 with Switch Set-up Run 2 - No Grid.

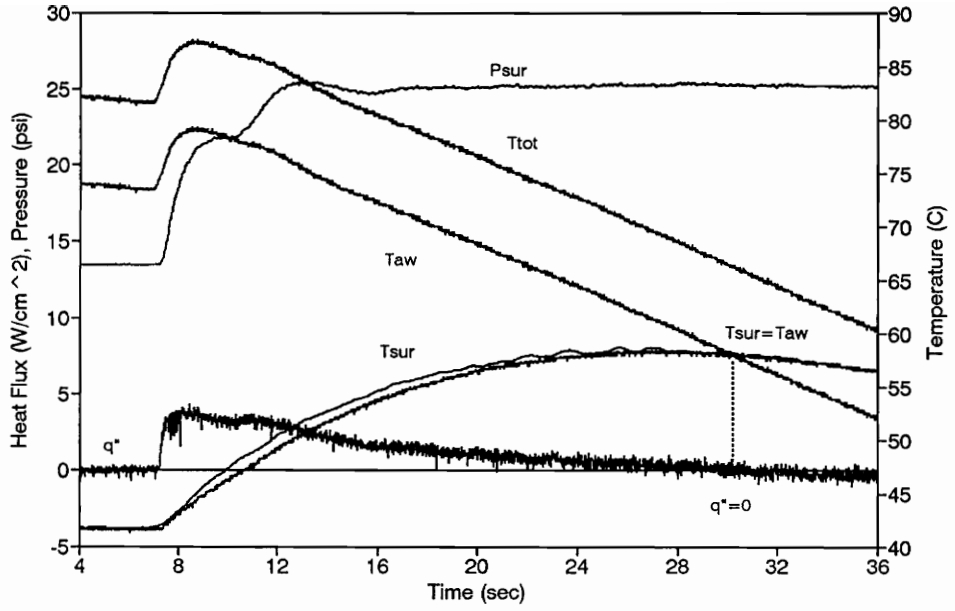

Figure D7. HFM-6 Leading Edge Gage with Switch Set-up - Run 3 - No Grid.

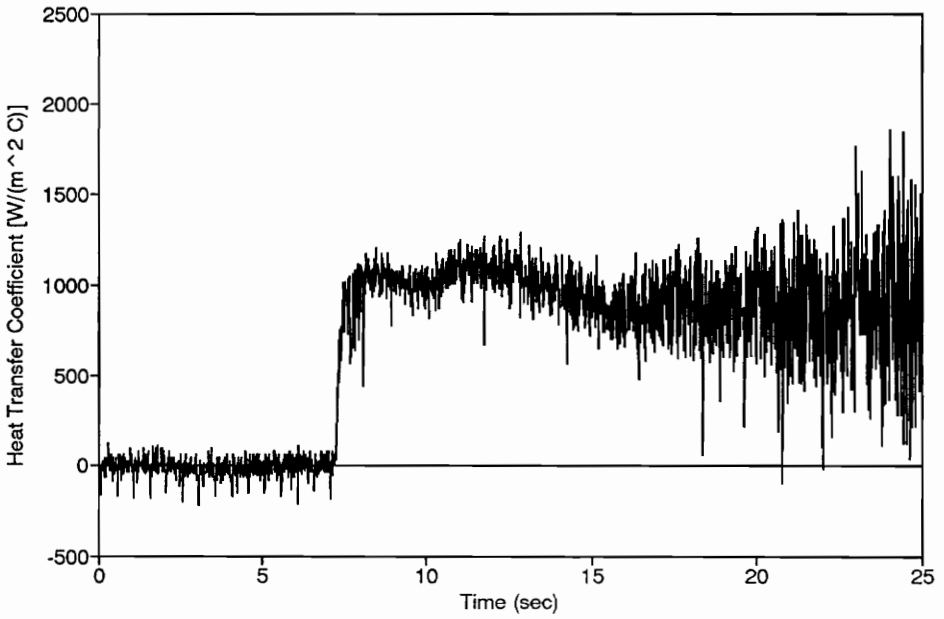

Figure D8. HTC from HFM-6 with Switch Set-up Run 3 - No Grid.

Appendix E

LABVIEW PROGRAMS

The following pages are printouts of the programs from LABVIEW that performed post-processing on the data. These programs were originally written or modified by David G. Holmberg, at Virginia Tech, Blacksburg, Virginia.

There are four programs

(1) A hot wire calibration program entitled Tunnel Single HW Cal.vi.

(2) A voltage to velocity program entitled LORENHW.VI

(3) A filtering program that also measured turbulence intensity and integral length scales entitled DGHSPCTM.VI

(4) A program for the switch box set-up to alternate the HFS and RTS signals called SWITCH.VI

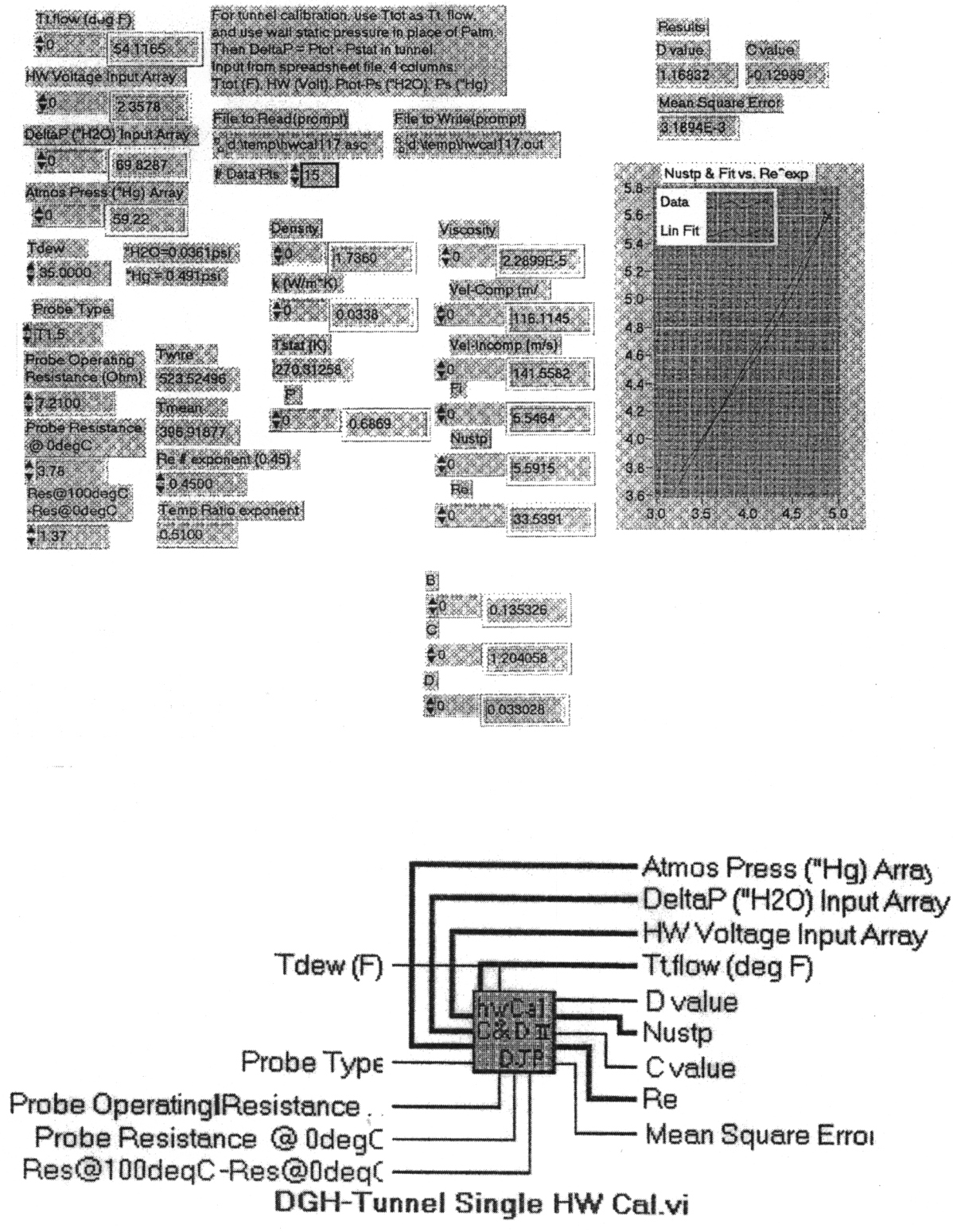

Figure E1. Tunnel Single HW Cal.vi

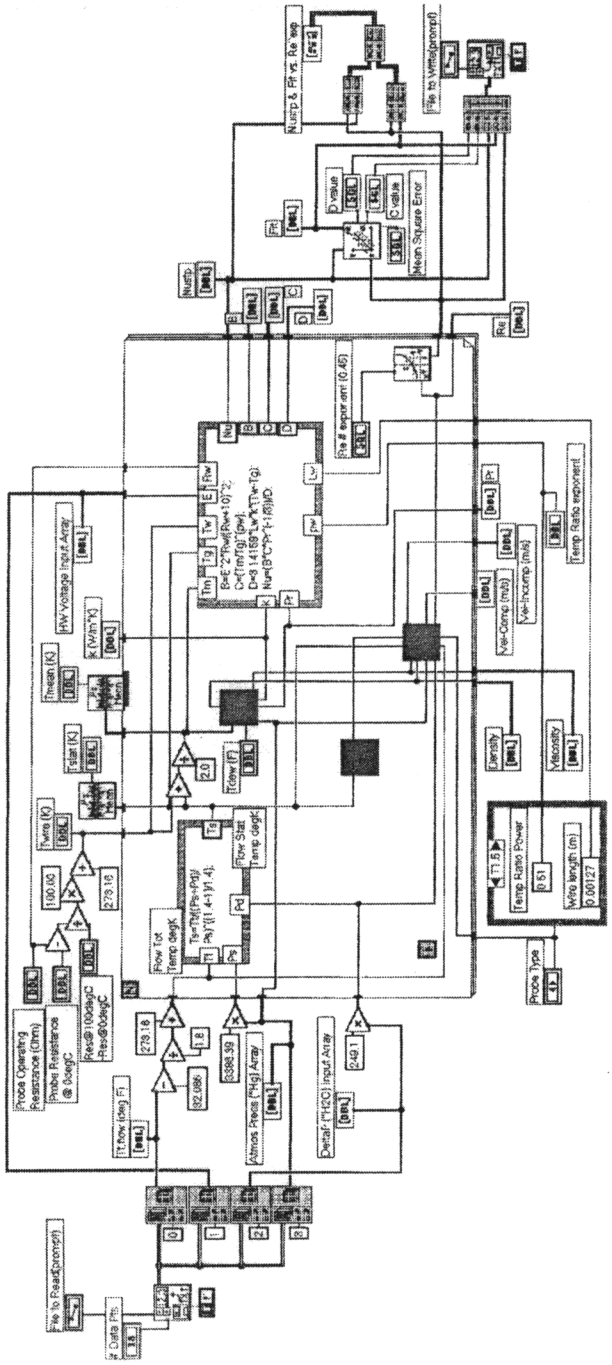

Figure E2. Tunnel Single HW Cal.vi (Con't)

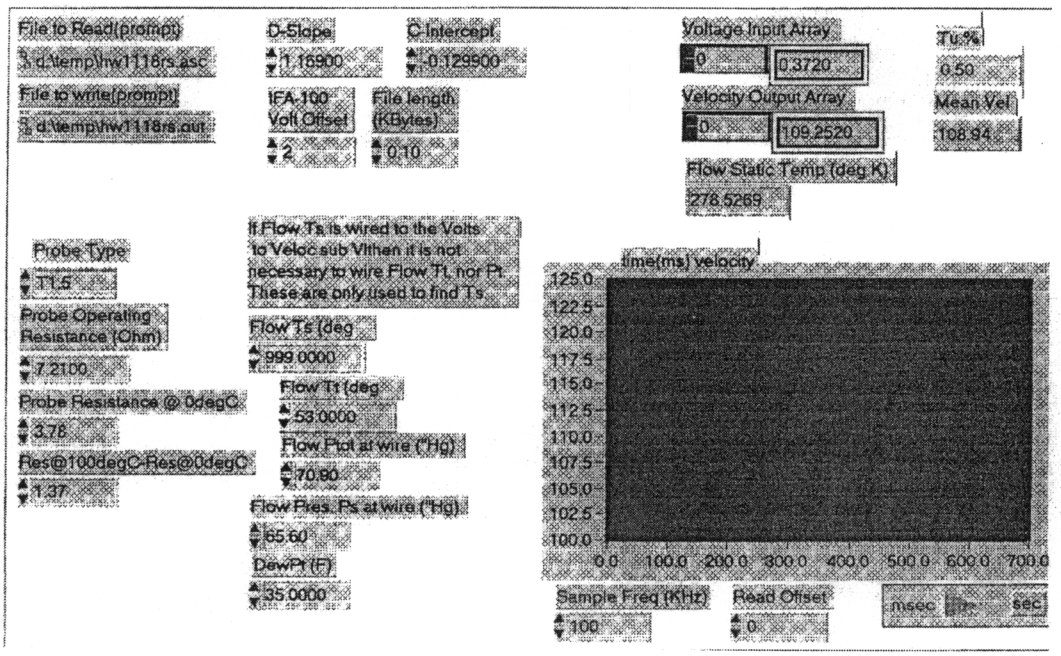

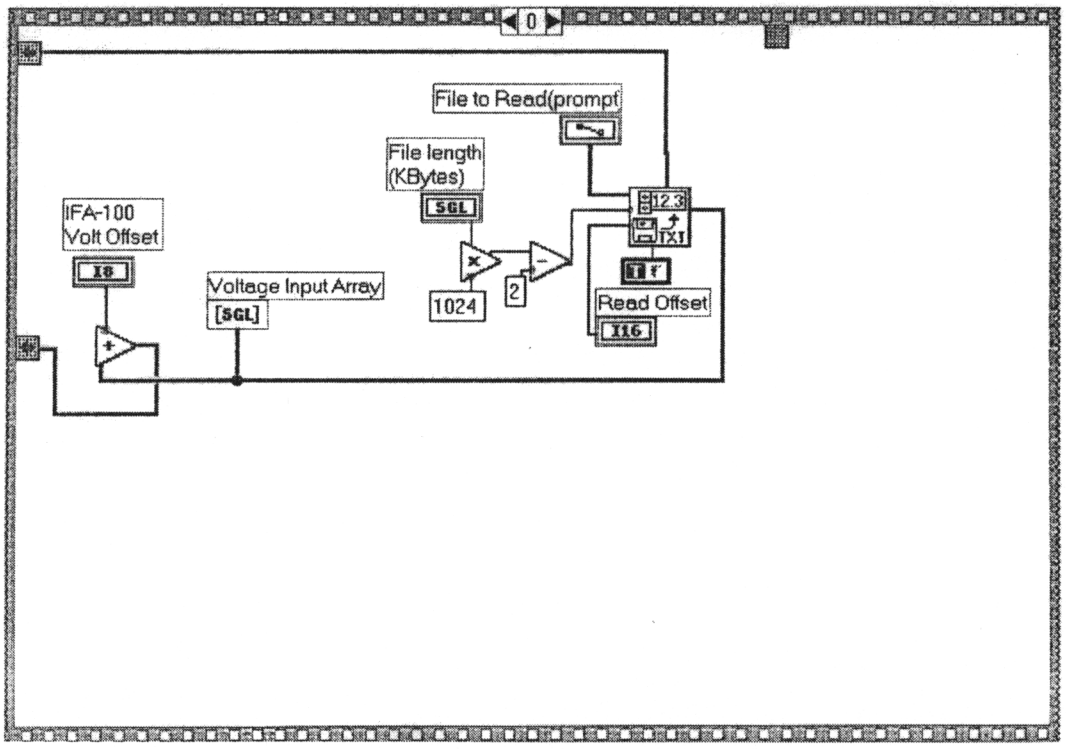

Figure E3. LORENHW.VI

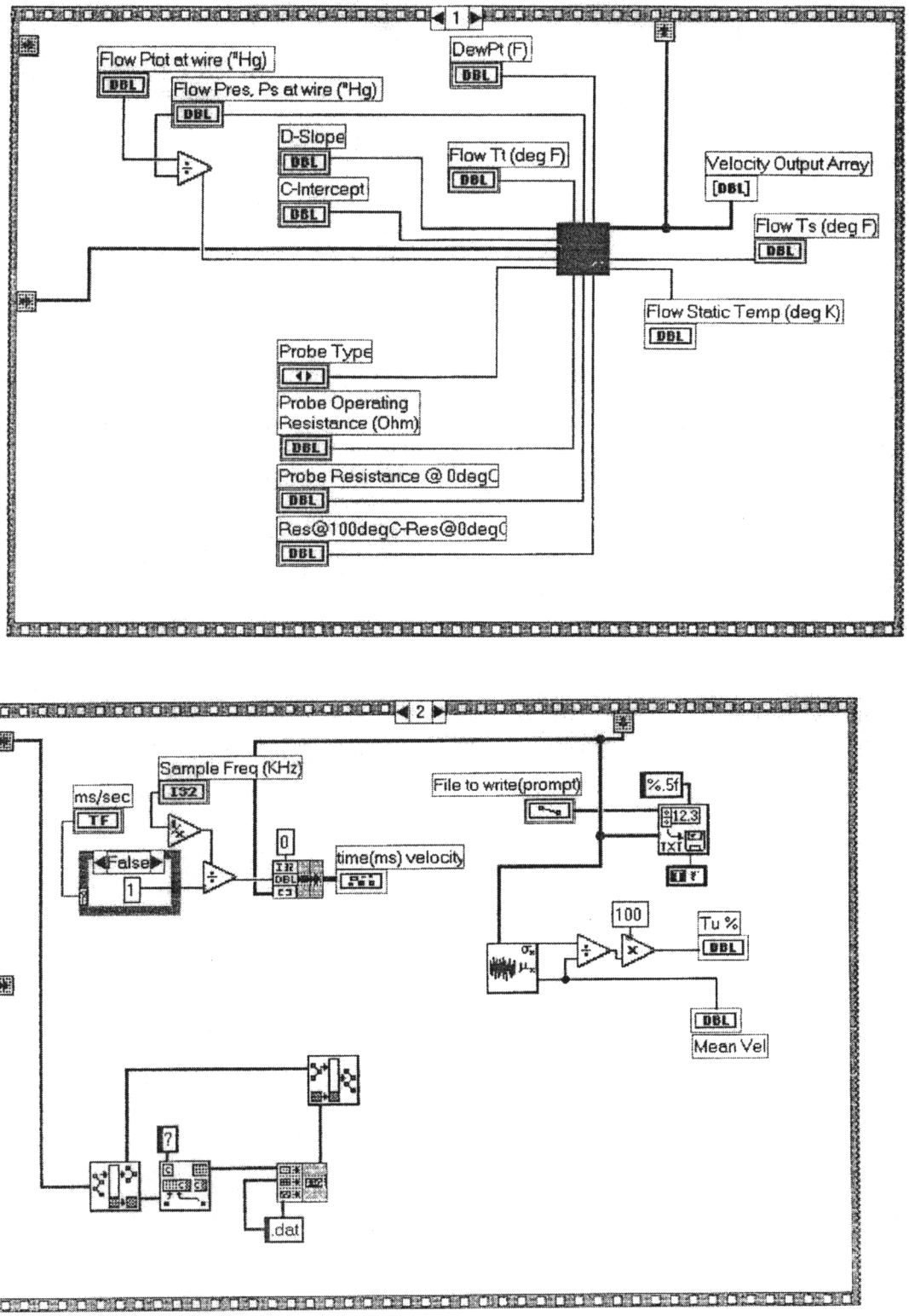

Figure E4. LORENHW.VI (Con't)

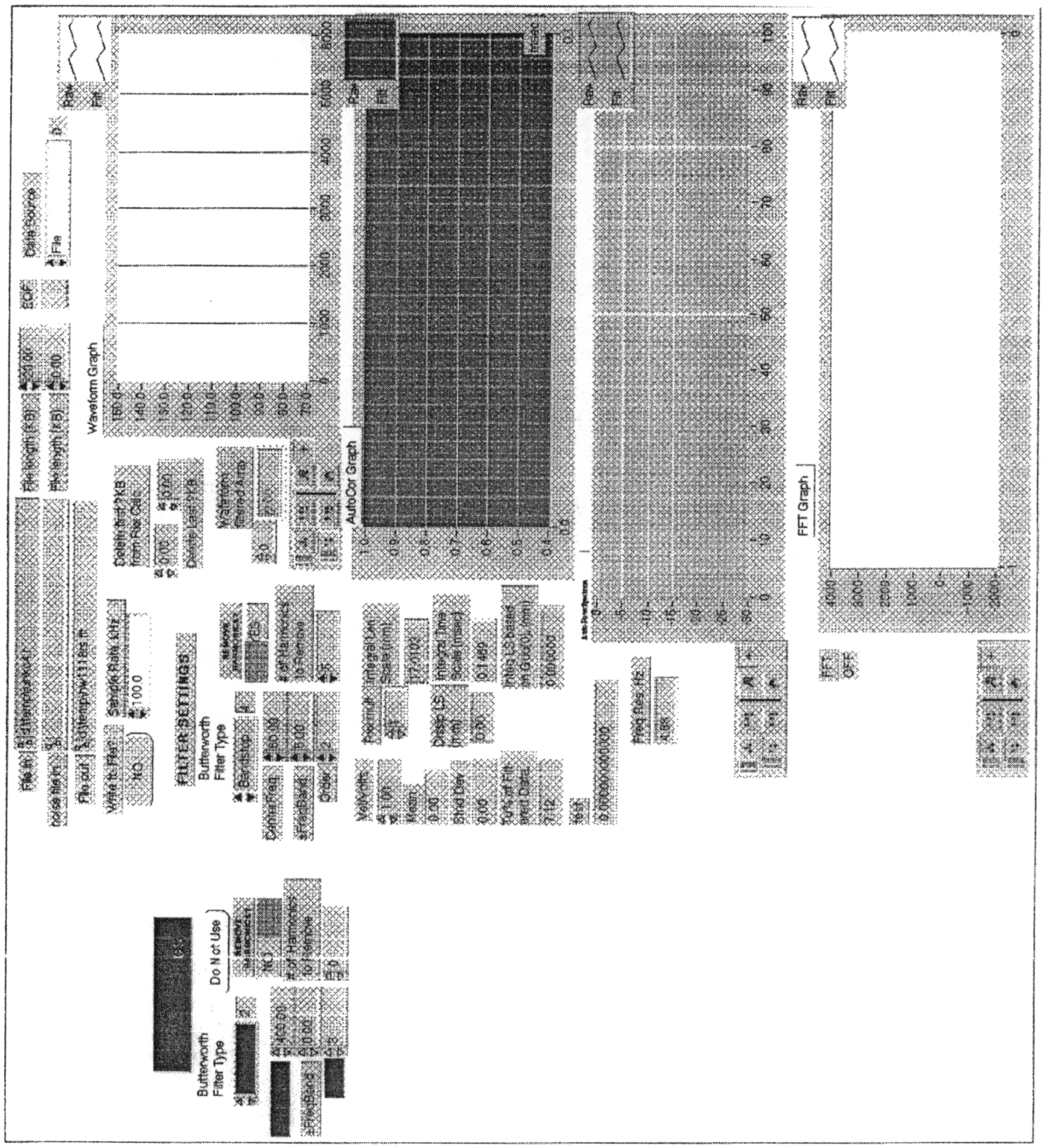

Figure E5. DGHSPCTM.VI

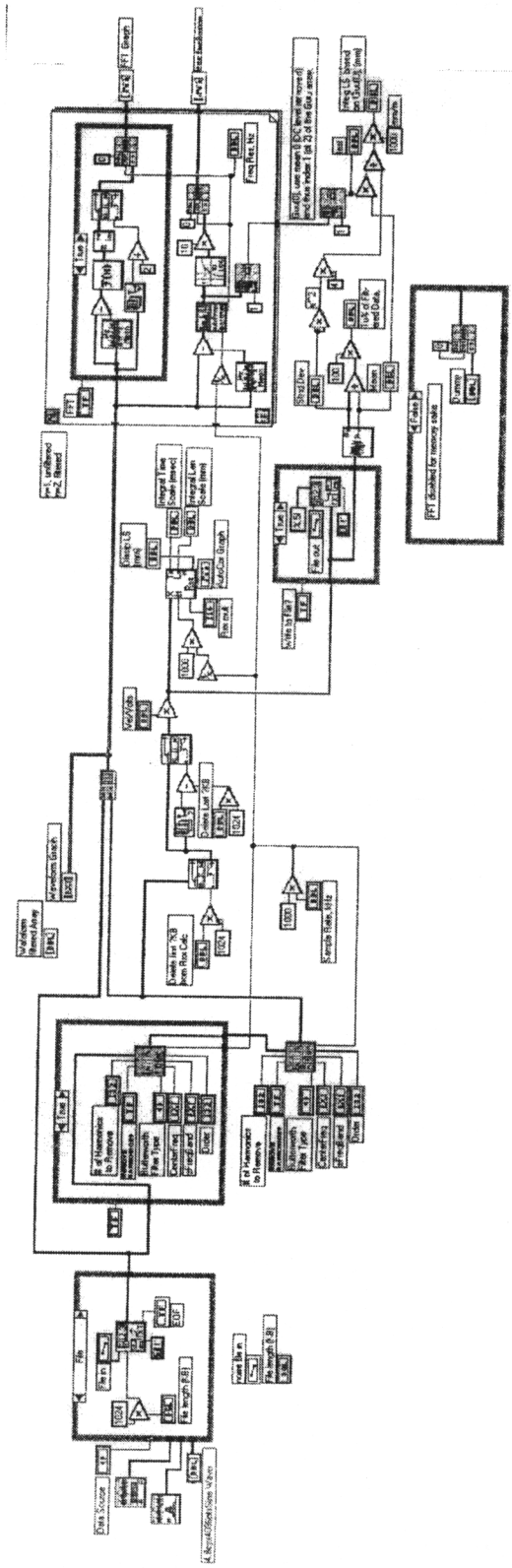

Figure E6. DGHSPCTM.VI (Con't)

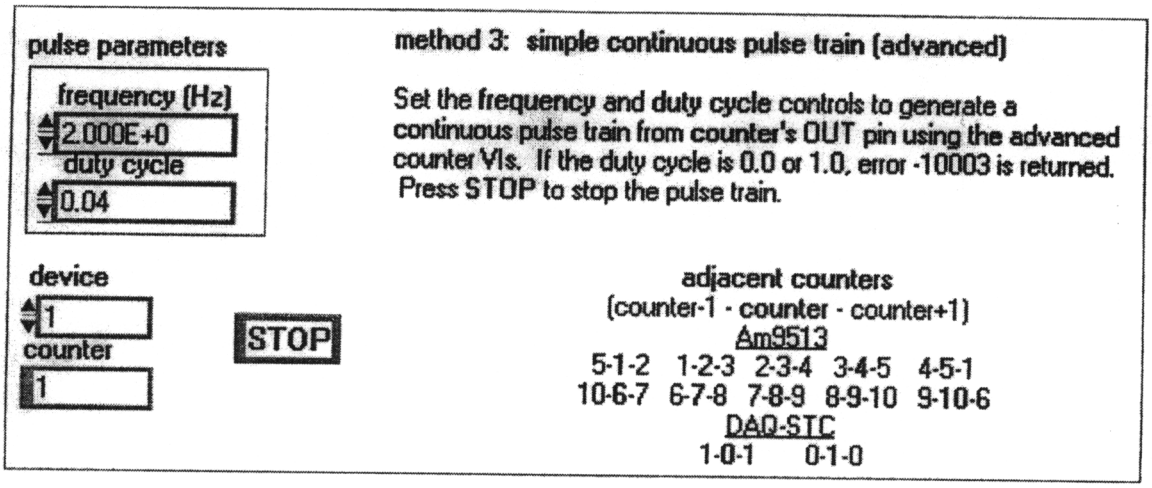

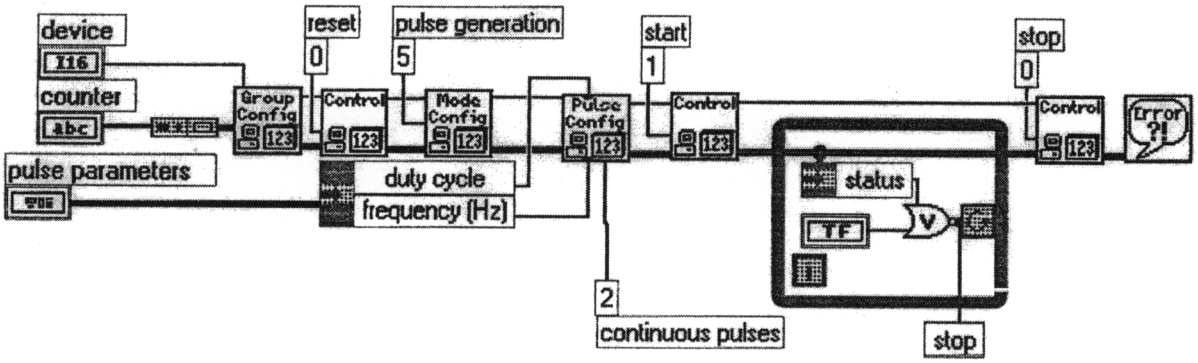

Figure E7. SWITCH.VI

Appendix F

CONDUCTION CALIBRATION OF HFM-2A LINE GAGE

The conduction calibration program (QT.FOR) was originally written by Karen Baker [1993] and later modified by David Holmberg [1995]. The program is designed to convert an **HFM** surface heat flux signal to the corresponding surface temperature according to a one dimensional semi-infinite model of heat conduction into a substrate of known thermal properties and initially constant temperature. The thermal properties of the aluminum blades are shown in Table F.1

Table F.1 - Properties of aluminum blades

k =	129 W/(m K)
Cp =	921 J/(kg K)
ρ =	2770 kg/m^3
α =	5.09 x 10^{-5} m^2/s

The model is valid for short times where the 1-D, semi-infinite assumptions are valid. The program utilizes the Green's function method to integrate the heat flux with respect to time to yield temperature. The program output contains the **HFS** signal, **RTS** signal, and calculated surface temperature signal.

A sensitivity value was calculated for five of the six runs from the leading edge line gage. Run 2 was not examined due to initial signal problems from the **RTS**. The 1 kHz, 64 second heat flux signal was reduced to 1 second (1000 points) near the initial start-up of the tunnel. The **RTS** signal was also reduced to 1 second at the exact time as the **HFS**. Using a spreadsheet, these two data sets were linked in a two column format for input into the program. Approximately 100 data points were averaged before the initial increase in

temperature and heat flux. The remaining 900 points were located on the increasing slope of the temperature and heat flux signals. The sensitivity was varied within the program to obtain the optimum sensitivity value for the particular run. Table F.2 shows the results from the five runs.

Table F.2 - Experimental vs. Manufacturer Sensitivity

Run	Intial Temperature (°C)	Calculated Sensitivity	Sensitivity from Manufacturer
1	27.0	11.4	12.4
3	33.3	10.7	12.5
4	18.6	12.7	12.2
5	33.0	10.7	12.5
6	39.3	12.1	12.7

Figure F1 shows the sensitivity value at the respective temperature for each run compared with the manufacturer's equation of

HFM-2a Leading Edge $$S(T) = 11.86\,\mu V/W/cm^2 + 0.02T_{SUR}(^\circ C) \qquad (10c)$$

The average sensitivity for all the runs was 11.5 μv/W/cm^2 and 8.4% lower than Thermateq's sensitivity value of 12.5 μv/W/cm^2 over all the runs. Figures F2-F6 show the comparison between the experimental temperature and the calculated temperature for each of the runs based on the calculated sensitivity.

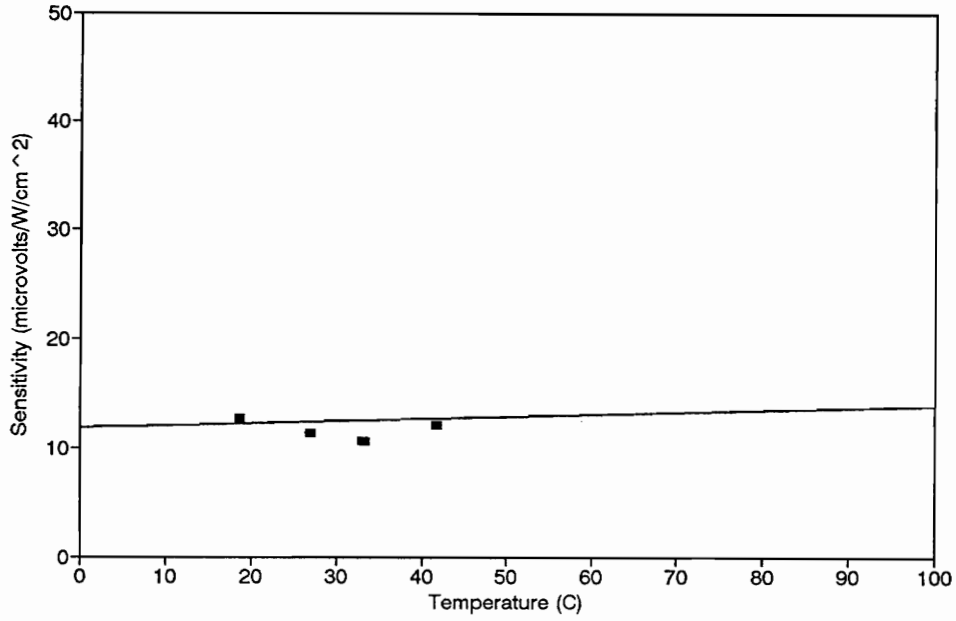

Figure F1. HFM Conduction Calibration from Program vs. Manufacturer

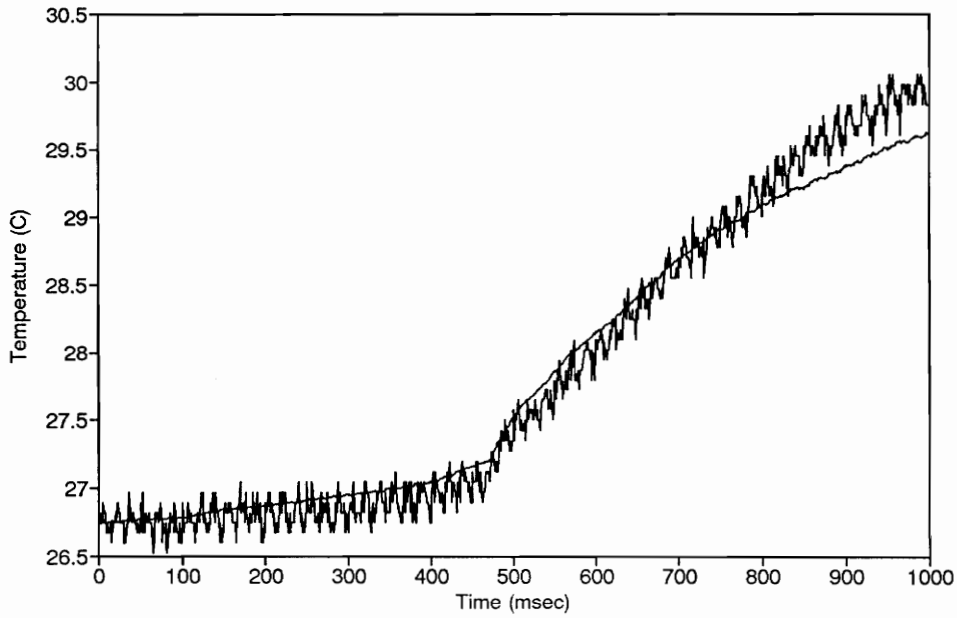

Figure F2. Experimental vs. Calculated Temperature for Line Gage Run 1.

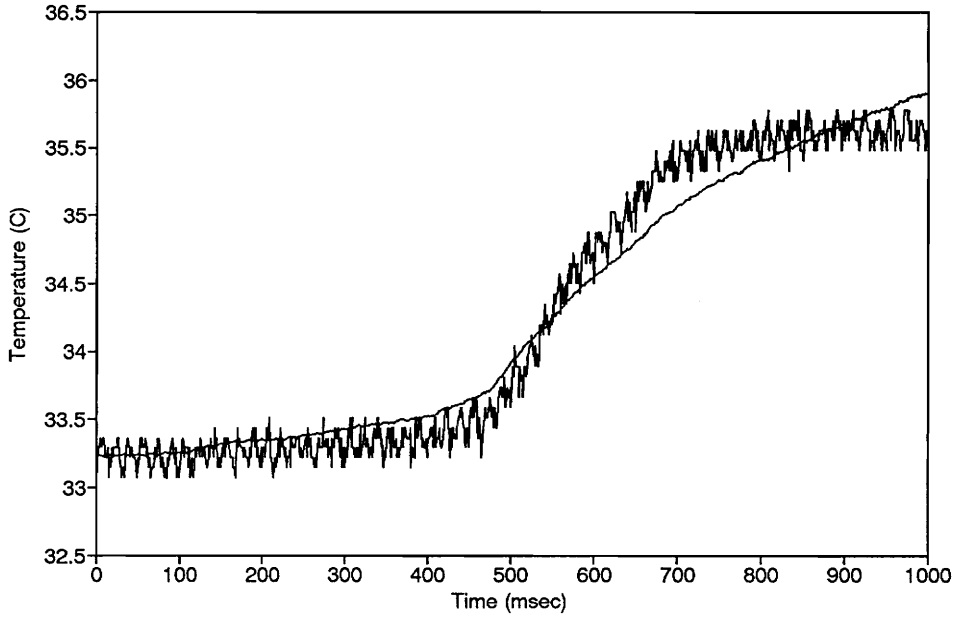

Figure F3. Experimental vs. Calculated Temperature for Line Gage Run 3.

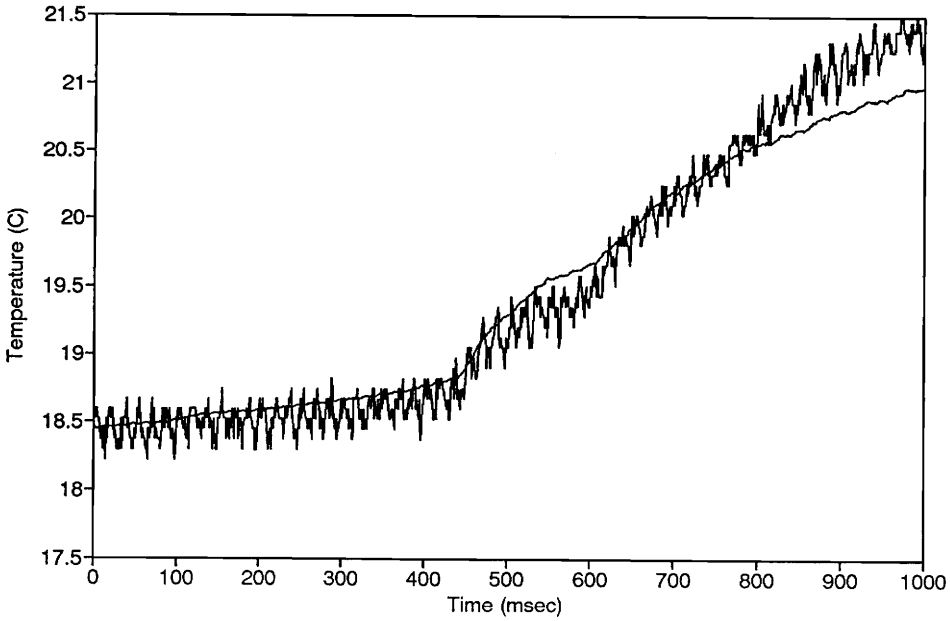

Figure F4. Experimental vs. Calculated Temperature for Line Gage Run 4.

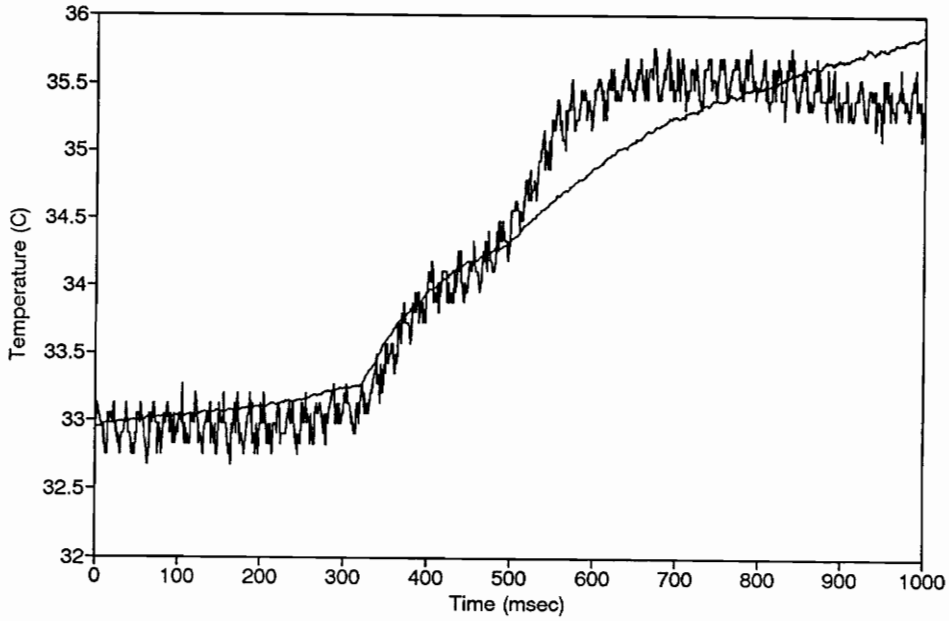

Figure F5. Experimental vs. Calculated Temperature for Line Gage Run 5.

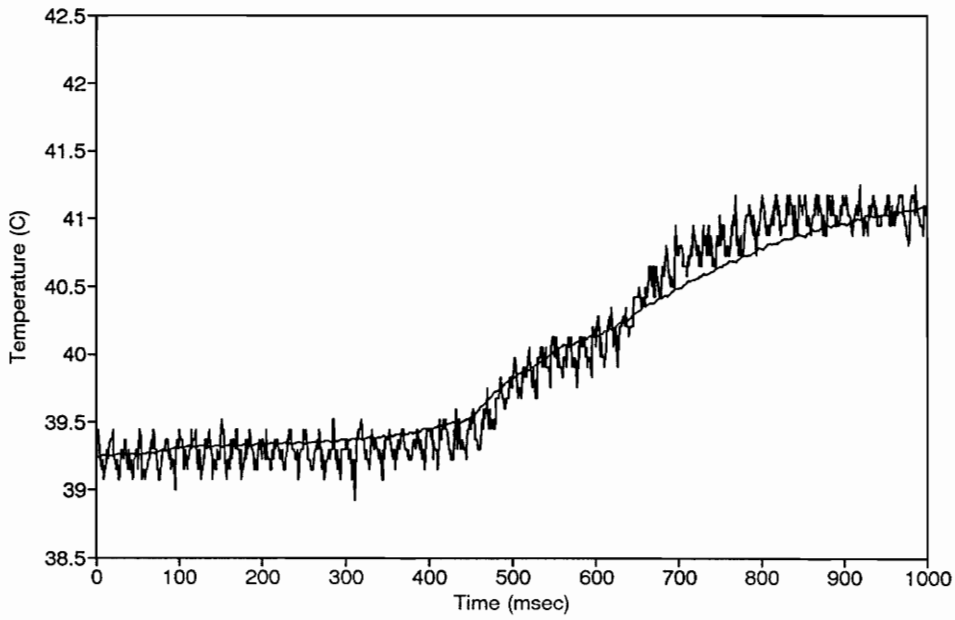

Figure F6. Experimental vs. Calculated Temperature for Line Gage Run 6.

```
************************************************************
*   QT.FOR                                                 *
*                                                          *
*   Originally written by Karen Baker                      *
*   Expanded by David Holmberg                             *
*   Last modified   5/22/95                                *
*   Latest modification improves convergence routine.      *
*                                                          *
*     This program is designed to convert an HFM surface heat flux  *
*  signal to the corresponding surface temperature according to a    *
*  one dimensional semi-infinite model of heat conduction into a     *
*  substrate of known thermal properties and initially constant      *
*  temperature. This model is valid for short times where the 1-D,   *
*  semi-infinite assumptions are valid. Documentation of this method *
*  can be found in HFM related publications.                         *
*     Data is input from a two column text file with the first       *
*  column temperature and the second heat flux with a space between  *
*  columns. The temperature and heat flux signals should be the same *
*  output by the HFM amplifier. Then this program converts the       *
*  voltages obtained from the heat flux microsensor to their corr-   *
*  esponding heat flux and temperature responses.  The amplifier     *
*  gains, RTS calibration, and substrate properties are entered into *
*  the uncompiled code as constants. If you want any of these to be  *
*  entered as inputs, then the source code must be changed.          *
*     This program utilizes the Cook and Felderman method to         *
*  differentiate temperature with respect to time to obtain the      *
*  corresponding heat flux and Green's function method to integrate  *
*  the heat flux with respect to time to yield temperature.          *
*     While the RTS calibration is entered as a known constant, the  *
*  HFS sensitivity is only entered as a guess value and this program *
*  iterates to find the best value of gage sensitivity for each data *
*  set such that the difference between experimental temperature and *
*  the temperature converted from the experimental heat flux is      *
*  minimized. A secant method algorithm is used to close on the      *
*  best solution for S (the HFS sensitivity).                        *
*     This program should not be used without looking at plotted     *
*  results to check PREPT and match in temps as time increases. If   *
*  the program crashes, try a different initial guess for S.         *
*                                                          *
*     Variables  used are:                                 *
*                                                          *
*   K.....Thermal conductivity of substrate (W/cmK)        *
*   RHO.....Density of substrate (kg/cm^3)                 *
*   CP.....Specific heat of substrate (J/kgK)              *
*   ALPHA.....Thermal diffusivity of substrate (cm^2/s)    *
*   QEXP().....Heat flux calc from experimental voltage (W/cm2)  *
*   TEXP().....Temperature calc from experimental voltage (degC) *
*   QCALC()....Heat flux calculated from temperature       *
```

```
*    TCALC()....Change in temp calc from heat flux based on SENS,          *
*          not final sensitivity. TCALC is an offset from TAVG             *
*    TEMPIN.....Input temperature (Volts), with or without gain            *
*    QIN.....Input heat flux (Volts)                                       *
*    RTSREF.....Reference temperature in RTS calibration (degC)            *
*          This is an offset, and not used in calculations.                *
*    RTSLOPE....Slope of RTS calibration curve; sensitivity(degC/V)        *
*    RTSGAIN....Ampilfier gain setting for RTS                             *
*    HFSGAIN....Amplifier gian setting for HFS                             *
*    SAMPFREQ...Sampling Frequency (kHz)                                   *
*    DT.....Time step (s), SAMPFREQ(Hz)^-1                                 *
*    TAVG.....Average temp of first PREPT points, substrate Tinit          *
*    TDIF.....Individual TCALC(J) - TEXP(J); individual errors             *
*    SUMTDIF....Sum of errors                                              *
*    SENS.....Input sensitivity of sensor (uV/W/cm^2)                      *
*    S().....Sensitivity output from convergence routine                   *
*    E().....Absolute error, equals ABS(SUMTDIF)                           *
*    MAXERR.....Error level defining convergence on S                      *
*    TIMEF.....Number of data points taken                                 *
*    STEPMAX....Max number of iterations in convergence routine            *
*    SKIP.....Input file size reduction factor                             *
*    LONGDATA...Length of unreduced input file                             *
*    PREPT.....Initial number of pts where T ~ constant, and q" ~ 0        *
*    VARYS.....Yes/No to vary input sensitivity                            *
************************************************************************

      REAL K, RHO, CP, ALPHA,
     + QEXP(3500), TEXP(3500), QCALC(3500), TCALC(3500),
     + TEMPIN, QIN, RTSREF, RTSLOPE, RTSGAIN, HFSGAIN, SAMPFREQ,
     + DT, TAVG, TDIF, SUMTDIF(100), SENS, S(100), E(100), MAXERR
      INTEGER TIMEF, STEPMAX, SKIP, LONGDATA, PREPT, VARYS
      CHARACTER INFILE*50, OUTFILE*50
      PARAMETER (PI=3.141592654)

************************************************************************
*     Definition of thermal properties of substrate, and other         *
*          parameters related to temp and S iteration.                 *
*        THESE MUST BE CHANGED FOR A GIVEN GAGE SUBSTRATE,             *
*           RTS CALIBRATION, AND GAIN SETTINGS                         *
*     PREPT is sensitive to starting length of individual data sets.   *
*     STEPMAX and MAXERR should be fine for all cases.                 *
************************************************************************

      K=1.29
      RHO=2.77E-3
      CP=921
      ALPHA=K/RHO/CP
      RTSREF = 25.
      RTSLOPE = 5000.
      RTSGAIN = 1.
      HFSGAIN = 1.
```

```
      PREPT = 10
      STEPMAX = 100
      MAXERR = 0.0001

*****************************************************************
*     Input filenames, open the ASCII input data file and create the      *
*     output file. Anything in the output file before running is erased   *
*     during each run.                                                    *
*****************************************************************

      PRINT*
      PRINT*
      PRINT*, '                - Program QT - '
      PRINT*
      PRINT*, '     The operation of this program is documented in the
     +source'
      PRINT*, 'code. Substrate properties, calibration constants, and am
     +plifier'
      PRINT*, 'gains must be entered there and the code recompiled.'
      PRINT*
      PRINT*
      PRINT*, 'Enter input filename:'
      READ(*,'(A)') INFILE
      PRINT*
      PRINT*, 'Enter output filename:'
      READ(*,'(A)') OUTFILE
      PRINT*

      OPEN (9, FILE = INFILE)
      OPEN (6, FILE = OUTFILE)

*****************************************************************
*      To use this program successfully, the number of data points,       *
*     TIMEF = LONGDATA/SKIP must be less than 3500, or the arrays will    *
*     overflow. By increasing the value of SKIP, longer data files can    *
*     be processed as if they were sampled at a lower frequency, but      *
*     it may be better to reduce LONGDATA than to increase SKIP.          *
*       SENS as entered is a known value or initial guess, depending      *
*     on VARYS. The final output value of S(N) is the best sensitivity    *
*     for the particular data set being analyzed.                         *
*****************************************************************

      PRINT*, 'Enter length of input file:'
      READ*, LONGDATA
      PRINT*, 'Enter sampling frequency of data (kHz):'
      READ*, SAMPFREQ
10    PRINT*, 'Enter input file size reduction factor (SKIP):'
      READ*, SKIP
      TIMEF = INT(LONGDATA/SKIP)
      IF (TIMEF.GT.3500) THEN
        PRINT*, 'SKIP value too small.'
```

```
      GOTO 10
      ENDIF
    DT = SKIP/SAMPFREQ/1000
    PRINT*, 'Enter heat flux sensitivity (known or initial guess)'
    PRINT*, 'used in converting V to W/cm2 (uV/W/cm2):'
    READ*, SENS
    PRINT*,'Do you want to vary this sensitivity value? (1=yes,0=no):'
    READ*, VARYS
    PRINT*
*****************************************************************
*   Do loop to read ASCII file and convert voltages to correspond-  *
*   ing temperature and heat flux according to given calibration    *
*   constants and gains.                                            *
*     DUM1,2 may be used to take up unwanted columns in the         *
*   input file. The IF stmt serves to remove all data pts where     *
*   (I-1)/SKIP is not an integer.                                   *
*****************************************************************

    J = 0
    DO 1 I = 1, LONGDATA
     READ (9, *) TEMPIN, QIN
*                        , DUM1IN, DUM2IN
     IF (INT((I-1)/SKIP).EQ.((REAL(I)-1)/REAL(SKIP))) THEN
      J = J + 1
      TEXP(J) = RTSLOPE*TEMPIN/RTSGAIN + RTSREF
      QEXP(J) = QIN*1000000./HFSGAIN/SENS
     ENDIF
1    CONTINUE

*****************************************************************
*   Do loop to find average of the first PREPT points of TEXP(I).   *
*   PREPT is the initial number of data points where TEXP is approx-*
*   imately constant, and where QEXP is approximately 0, before the *
*   heat flux pulse arrives. PREPT should be as large as possible.  *
*   This average serves as the starting temp (TCALC(1)) in "DO 4..." *
*   below, and minimizes error due to noise on the temp signal.     *
*****************************************************************

    DO 33 I = 1, PREPT
     TAVG = TAVG + TEXP(I)/PREPT
33   CONTINUE

*****************************************************************
*   Do loop to perform numerical expression developed by Cook and   *
*   Felderman to calculate heat flux from surface temperature       *
*****************************************************************

    DO 2 M = 1, TIMEF
     QCALC(M) = 0
    DO 3 L = 2, M
     QCALC(M) = QCALC(M) + (TEXP(L) - TEXP(L-1))/(SQRT((M -L)*DT)
```

```
     + +SQRT((M-L+1)*DT))
3    CONTINUE
      QCALC(M) = 2.*SQRT(K*RHO*CP)/SQRT(PI)*QCALC(M)
2    CONTINUE

*****************************************************************
*    Do loop to perform method of Green's function to calculate  *
*    temperature from heat flux                                  *
*****************************************************************

     DO 4 I = 1, TIMEF
      TCALC(I) = 0
     DO 5 J = I, 1, -1
      IF (J.EQ.1) THEN
       TCALC(I) = TCALC(I) - 2.*SQRT(ALPHA)/K/SQRT(PI)*QEXP(J)
    +   *(SQRT(((I-.5)-(J-.5))*DT)-SQRT((I-.5)*DT))
      ELSE
       TCALC(I) = TCALC(I) -2.*SQRT(ALPHA)/K/SQRT(PI)*QEXP(J)
    +   *(SQRT(((I-.5)-(J-.5))*DT)-SQRT(((I-.5)-(J-1.5))*DT))
      ENDIF
5    CONTINUE
4    CONTINUE

*****************************************************************
*    Do loop where S is iteratively reduced to find the best least  *
*    error fit between the actual temperature data, TEXP, and the   *
*    temperature converted from the actual heat flux, QEXP. The loop*
*    also contains IF statements to govern the value and direction  *
*    of the next step in determining a more accurate value of S.    *
*****************************************************************

     N = 0
     S(0) = SENS
     S(1) = SENS
     Smin = 0.
     Smax = 100*SENS
     IF (VARYS.EQ.0) GOTO 100
     WRITE (*, *) ' Sensitivity   Convergence Error'

     DO 77 N = 1, STEPMAX
      SUMTDIF(N) = 0
      DO 7 J = 1, TIMEF
       IF(N.EQ.1) THEN
        TDIF = TCALC(J) + TAVG - TEXP(J)
        SUMTDIF(N) = SUMTDIF(N) + TDIF
       ELSE
        SUMTDIF(N) = SUMTDIF(N) + (S(1)/S(N)-1)*TCALC(J)
       ENDIF
7     CONTINUE
      IF(N.GT.1) SUMTDIF(N) = S
UMTDIF(N) + SUMTDIF(1)
```

```
      E(N) = ABS(SUMTDIF(N))

      IF (N.EQ.1) THEN
        S(2) = S(1) + SENS/1000
        GOTO 76
        ENDIF
      IF (E(N).GT.E(N-1)) THEN
        IF(S(N).GT.S(N-1))  Smax = S(N)
        IF(S(N).LT.S(N-1))  Smin = S(N)
        ENDIF
      IF (E(N).LT.E(N-1)) THEN
        IF(S(N).GT.S(N-1))  Smin = S(N-1)
        IF(S(N).LT.S(N-1))  Smax = S(N-1)
        ENDIF

      S(N+1) = S(N-1) - (S(N)-S(N-1))*E(N-1)/(E(N)-E(N-1))

      IF (S(N+1).GT.Smax.OR.S(N+1).LT.Smin) THEN
        IF ((Smax-S(N)).GT.(S(N)-Smin))  S(N+1) = (Smax+S(N))/2
        IF ((Smax-S(N)).LT.(S(N)-Smin))  S(N+1) = (Smin+S(N))/2
        ENDIF
      IF (ABS(S(N+1)-S(N)).LT.MAXERR) GOTO 100

76     WRITE (*, '(1X, F10.3, 8X, F10.6)') S(N), E(N)
77    CONTINUE

*****************************************************************
*    Do loop to write final values to file opened above                    *
*****************************************************************

100   WRITE (6, '(1X, A14, F7.3)') 'Sensitivity = ', S(N+1)
      WRITE (*, '(1X, F10.3, 8X, F10.6)') S(N+1), E(N+1)
      PRINT*
      WRITE (*, *) 'Total time (ms) =', TIMEF*DT*1000
      WRITE (*, *) 'Total # of points =', TIMEF
      WRITE (*, *) 'dt (ms) =  ', DT*1000
      WRITE (*, *) 'Data infile = ', INFILE
      WRITE (*, *) 'Data saved to: ', OUTFILE
      WRITE (*, *) 'SKIP = ', SKIP

      WRITE (6, *) 'Total time (ms) =', TIMEF*DT*1000
      WRITE (6, *) 'Total # of points =', TIMEF
      WRITE (6, *) 'dt (ms) =  ', DT*1000
      WRITE (6, *) 'Data infile = ', INFILE
      WRITE (6, *) 'SKIP = ', SKIP
      WRITE (6, *)
      WRITE (6, *) '   Time (msec)     q" exp       T exp       q"calc
     +       T calc '

      DO 12 I = 1, TIMEF
20    FORMAT (1X, F12.7, 4(2X, F12.7))
```

```
      WRITE (6, 20) (I-1)*DT*1000, QEXP(I), TEXP(I), QCALC(I),
     +                        TCALC(I)*SENS/S(N+1)+TAVG
12    CONTINUE
      PRINT*
      STOP
      END
```

VITA

Loren Patton Johnson was born on April 8, 1970, in Corpus Christi, Texas. He has lived most of his life in Great Falls, Virginia, and graduated from Herndon High School, in June 1988. In August of 1988, he began his undergraduate studies at Virginia Tech where he eventually received his bachelor of science degree in Mechanical Engineering, in May of 1993 with a minor in French. He spent the 1990-1991 academic year attending L'Université de Technologie de Compiègne, France. Recently, he has been an active alumni in ΦΣΠ National Honor Fraternity in which he was a founding father at VA Tech. Upon graduation in May 1995, he will meet up with his mother, father, brother and sister in Seattle, Washington.